

**Sudan University of Science & Technology**  
**College of Engineering**  
**School of Mechanical Engineering**  
**Power Department**

**DESIGN AND STUDY OF A PARABOLIC TROUGH  
COLLECTOR FOR GENERATING ELECTRICITY**

A project submitted in partial Fulfillment for Requirements of Degree of  
B.Sc Honor in Mechanical Engineering

**Prepared by**

- 1- Ahmed Mohammed Amasaib Khalaf Allah.
- 2- Mohammed Al-Mujtaba abd Al-bagi Mohammed Farah.
- 3- Ashraf abd Allah Hamed Mohammed.
- 4- Mohammed Ebrahim Abd al-Razig Hassan.

**Supervised by**

**A.A.A.Abuelnuor**

October 2015

بِسْمِ اللَّهِ الرَّحْمَنِ الرَّحِيمِ

قُلْ هُوَ اللَّهُ أَحَدٌ ﴿١﴾ اللَّهُ الصَّمَدُ ﴿٢﴾ لَمْ يَكُنْ لَهُ  
وَلَمْ يُولَدْ ﴿٣﴾ وَلَمْ يَكُنْ لَهُ كُفُوًا أَحَدٌ ﴿٤﴾

## **DEDICATION**

*To the fountain of patience and optimism and hope.*

*To each of the following in the presence of God and His Messenger, my mother dear.*

*To those who have demonstrated to me what is the most beautiful of my brothers life.*

*To the big heart my dear father.*

*To the people who paved our way of science and knowledge all our teachers distinguished.*

*To the taste of the most beautiful moments with my friends.*

*...I guide this research...*

## **ACKNOWLEDGEMENT**

**Dr. Mnahel Zkki.**

**Eng. Abd Alhakm Ahmed noralden.**

**Eng. Alsadig Mustafa Abo daber.**

**Eng. Omnia abd- almagded.**

**Eng. Al Hassan Habib.**

**Eng. Alkhansaa abd Alhfeez abdallah.**

***All thanks and appreciation to our supervisor***

***A.A.A.Aboalnoor***

## مستخلص :

تم استخدام نماذج حسابيه في هذا المشروع لايجاد الاشعاعات الشمسيه المباشره والمنعكسه من طبقه الجو على سطح الارض لكل ساعه بناء على الاشعاع الشمسي الكلي اليومي على سطح افقي , بالاضافه الى ذلك فقد تم استخدام نماذج حسابيه لحساب هذه الاشعاعات للاسطح المائله. ان معظم المقادير المستخدمه في هذا المشروع مطلوبه كبيانات اوليه في عده تطبيقات للمحاكه الحراريه ولمحاكه انظمه الطاقه الشمسيه. كما تم استخدام نماذج حسابيه لدراسه حركه المائع داخل الانبوب (المستقبل) ودراسه تاثير الاشعاع الشمسي المباشر والمنعكس على ضغط ودرجه حراره وسرعه وطاقه حركه وقوه المائع داخل الانبوب. كما تم استخدام نماذج حسابيه لدراسه خواص المجمع الشمسي ذو القطع المكافئ ويجاد الكفاءه الحراريه .

تم عرض ومناقشه التغيرات التي تحدث لمقدار الاشعاع الشمسي الساقط على الاسطح مع تغير الوقت واتجاه السطح قورنت النتائج مع الدراسات الميدانيه لشهر اكتوبر ووجد ان هناك توافق بين الدراسات النظرية والعملية بنسبه خطأ 9.5 درجه. كما تم عرض ومناقشه التغيرات التي تحدث لخواص المائع داخل الانبوب (المستقبل) وذلك باستخدام برنامج المحاكاه FLUENT , كما تم عرض ومناقشه التغيرات التي تحدث لخواص المجمع الشمسي ذو القطع الكافئ مع الزمن واتجاه السطح العاكس ومعدل الانسياب الكتلي ونسبه التركيز. قورنت نتائج البحث مع التجارب المعملية ووجد هناك اختلاف بين نتائج الدراسه النظرية والعملية وذلك لاسباب تم مناقشتها وعرضها .

ان النتائج التي تم الحصول عليها في هذا البحث مفيده كبيانات اوليه للحصول على تقديرات سريعه للاشعاع الشمسي وكيفيه استخدامه في حسابات طاقه التبريد في المباني وحسابات الاحمال الحراريه للتكيف والتجفيف النباتي وتطبيقات المجمعات الشمسيه بنوعيهما الكهربيه والحراريه.

كما تم التوصل الى ان تطبيقات الطاقه الشمسيه الحراريه يمكن تطبيقها في السودان وذلك بناء على نتائج الدراسه حيث يبلغ متوسط الاشعاع الشمسي المباشر في اليوم 5231.8 واط على المتر المربع.

## Abstract

Mathematical models were used in this project to find the direct and reflected solar radiation from the air layer on the surface of the earth per hour based on the total daily solar radiation on a horizontal surface, also mathematical models has been used to calculate the radiation of the tilted surfaces. Most of the ingredients used in this project as data required previews of several solar energy applications thermal simulation and solar power systems. In addition mathematical models it has been used to study the movement of the fluid inside the tube (receiver), and study the effect of direct and reflected solar radiation on the pressure, temperature ,speed, kinetic energy and forces of fluid inside the tube. As it has been the use of mathematical models to study the parabolic trough solar collector performances and estimate its efficiency. present and discuss of changes in amount of solar radiation incident occur on the surfaces with the changing time and the direction of the surface results were compared with field studies for October and found that there is a consensus between the studies theoretical and practical studies by error of 9.5 Degree . also has been present and discuss the changes that occur to the properties of the fluid inside the tube (receiver) using the FLUENT simulation program, were also present and discuss the changes that occur to the properties of parabolic trough solar collector with time and direction of the surface of the reflector and the mass flow rate and the concentration ratio. The theoretical studies compared with the results of laboratory experiments and found there is a difference between the results of the theoretical study and practical for reasons that have been discussed and presented. The results obtained in this research useful as data Initial to get quick estimates of solar radiation and use this results to calculate cooling loads in buildings ,vegetable drying and solar energy application both electric and thermal.

# TABLE OF CONTENTS

Number	Object	Page
i.	الآية	-
ii.	<i>DEDICATION AND ACKNOWLEDGEMENT</i>	-
iii.	مستخلص	-
iv.	<i>Abstract</i>	-
v.	TABLE OF CONTENTS	-
vi.	LIST OF FIGURES	-
vii.	LIST OF TABLES	-
viii.	LIST OF SYMBOLS	-
ix.	LIST OF ABBREVIATIONS	-
<i>CHAPTE ONE</i>		
1.1	<i>Introduction</i>	2
1.2	<i>problem Statement</i>	2
1.3	<i>Objectives of the research</i>	2
1.4	<i>Methodology</i>	3
1.5	<i>Thesis outlets</i>	3
<i>CHAPTER TWO</i>		
2.1	<i>Introduction</i>	5
2.2	<i>Source of solar energy</i>	7
2.3	<i>Characterization</i>	11
2.4	<i>Distribution</i>	13
2.5	<i>Energy related environmental problems</i>	14
2.6	<i>Type of solar energy</i>	17
2.7	<i>Application of solar energy</i>	19
2.8	<i>Solar Thermal collector</i>	22
2.9	<i>Definition of PTC</i>	34
2.10	<i>Power plant components</i>	35
2.11	<i>parabolic trough collector</i>	36
2.12	<i>Heat transfer fluid</i>	51
2.13	<i>Direct steam generation</i>	56
2.14	<i>Advantages and challenges of DSG</i>	57
2.15	<i>Challenges</i>	58
2.16	<i>Solar field orientation</i>	61

CHAPTER THREE		
3.1	Abstract	64
3.2	Location of study	65
3.3	Estimation of Hourly Solar Radiation in horizontal surface Using Mathematical Model	66
3.4	The algorithm of horizontal surface	74
3.5	Estimation of Hourly Solar Radiation in Inclined surface Using Mathematical Model	75
3.6	the algorithm of tilted surface	77
3.7	Computational procedures	78
3.8	Model Parameters	79
3.9	Software Tools	79
3.10	Theoretical Study of a Parabolic Trough Solar Collector using Mathematical Model	80
3.11	Simulation and analyzing the flow inside the tube	88
3.12	TUBE in GAMBIT	89
3.13	Steps of solution in FLUENT	89
3.14	experimental model	98
CHAPTER FOUR		
4.1	The number of day in year	104
4.2	Results for horizontal surface	105
4.3	Results for Inclined surface	118
4.4	Results for theoretical Study of a Parabolic Trough Solar Collector	132
4.5	Numerical result of FLUENT	137
4.6	Results of measured Data	143
4.7	Comparison with Measured Data	144
4.8	Result of experimental model	145
4.9	Discussion	146
CHAPTER FIVE		
5.1	Conclusion	148
5.2	Recommendation	148
x.	REFERENCES	149
xi.	Appendix	151

## LIST OF FIGURES

figure	Title	page
2.1	Solar furnace used by Lavoisier in 1774.	5
2.2	Parabolic collectors powering a printing press at the 1878 Paris Exposition.	6
2.3	Sun earth relationships.	8
2.4	Anatomy of a Star.	8
2.5	Yearly variation of solar declination.	10
2.6	Declination of the sun.	10
2.7	Solar Radiations and the Earth-Atmosphere System.	11
2.8	Radiation flux distribution.	13
2.9	roof overhangs	18
2.10	Thermal Conductivity of an Insulated Wall.	18
2.11	Solar Distillation.	19
2.12	Schematic of Solar Home Lighting System.	20
2.13	Schematic of Solar Water pumping System	21
2.14	Solar Power Plants.	22
2.15	Pictorial view of a flat plate collector.	24
2.16	Schematic diagram of a compound parabolic collector	25
2.17	schematic diagram of an evacuated tube collector	27
2.18	Schematic diagram of a downward facing receiver illuminated from an LFR field.	28
2.19	Schematic diagram showing interleaving of mirrors in a CLFR with reduced shading between mirrors.	29
2.20	Schematic of a parabolic dish collector.	30
2.21	Schematic of central receiver system.	32
2.22	Schematic of a parabolic trough collector.	34
2.23	Energy conversion chain in a parabolic trough power plant and corresponding plant components	35
2.24	Focal length of parabolic shape.	36
2.25	paths of parallel rays at a parabolic mirror	37
2.26	Geometrical parabolic trough parameters.	37
2.27	Relation between the focal length and the rim angle for a constant trough aperture width.	38
2.28	Effects of slope errors in dependence on the rim angle.	39
2.29	Collector aperture area and receiver aperture area.	40
2.30	Mounting of a parabolic trough with silver coated glass mirror.	41
2.31	Reflectivity of silver.	42
2.32	multilayered mirrors	42
2.33	Reflect Tech film	43
2.34	Space frame structure of a Euro trough collector module	45
2.35	schematic of Euro trough module structural elements: (a) front and rear endplates for mounting to the pylons, (b) space frame structure, (c) receiver supports, (d) cantilever	45



	arm, (e) mirror facet	
2.36	Schott PTR 70	47
2.37	Siemens UVAC 2010	47
2.38	Archimede HEMS08	47
2.39	Structure of a parabolic trough receiver	48
2.40	Multi-layer coating of the absorber tube.	49
2.41	41 Transmittance of borosilicate glass without antireflective coating (blue line) Solar spectrum (orange line) Thermal radiation at about 380 °C (green line)	50
2.42	HTF selection criteria.	53
2.43	Direct steam generation systems.	56
2.44	operation concepts	59
2.45	DISS test facility at Plataforma Solar de Almería	60
2.46	Schema of DISS test facility	60
3.1	location of study	65
3.2	Definition of Latitude l, Hour angle h and Declination d angles	68
3.3	Definition of altitude, zenith and azimuth angles.	69
3.4	incidence angle in horizontal surface	71
3.5	Flowchart to calculate the potential solar radiation in horizontal surface.	74
3.6	Flowchart to calculate the potential solar radiation in Inclined surface.	77
3.7	flowchart to calculate Thermal Efficiency of parabolic trough solar collector	88
3.8	Design the tube in gambit.	89
3.9	Scale grid.	90
3.10	Grid Display.	90
3.11	Grid.	91
3.12	Solver.	91
3.13	Energy.	92
3.14	Viscous Model.	92
3.15	Materials.	93
3.16	Boundary Condition for inlet	94
3.17	Boundary Condition for lower arch.	94
3.18	Boundary Condition for wall.	95
3.19	Boundary Condition for upper arch.	95
3.20	Boundary Condition for outlet.	96
3.21	Residual Monitors.	96
3.22	Initialize the flow.	97
3.23	Iterate.	97
3.24	Experimental model.	100
3.25	Pyranometer and avometer.	101
3.26	Pressure gauges.	102
3.27	thermometers (hioki)	102
4.1	Direct, diffuse, and total solar radiation components during 15 January 2015.	111
4.2	Direct, diffuse, and total solar radiation components during 15 February 2015.	112
4.3	Direct, diffuse, and total solar radiation components during 15 March 2015.	112
4.4	Direct, diffuse, and total solar radiation components during 15 April 2015.	113

4.5	Direct, diffuse, and total solar radiation components during 15 May 2015.	113
4.6	Direct, diffuse, and total solar radiation components during 15 June 2015.	114
4.7	Direct, diffuse, and total solar radiation components during 15 July 2015.	114
4.8	Direct, diffuse, and total solar radiation components during 15 August 2015.	115
4.9	Direct, diffuse, and total solar radiation components during 15September2015	115
4.10	Direct, diffuse, and total solar radiation components during 15 October 2015.	116
4.11	Direct, diffuse, and total solar radiation components during 15 November2015.	116
4.12	Direct, diffuse, and total solar radiation components during 15December 2015.	117
4.13	Average Direct, diffuse, and total solar radiation components during 2015.	118
4.14	Tilted surface Solar radiation in 15 February collector facing south	124
4.15	Tilted surface Solar radiation in 15 February collector facing west	124
4.16	Tilted surface Solar radiation in 15 February collector facing north	125
4.17	Tilted surface Solar radiation in 15 February collector facing east	125
4.18	Tilted surface Solar radiation in 15 May collector facing south	126
4.19	Tilted surface Solar radiation in 15 May collector facing west	126
4.20	Tilted surface Solar radiation in 15 May collector facing north	127
4.21	Tilted surface Solar radiation in 15 May collector facing east	127
4.22	Tilted surface Solar radiation in 15 August collector facing south	128
4.23	Tilted surface Solar radiation in 15 August collector facing west	128
4.24	Tilted surface Solar radiation in 15 August collector facing north	129
4.25	Tilted surface Solar radiation in 15 August collector facing east	129
4.26	Tilted surface Solar radiation in 15 November collector facing south	130
4.27	Tilted surface Solar radiation in 15 November collector facing west	130
4.28	Tilted surface Solar radiation in 15 November collector facing north	131
4.29	Tilted surface Solar radiation in 15 November collector facing east	131
4.30	Variation in efficiency of Parabolic Trough Solar Collector with different mass flow rate.	133
4.31	Variation in useful energy with different mass flow rate.	134
4.32	Rate of energy gained as the concentration ratio increases.	134
4.33	Variation in efficiency of Parabolic Trough Solar Collector during summer and winter.	135
4.34	Variation of efficiency and heat removal factor of PTC with different mass flow rate.	136
4.35	Total Temperature	137
4.36	Contours of Total Temperature	138
4.37	Contour of Total Temperature	138
4.38	Contours of Static Pressure	139
4.39	Contours of Static Pressure	139
4.40	Velocity Vector Colored by Static Pressure	140
4.41	Velocity Vector Colored by Velocity Magnitude.	140
4.42	Contours of Turbulent kinetic Energy.	141
4.43	Velocity Vector Colored by Turbulent kinetic Energy.	141
4.44	Variation between measured data and theoretical results.	144

## LIST OF TABLES

Table	Title	Page
2.1	Type of radiation and there wavelength	12
2.2	Comprehensive list:	23
2.3	Types of parabolic trough collectors and their technical data	46
2.4	Nearly all parabolic trough power plants use synthetic thermo oil as HTF.	53
3.1	Percentage of the ground reflectivity	67
3.2	Parabolic chap	98
3.3	Experimental parabolic trough collector parameters	100
4.1	The number of day in year	104
4.2	Solar radiation in horizontal surface results of 15 January	105
4.3	Solar radiation in horizontal surface results of 15 February	106
4.4	Solar radiation in horizontal surface results of 15 March	106
4.5	Solar radiation in horizontal surface results of 15 April	107
4.6	Solar radiation in horizontal surface results of 15 May	107
4.7	Solar radiation in horizontal surface results of 15June	108
4.8	Solar radiation in horizontal surface results of 15 July	108
4.9	Solar radiation in horizontal surface results of 15 August	109
4.10	Solar radiation in horizontal surface results of 15 September	109
4.11	Solar radiation in horizontal surface results of 15 October	109
4.12	Solar radiation in horizontal surface results of 15 November	110
4.13	Solar radiation in horizontal surface results of 15 December	110
4.14	The daily average solar radiation components for 2015.	117
4.15	Total radiation with different tilted angles during 15 February 2015	120
4.16	Total radiation with different tilted angles during 15 May 2015	121
4.17	Total radiation with different tilted angles during 15 August 2015	122
4.18	Total radiation with different tilted angles during 15 November 2015	123
4.19	Theoretical model parameters.	132
4.20	Efficiency, useful energy and input power with different mass flow rate.	133
4.21	Useful energy and input power with different concentration ratio.	134
4.22	the efficiency during summer and winter	135
4.23	variation of efficiency and heat removal factor of PTC with different mass flow rate	136
4.24	Mass flow rate.	142
4.25	Total heat transfer.	142
4.26	Force report.	142
4.27	Moment report.	143
4.28	The measured Data for 15 October 2015.	143
4.29	The comparison between MATLAB R2010b outputs and measured data.	144

## LIST OF SYMBLS

H	altitude of the site	[m]
I	latitude of the site	degree
S	Solar constant	$W/m^2$
LON	local Longitude of site	degree
LSM	standard Longitude of the site	degree
$\rho$	ground reflectivity	[dimensionless]
N	The day number in the year	[dimensionless]
N	factor to calculate Equation of Time	[dimensionless]
EOT	Equation of Time	[dimensionless]
LST	local solar time	[dimensionless]
H	Hour angle	degree
$I_o$	Extraterrestrial radiation	$W/m^2$
$\theta$	Incident angle of sun's rays	degree
A	the apparent solar irradiation	$W/m^2$
B	the atmospheric extinction coefficient	[dimensionless]
$I_{dn}$	Direct radiation from the sun	$W/m^2$
M	Air mass ratio	[dimensionless]
F.ws	view factor or configuration factor	[dimensionless]
$\varepsilon$	tilt angle	degree
$I_b$	Beam (direct) radiation	$W/m^2$
$I_d$	Diffuse radiation from sky	$W/m^2$
$I_t$	total solar radiation	$W/m^2$
D	declination angle	degree
$\beta$	altitude angle	degree
$\psi$	Zenith angle	degree
$\gamma$	Solar azimuth angle	degree

Dr	$360/365$ factor to convert	[dimensionless]
LStT	local standard time	[dimensionless]
Qt	total radiation received by an inclined surface	$W/m^2$
Qb	direct (beam) radiation in an inclined surface	$W/m^2$
$\gamma_s$	the surface azimuth angle	degree
Qd	diffuse radiation in an inclined surface	$W/m^2$
Qr	reflected radiation from the surrounding ground	$W/m^2$
R	hourly geometric factor	[dimensionless]
Aap	aperture area	$[m^2]$
Ar.ext	external surface area of receiver	$[m^2]$
Ar.int	internal surface area of receiver	$[m^2]$
Cr	concentration ratio	[dimensionless]
Dr.ext	external diameter of receiver	$[m]$
Dr.int	internal diameter of receiver [	$[m]$
Fr	heat removal factor of collector	[dimensionless]
Hp	absorbed radiation	$W/m^2$
Z	efficiency factor of collector	[dimensionless]
Cp	specific heat	$J/kg \cdot ^\circ C$
Hr	radiation heat transfer coefficient between receiver and ambient	$W/M^2 \cdot ^\circ C$
Hw	convective heat transfer coefficient between receiver and ambient	$W/M^2 \cdot ^\circ C$
Ib	beam solar radiation	$W/m^2$
Ka	conductivity of air	$W/m \cdot ^\circ C$
L	collector length	$[m]$
W	collector width	$[m]$
F	focus length	$[m]$
M	mass flow rate	$[kg/hr]$
Nu.a	Nussle number of air	[dimensionless]
Re.a	Reynolds number of air	[dimensionless]
T.amb	ambient temperature	$[^\circ C]$
Tr	receiver temperature	$[^\circ C]$
Tf.i	inlet fluid temperature	$[^\circ C]$
Tf.o	outlet fluid temperature	$[^\circ C]$
Ul	overall heat loss coefficient	$W/M^2 \cdot ^\circ C$
V	wind velocity	$M/s$
Qi	Power input to collector	$W/m^2$
Qo	theoretical useful energy	$W/m^2$
$\sigma$	Stefan–Boltzmann constant	$W/M^2 \cdot K^4$
$\rho$	Reflectivity	[dimensionless]
$\alpha$	Absorptance	[dimensionless]
$\eta_{th}$	theoretical thermal efficiency	[dimensionless]

## LIST OF ABBREVIATIONS

PTC	Parabolic trough collector
PV	Photovoltaic
STC	Solar thermal collectors
NCC	Non- Concentrating collectors
CC	Concentrating collectors
FPC	Flat plat collector
CPC	Compound parabolic collector
ETC	Evacuated tube collector
LFR	Linear Fresnel reflector
PDC	Parabolic dish collector
HFC	Heliostat field collector
CG	Geometrical concentration ratio
HCE	Heat collector element
ASE	Archimede solar energy
HTF	Heat transfer fluids
DSG	Direct steam generation
SFO	Solar field orientation
EWD	East – west direction
NSD	North –south direction
SA	Solar angles
SRHS	Solar radiation in horizontal surface
SRIS	Solar radiation in inclined surface
HRF	Heat removal factor
UEG	Useful energy gained
SRC	Solar radiation components

# CHAPTER ONE

## 1.1 Introduction

This Research is a design of parabolic trough collector and a study of the relationship between the concentrating ratio of sun radiation and the generated heat. And study the flow of the fluid inside the collector tube .The Importance of producing electricity in respect of reducing air pollution is raising every day. Therefore this research will focus only on concentrating sun rise by (PTC) aiming to generate steam to produce electricity. It is our hope and aspiration that this research raises public awareness and that people can live in a clean world someday.

## 1.2 Statement of the problem

It is clear that Sudan depends on hydropower for electricity production, and this dependence is a danger in the future as to agreements of Nile Basin Countries and increasing investment in agricultural projects. Hence, there must be other sources to generate electricity to meet the shortfall in the growing energy demand. Also highly cost and magnitude of fuel used to operate boiler and super heater. In addition to reducing the use of bio-fuel which causing the emission of greenhouse gases which effect directly on the environment in terms of emission damage or removal of trees to use charcoal. Where majority of the population in Sudan depends on bio-fuel ranges almost 68.4%.

## 1.3 Objectives of the research

- 1- Design high performance parabolic trough collector.
- 2- Study the sun radiation numerically and experimentally.
- 3- Produce electricity.



## 1.4 Methodology

The parabolic trough collector will be designed and built actually to obtain the required data of a study, such as the concentrating ratio, the temperature of fluid, pressure inside the tube and the electricity product. Simulate and analyze the flow inside the tube using GAMBIT 2.3.16 to build it and FLUENT 6.3.26 to analyze the flow of fluid, and extract the temperature and the pressure of the fluid and there effects on the tube, heat transfer through the tube and the velocity of the steam across the nozzle. Extract the amount sun radiation (beam, defuse and total radiation) reach the surface of Khartoum numerically by calculation and experimentally by pyranometer and avometer .

## 1.5 Thesis outlets

- 1- Introduction: in which the research problem is defined and also the goals and the approach.
- 2- Literature review: this chapter introduces the sun star and its energy demand and utilized in numeration. Also proportion of sunlight reaches earth relatively to location of Sudan. And defining parabolic trough collector and introduce the parts of its construction. Also introduce three main concepts: (reflective surface, evacuated tube, heat fluid transfer).
- 3- Methodology: Calculate solar radiation, study of the flow inside the tube, calculate the theoretical efficiency of PTC and design an experimental model.
- 4- Results and discussion: this chapter displays the MATLAB, FLUENT and practical results. Also discusses the effect of sun radiation on the tube(receiver) and compared the theoretical results with experimental results
- 5- conclusion: this chapter provides a conclusion on the results, appendix and bibliography of the research.

# CHAPTER TWO

## 2.1 Introduction

Solar energy is the oldest energy source ever used. The sun was adored by many ancient civilizations as a powerful god. The first known practical application was in drying for preserving food probably the oldest large-scale application known to us is the burning of the Roman fleet in the bay of Syracuse by Archimedes, the Greek mathematician and philosopher (287–212 B.C.). Scientists discussed this event for centuries. A Polish mathematician described the burning of the Roman fleet in detail: “The burning glass of Archimedes composed of 24 mirrors, which conveyed the rays of the sun into a common focus and produced an extra degree of heat.” [1]. Amazingly, the very first applications of solar energy refer to the use of concentrating collectors, which are, by their nature (accurate shape construction) and the requirement to follow the sun, more difficult to apply. During the 18th century, solar furnaces capable of melting iron, copper, and other metals were being constructed of polished iron, glass lenses, and mirrors. The furnaces were in use throughout Europe and the Middle East. One of the first large-scale applications was the solar furnace built by the well-known French chemist Lavoisier, who, around (1774) constructed powerful lenses to concentrate solar radiation (see Figure 2.1). This attained the remarkable temperature of 1750°C. The furnace used a 1.32 m lens plus a secondary 0.2 m lens to obtain such temperature, which turned out to be the maximum achieved for 100 years [1].

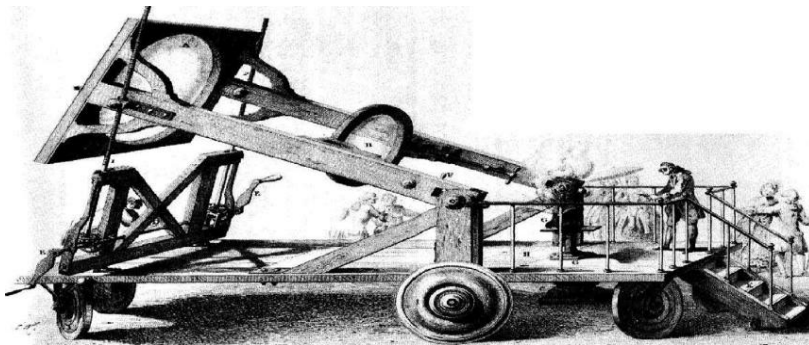


Figure 2.1 Solar furnace used by Lavoisier in 1774 [1]

During the 19th century, attempts were made to convert solar energy into other forms based upon the generation of low-pressure steam to operate steam engines. August Monchot pioneered this field by constructing and operating several solar powered steam engines between the years 1864 and 1878 in Europe and North Africa. One of them was presented at the 1878 International Exhibition in Paris (see Figure 2.2). The solar energy gained was used to produce steam to drive a printing machine. Evaluation of one built at Tours by the French government showed that it was too expensive to be considered feasible [1].

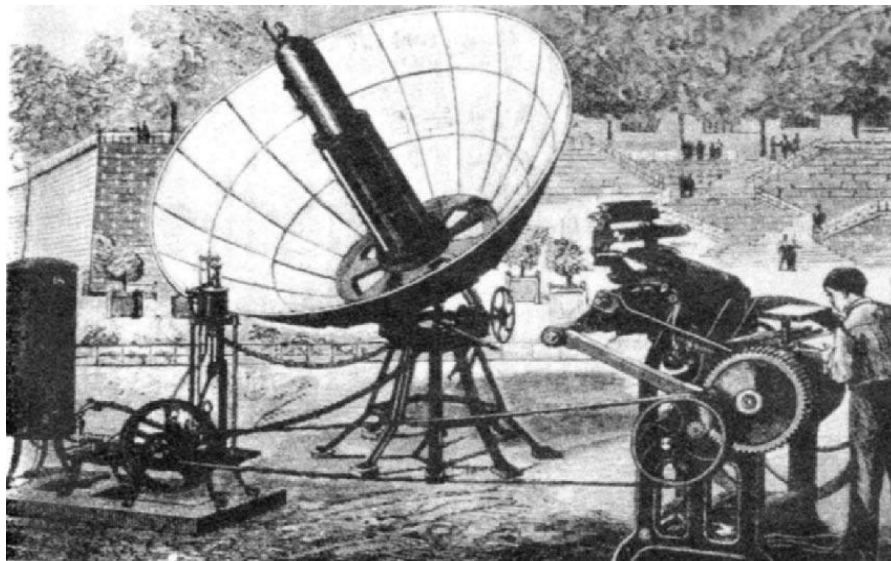


Figure 2.2 parabolic collectors powering a printing press at the 1878 Paris Exposition[1]

In 1901 A. G. Eneas installed a 10 m diameter focusing collector that powered a water-pumping apparatus at a California farm. The device consisted of a large umbrella-like structure open and inverted at an angle to receive the full effect of the sun's rays on the 1788 mirrors that lined the inside surface [1]. In 1904, a Portuguese priest, Father Himalaya, constructed a large solar furnace. This was exhibited at the St. Louis World's Fair. This furnace appeared quite modern in structure, being a large, off-axis, parabolic horn collector [1]. In 1912, Frank Shuman, in collaboration with C.V. Boys, undertook to build the world's largest pumping plant in Meadi, Egypt.

The system was placed in operation in 1913, using long parabolic cylinders to focus sunlight onto a long absorbing tube. Each cylinder was 62 m long, and the total area of the several banks of cylinders was 1200 m<sup>2</sup>. The solar engine developed as much as 37 to 45 k W continuously for a five-hour period. Despite the plant's success, it was completely shut down in 1915 due to the onset of World War I and cheaper fuel prices [1]. Today, many large solar plants have output in the megawatt range to produce electricity or process heat. The first commercial solar plant was installed in Albuquerque, New Mexico, in 1979. It consisted of 220 heliostats and had an output of 5 MW. The second was erected at Barstow, California, with a total thermal output of 35 MW. Most of the solar plants produce electricity or process heat for industrial use and they provide superheated steam of 673 K. Thus, they can provide electricity or steam to drive small-capacity conventional desalination plants driven by thermal or electrical energy [1]. Another area of interest, hot water and house heating, appeared in the mid- 1930s but gained interest in the last half of the 1940s. Until then, millions of houses were heated by coal-burning boilers. The idea was to heat water and feed it to the radiator system that was already installed [1].

## 2.2 Source of solar energy

The sun is the only star of our solar system located at its center. About 74% of the sun's mass is hydrogen, 25% is helium, and the rest is made up of trace quantities of heavier elements. The sun has a surface temperature of approximately 5500 K, giving it a white color, which, because of atmospheric scattering, appears yellow. The sun generates its energy by nuclear fusion of hydrogen nuclei to helium [1]. The sun is a sphere of intensely hot gaseous matter with a diameter of  $1.39 \times 10^9$  m. The sun is about  $1.5 \times 10^{11}$  m away from earth (see Figure2.3).

so, because thermal radiation travels with the speed of light in a vacuum (300,000 km/s), after leaving the sun solar energy reaches our planet in 8 min and 20 sec [1].

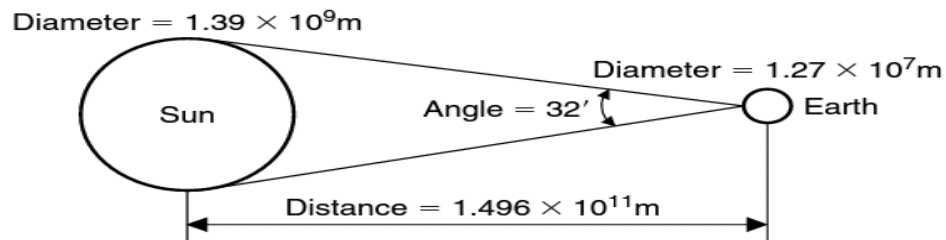


Figure 2.3 sun earth relationships[1]

Energy emitted by a star is generated by nuclear fusion. The fusion process occurs in the core, or center, of the star. Energy released by the fusion process propagates away from the core by radiating from one atom to another in the radiation zone of the star. As the energy moves away from the core and passes through the radiation zone, it reaches the part of the star where the energy continues its journey towards the surface of the star as heat associated with thermal gradients. This part of the star is called the convection zone. The surface of the star, called the photosphere, emits light in the visible part of the electromagnetic spectrum. The star is engulfed in a stellar atmosphere called the chromospheres. The chromospheres are a layer of hot gases surrounding the photosphere [1] (see Figure 2.4).

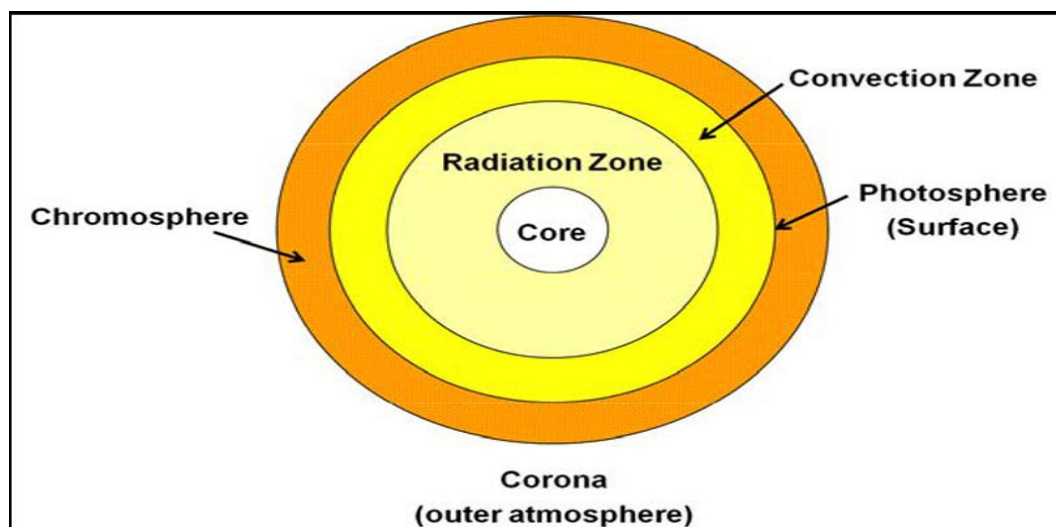


Figure 2.4 Anatomy of a Star[1]

As observed from the earth, the sun disk forms an angle of 32 min of a degree. This is important in many applications, especially in concentrator optics, where the sun cannot be considered as a point source and even this small angle is significant in the analysis of the optical behavior of the collector. The sun has an effective black-body temperature of 5500 K. The temperature in the central region is much higher. In effect, the sun is a continuous fusion reactor in which hydrogen is turned into helium. The sun's total energy output is  $3.8 * 10^{20}$  MW, which is equal to 63 MW/m<sup>2</sup> of the sun's surface. This energy radiates outward in all directions. The earth receives only a tiny fraction of the total radiation emitted, equal to  $1.7 * 10^{14}$  kW; however, even with this small fraction, it is estimated that 84 min of solar radiation falling on earth is equal to the world energy demand for one year (about 900 EJ). As seen from the earth, the sun rotates around its axis about once every four weeks [1]. As observed from earth, the path of the sun across the sky varies through-out the year. The shape described by the sun's position, considered at the sometime each day for a complete year, is called the analemma and resembles a figure 8 aligned along a north-south axis. The most obvious variation in the sun's apparent position through the year is a north-south swing over 47° of angle (because of the 23.5° tilt of the earth axis with respect to the sun), called declination (see Figure 2.5 2.6). The north-south swing in apparent angle is the main cause for the existence of seasons on earth. Knowledge of the sun's path through the sky is necessary to calculate the solar radiation falling on a surface, the solar heat gain, the proper orientation of solar collectors, the placement of collectors to avoid shading, and many more factors that are not of direct interest in this book. The objective of this chapter is to describe the movements of the sun relative to the earth that give to the sun its east-west trajectory across the sky. The variation of solar incidence angle and the amount of solar energy received are

analyzed for a number of fixed and tracking surfaces. The environment in which a solar system works depends mostly on the solar energy availability [1].

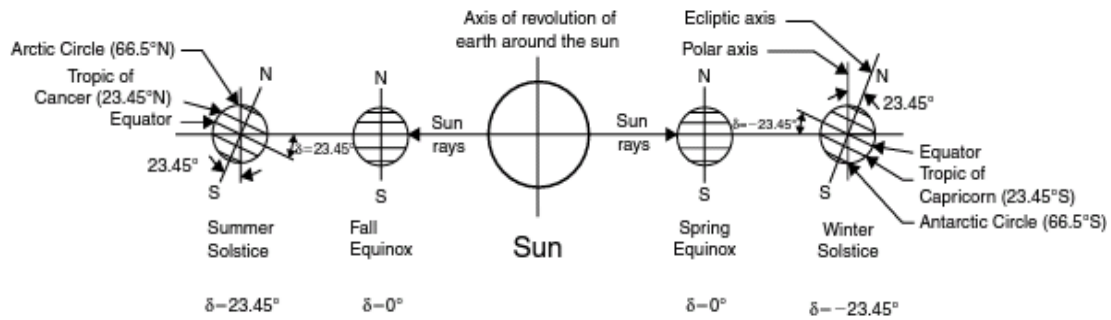


Figure 2.5 Yearly variation of solar declination[1]

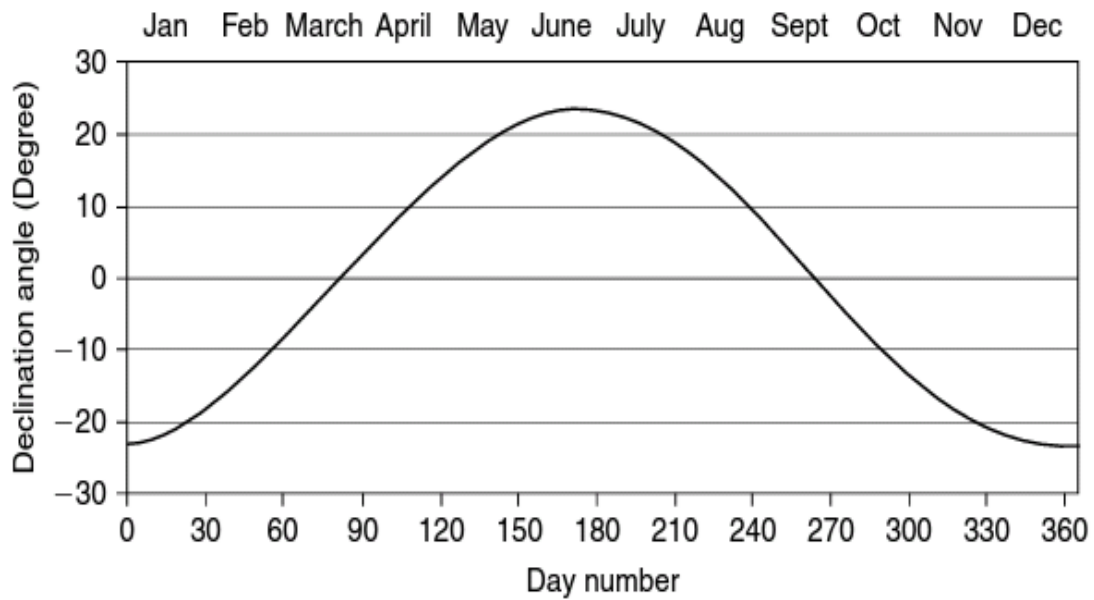


Figure 2.6 declination of the sun[1]



## 2.3 Characterization

In terms of energy strength, the sun constantly delivers ( $1.7 \times 10^{14}$  kW) to the earth. However, some of this power is absorbed by the atmosphere so that, even under ideal conditions, a receptor on Earth may receive less than 1,000 W/m<sup>2</sup> [1]. From an overall global perspective, of the total annual radiation reaching the earth's atmosphere its ultimate distribution is as follows:

- 50% is reflected back into space by the cloud
- 27.8% is absorbed in evaporating water
- 15% is reflected back by the Earth's surface
- 5.3% is absorbed by bare soil
- 1.7% is absorbed by marine vegetation
- 0.2% is absorbed by land vegetation

Some of the light that is scattered by the atmosphere eventually reaches the surface of the earth as diffused light (see Figure 2.7). Solar radiation that reaches the earth's surface from the disk of the sun is called direct solar radiation if it has experienced negligible change in its original direction propagation [6].

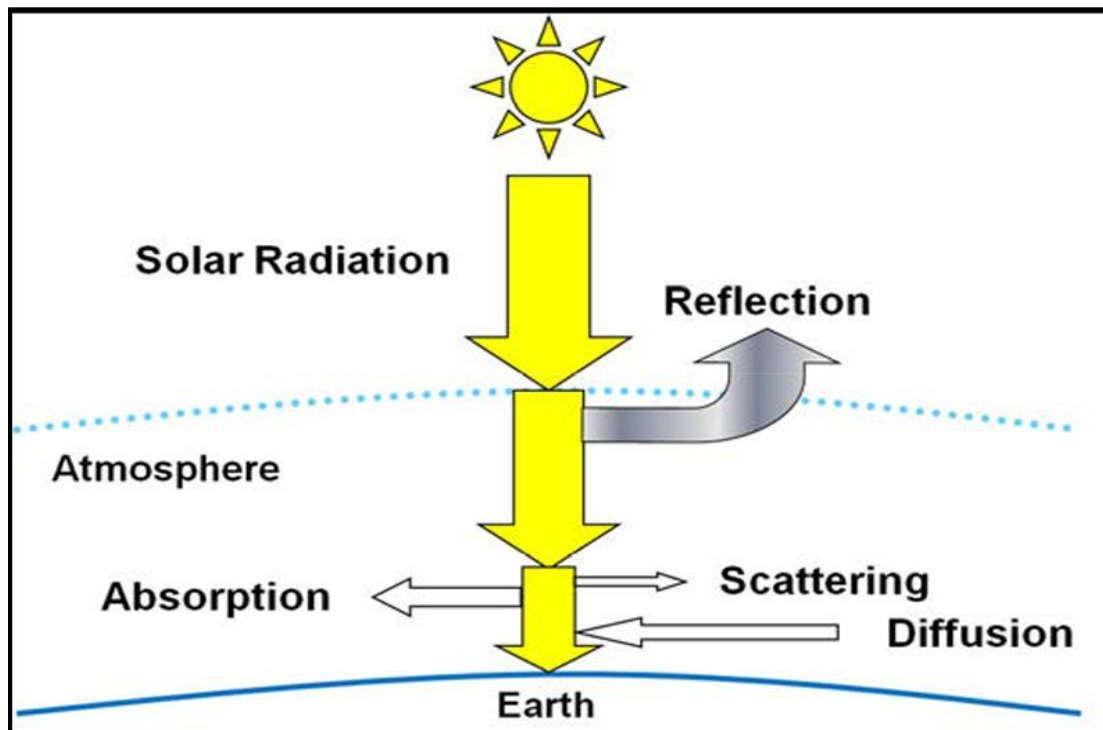


Figure 2.7 Solar Radiations and the Earth-Atmosphere System[6]

Radiant energy received from the sun passes through the Earth's atmosphere, which absorbs some of the energy and thus affects the quality of visible light as it is received. The units of wavelength may be expressed in meters (m) centimeters (cm) micrometers or angstroms ( $1.0 \text{ \AA} = 10 \mu$ ) with meters and centimeters being the usual units of choice. The speed of electromagnetic radiation is approximately  $3 \times 10^{18} \text{ m/s}$  in a vacuum. This velocity is given by the product of the wavelength ( $\lambda$ ) and the frequency ( $f$ ) of the radiation [7].

$$c = \lambda \cdot f \text{ consistent units}$$

Table2.1 type of radiation and there wavelength [6]

<b>Type of Radiation</b>	<b>Wavelength (m)</b>
Gamma rays	$10^{-13} - 10^{-11}$
X-rays	$10^{-11} - 10^{-9}$
Ultraviolet rays	$10^{-9} - 4 * 10^{-7}$
Visible rays	$4 * 10^{-7} - 8 * 10^{-7}$
Infrared rays	$8 * 10^{-7} - 10^{-4}$
Micro waves	$10^{-4} - 10^{-1}$
Radio waves	$10^{-1} - 10$

The radiant energy received by Earth is distributed as follows [8]:

- 7.82 percent: ultraviolet spectrum.
- 47.33 percent: visible spectrum.
- 44.85 percent: infrared spectrum.

The amount of sunlight available is one factor to take into account when considering using solar energy. There are a few other factors, however, which need to be looked at when determining the viability of solar energy in any given location These are as follows[8].

- Geographic location.
- Time of day.
- Season.
- Local landscape.
- Local weather.

## 2.4 Distribution

The average amount of solar radiation flux striking the Earth's surface is approximately 630 W/m<sup>2</sup>. This is an average figure; the actual radiation received at a specific location can be higher or lower. As noted earlier, essentially no radiation is received at night, and a reduced amount is received at times other than noon (see Figure 2.8). The solar energy received also varies significantly with latitude, as well as with time of year [2].

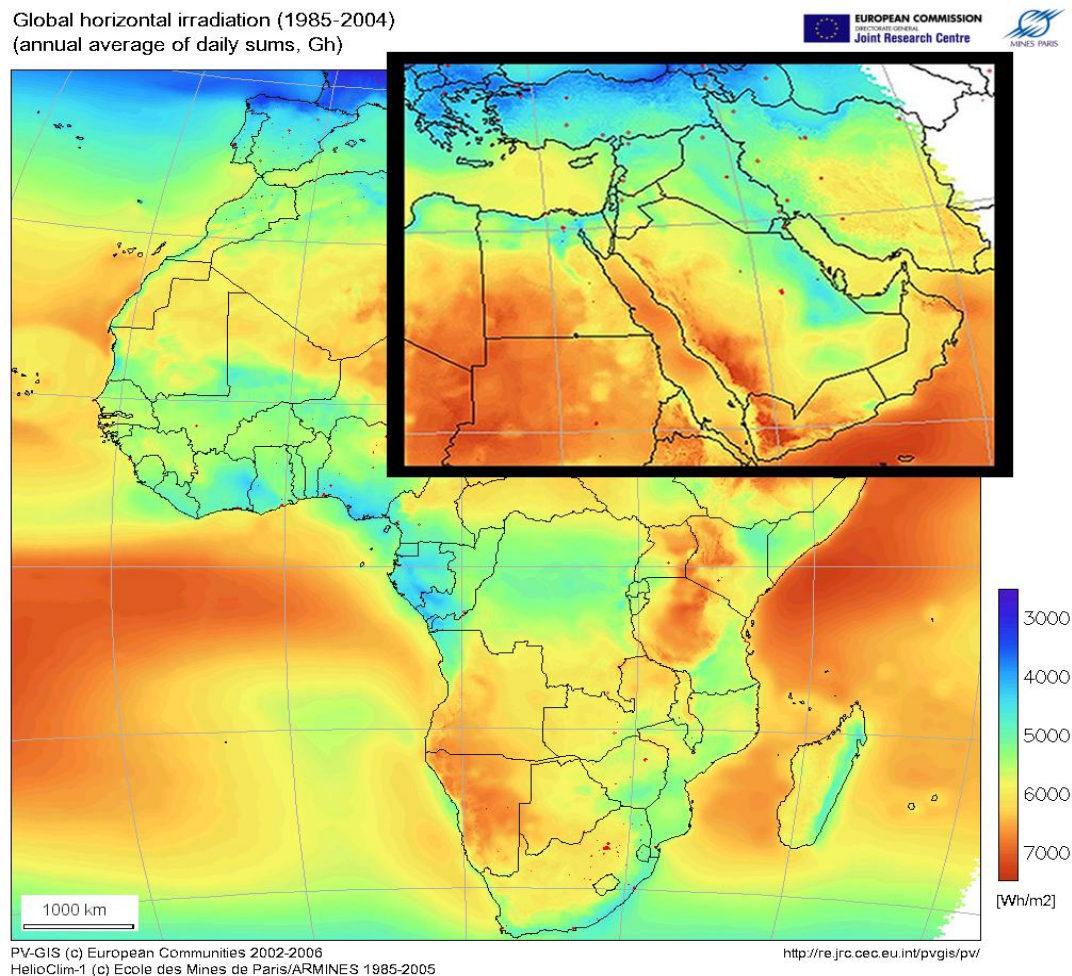


Figure2.8 radiation flux distribution[2]

## 2.5 Energy related environmental problems

Energy is considered a prime agent in the generation of wealth and a significant factor in economic development. The importance of energy in economic development is recognized universally and historical data verify that there is a strong relationship between the availability of energy and economic activity. Although at the early 70s, after the oil crisis, the concern was on the cost of energy, during the past two decades, the risk and reality of environmental degradation have become more apparent. The growing evidence of environmental problems is due to a combination of several factors since the environmental impact of human activities has grown dramatically. This is due to the increase of the world population, energy consumption and industrial activities. Achieving solutions to environmental problems that humanity faces today requires long-term potential actions for sustainable development. In this respect, renewable energy resources appear to be one of the most efficient and effective solutions [4].

A few years ago, most environmental analysis and legal control instruments concentrated on conventional pollutants such as Sulphur dioxide ( $\text{SO}_2$ ), nitrogen oxides ( $\text{NOX}$ ), particulates, and carbon monoxide ( $\text{CO}$ ). Recently however, environmental concern has extended to the control of hazardous air pollutants, which are usually toxic chemical substances which are harmful even in small doses, as well as to other globally significant pollutants such as carbon dioxide ( $\text{CO}_2$ ). Additionally, developments in industrial processes and structures have led to new environmental problems [4].

Pollution depends on energy consumption. Today the world daily oil consumption is 76 million barrels. Despite the well-known consequences of fossil fuel combustion on the environment, this is expected to increase to 123 million barrels per day by the year 2025. There are a large number of factors which are significant

in the determination of the future level of the energy consumption and production. Such factors include population growth, economic performance, consumer tastes and technological developments. Furthermore, governmental policies concerning energy and developments in the world energy markets will certainly play a key role in the future level and pattern of energy production and consumption. Another parameter to be considered is the world population. This is expected to double by the middle of this century and as economic development will certainly continue to grow, the global demand for energy is expected to increase. Today much evidence exists, which suggests that the future of our planet and of the generations to come will be negatively impacted if humans keep degrading the environment. Currently, three environmental problems are internationally known; these are the acid precipitation, the stratospheric ozone depletion, and the global climate change. These are analyses in more detail below [4].

- **Acid rain**

This is a form of pollution depletion in which  $\text{SO}_2$  and  $\text{NO}_x$  produced by the combustion of fossil fuels are transported over great distances through the atmosphere and deposited via precipitation on the earth, causing damage to ecosystems that are exceedingly vulnerable to excessive acidity. Therefore, it is obvious that the solution to the issue of acid rain deposition requires an appropriate control of  $\text{SO}_2$  and  $\text{NO}_x$  pollutants. These pollutants cause both regional and transboundary problems of acid precipitation. Recently, attention is also given to other substances such as volatile organic compounds (VOCs), chlorides, ozone and trace metals that may participate in a complex set of chemical transformations in the atmosphere resulting in acid precipitation and the formation of other regional air pollutants [4].

- **Ozone layer depletion**

The ozone present in the stratosphere, at altitudes between 12 and 25 km, plays a natural equilibrium maintaining role for the earth, through absorption of ultraviolet (UV) radiation (240–320 nm) and absorption of infrared radiation [3]. A global environmental problem is the depletion of the stratospheric ozone layer which is caused by the emissions of CFCs, halons (chlorinated and brominated organic compounds) and  $\text{NO}_x$ . Ozone depletion can lead to increased levels of damaging UV radiation reaching the ground, causing increased rates of skin cancer and eye damage to humans and is harmful to many biological species. It should be noted that energy related activities are only partially (directly or indirectly) responsible depletion. The most significant role in ozone depletion have the CFCs, which are mainly used in air conditioning and refrigerating equipment as refrigerants, and  $\text{NO}_x$  emissions which are produced by the fossil fuel and biomass combustion processes, the natural denitrification and nitrogen fertilizers [4].

In 1998 the size of the ozone hole over Antarctica was 25 million  $\text{km}^2$ . It was about 3 million  $\text{km}^2$  in 1993. Researchers expect the Antarctic ozone hole to remain severe in the next 10–20 years, followed by a period of slow healing. Full recovery is predicted to occur in 2050; however, the rate of recovery is affected by the climate change [4].

- **Global climate change**

The term greenhouse effect has generally been used for the role of the whole atmosphere (mainly water vapour and clouds) in keeping the surface of the earth warm. Recently however, it has been increasingly associated with the contribution of  $\text{CO}_2$  which is estimated that contributes about 50% to the anthropogenic greenhouse effect. Additionally, several other gasses such as  $\text{CH}_4$ , CFCs, halons,

N<sub>2</sub>O, ozone and peroxyacetylnitrate (also called greenhouse gasses) produced by the industrial and domestic activities can also contribute to this effect, resulting in a rise of the earth's temperature. Increasing atmospheric concentrations of greenhouse gasses increase the amount of heat trapped (or decrease the heat radiated from the earth's surface), thereby raising the surface temperature of the earth. According to Colombo the earth's surface temperature has increased by about 0.6 8C over the last century, and as a consequence the sea level is estimated to have risen by perhaps 20 cm. These changes can have a wide range of effects on human activities all over the world [2].

## 2.6 Type of solar energy

- **PASSIVE SOLAR ENERGY**

Passive solar energy technology integrates building design with environmental factors that enable the capture or exclusion of solar energy. Mechanical devices are not used in passive solar energy applications. We illustrate passive solar energy technology by considering two simple but important examples: the roof overhang and thermal insulation [2].

- **Roof Overhang**

Sunlight that strikes the surface of an object and causes an increase in temperature of the object is an example of direct solar heat. Direct solar heating can cause an increase in temperature of the interior of buildings with windows. The windows that allow in the most sunlight are facing south in the northern hemisphere and facing north in the southern hemisphere (see Figure 2.9) illustrates two seasonal cases. The figure shows that the maximum height of the sun in the sky varies from season to season because of the angle of inclination of the earth's axis of rotation

relative to the ecliptic plane. The earth's axis of rotation is tilted  $23.5^\circ$  from a line that is perpendicular to the ecliptic plane [2].

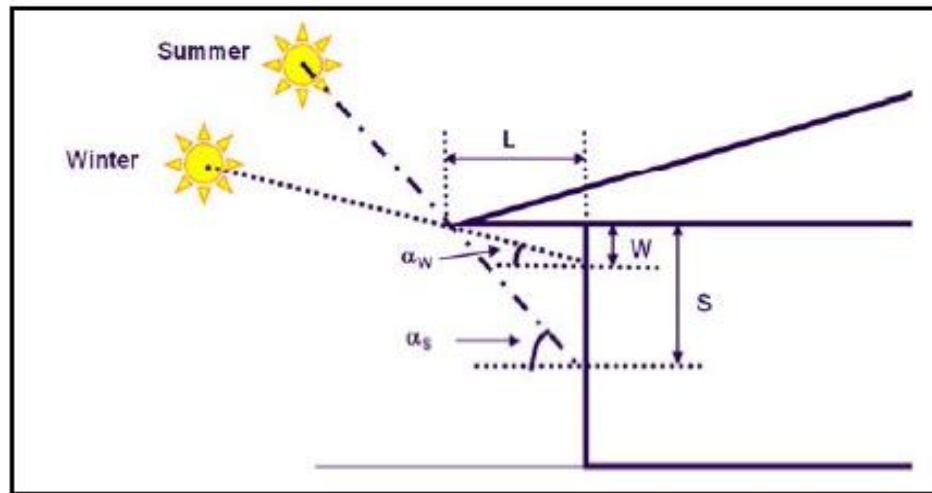


Figure 2.9 roof overhangs[2]

## Thermal Conductivity and Insulation

Solar energy may be excluded from the interior of a structure by building walls that have good thermal insulation. The quality of thermal insulation for a wall with the geometry shown in (see Figure 2.10) can be expressed in terms of thermal conductivity and thermal resistance. The rate of heat flow through the insulated wall shown in Figure 6-5 depends on wall thickness, the cross-sectional area perpendicular to the direction of heat flow, and the temperature difference between the exposed and inside faces of the wall. The rate of heat flow through the insulated wall depends on a property of the wall called thermal conductivity [2].

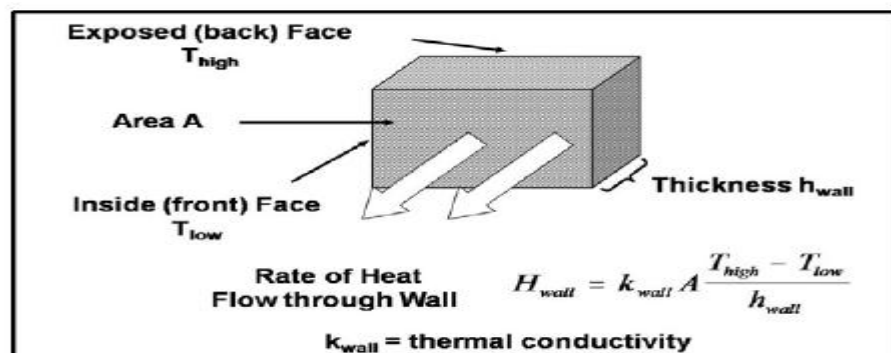


Figure 2.10 Thermal Conductivity of an Insulated Wall[2]



- **ACTIVE SOLAR ENERGY**

Active solar energy refers to the design and construction of systems that collect and convert solar energy into other forms of energy such as heat and electrical energy. Active solar energy technologies are typically energy conversion systems that are used to collect and concentrate solar energy, and convert it to a more useful form of energy such as collector, photovoltaic and PV/T systems [2].

## 2.7 application of solar energy

- **Solar Distillation system**

Water is the basic necessity for human along with food and air. There is almost no water left on Earth that is safe to drink without purification, only 1% of Earth's water is in a fresh. Solar distillation is a tried and true technology, the first "conventional" solar still plant was built in 1872 by the Swedish engineer Charles Wilson in the mining community of Las Salinas in what is now northern Chile. This still was a large basin-type still used for supplying fresh water using brackish feed water to a nitrate mining community. The plant used wooden bays which had blackened bottoms using logwood dye and alum. The total area of the distillation plant was 4,700 square meters. On a typical summer day this plant produced 4.9 kg of distilled water per square meter of still surface, or more than 23000 liters per day [3].

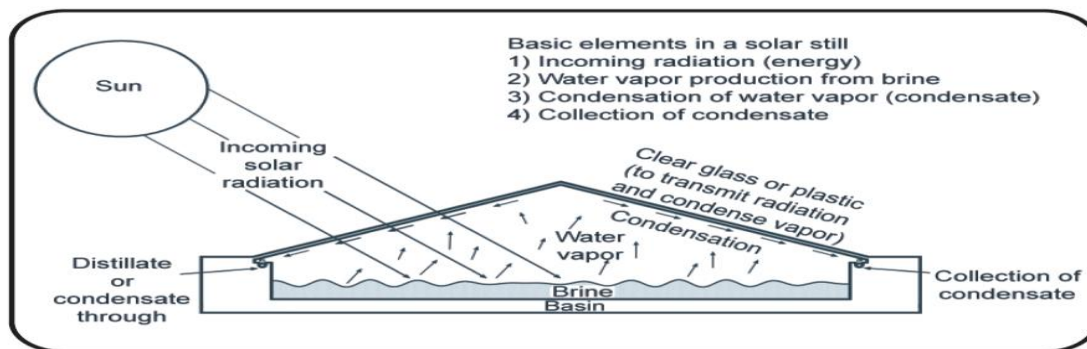


Figure 2.11 Solar Distillation[3]

- Solar Photovoltaic systems

Three most important and widely used applications of Solar PV have been considered here [5]. These are:

1. Solar home lighting systems.
2. Solar water pumping systems.
3. Solar power plants.
- 4.

## 1.Solar home lighting system

Home lighting systems are powered by solar energy using solar modules. The generated electricity is stored in batteries and used for the purpose of lighting whenever required. These systems are most widely used in non-electrified rural areas and as reliable emergency lighting system for important domestic, commercial and industrial applications (see Figure 2.12) [5].

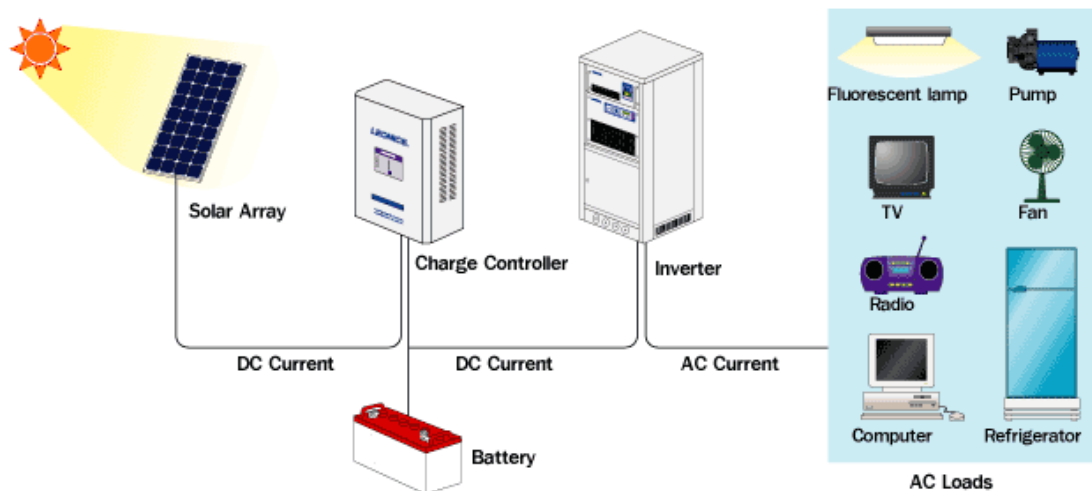


Figure 2.12 Schematic of Solar Home Lighting System[5]

## 2.solar water pumping system

These water pumping systems are powered by solar energy. It is a stand-alone system. The power generated by solar module is used for operating DC surface centrifugal mono-block pump set for lifting water from bore / open well or water reservoir for minor irrigation and drinking water purpose (see Figure 2-13). The system requires a shadow-free area for installation of the Solar Panel [5].

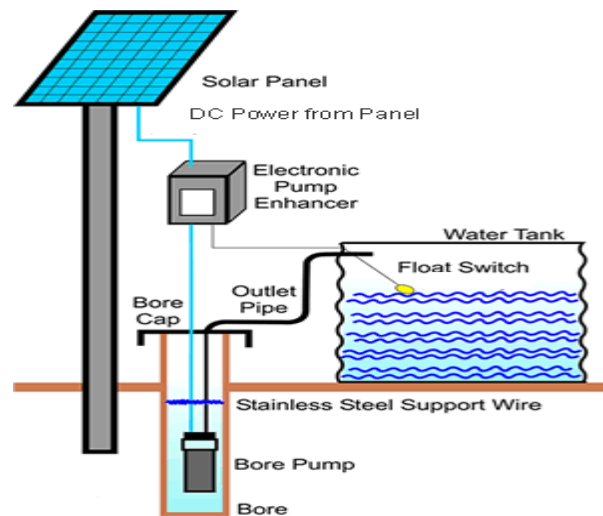


Figure 2.13 Schematic of Solar Water pumping System[5]

## 3.Solar Power Plants

Power supply in most of the cities and towns is unreliable, which has forced the people to use small generators. These generators are operated with fossil fuels like kerosene, petrol or diesel cause pollution. It also leads to increase dependence on oil imports. A solar power plant is a good option for electrification in areas that are located away from the grid line or where other sources are neither available nor can be harnessed in a techno economically viable manner. A solar power plant of the size 10–100 kW (kilowatt), depending on the load demand is preferable particularly with a liberal subsidy and low-interest soft loan from financial institutions. The idea is to raise the quality of life of the people subjected to

poverty in these areas. This coupled with low-gestation remote areas of many states that need electrification. Typical Stand alone solar power plant for the power generation comprises of Solar PV module array, Module mounting structures, Charge controller, Battery bank, Inverter and Load circuitry (see Figure 2-14) [5].



Figure 2.14 Solar Power Plants[5]

## 2.8 Solar Thermal collector

Solar energy collectors are special kind of heat exchangers that transform solar radiation energy to internal energy of the transport medium. The major component of any solar system is the solar collector. This is a device which absorbs the incoming solar radiation, converts it into heat, and transfers this heat to a fluid (usually air, water, or oil) flowing through the collector. The solar energy thus collected is carried from the circulating fluid either directly to the hot water or space conditioning equipment or to a thermal energy storage tank from which can be drawn for use at night and/or cloudy days [4].

There are basically two types of solar collectors:

- Non-concentrating or stationary.
- Concentrating.

A Non-concentrating collector has the same area for intercepting and for absorbing solar radiation, whereas a sun-tracking concentrating solar collector usually has concave reflecting surfaces to intercept and focus the sun's beam radiation to a smaller receiving area, thereby increasing the radiation flux. A large number of solar collectors are available in the market [4].

Table 2.2 acomprehensive list[4]

<b>Motion</b>	<b>Collector type</b>	<b>Absorber type</b>	<b>Concentration ratio</b>	<b>temperature range (C)</b>
<b>Stationary</b>	Flat plate collector (FPC)	Flat	1	30-80
	Evacuated tube collector (ETC)	Flat	1	50-200
	Compound parabolic collector (CPC)	Tubular	1-5	60-240
<b>Single-axis tracking</b>	Linear Fresnel reflector (LFR)	Tubular	10-40	60-250
	Parabolic trough collector (PTC)	Tubular	15-45	60-300
	Cylindrical trough collector (CTC)	Tubular	10-50	60-300
<b>Two-axes tracking</b>	Parabolic dish reflector (PDR)	Point	100-1000	100-500
	Heliostat field collector (HFC)	Point	100-1500	150-2000

## 2.8.A Non-concentrating or stationary collector

Solar energy collectors are basically distinguished by their motion, i.e. stationary, single axis tracking and two axes tracking, and the operating temperature. Initially, the stationary solar collectors are examined. These collectors are permanently fixed in position and do not track the sun [4]. Three types of collectors fall in this category:

Flat plate collectors (FPC).

Stationary compound parabolic collectors (CPC).

Evacuated tube collectors (ETC).

- Flat-plate collectors (FPC)

A typical flat-plate solar collector is shown in (Figure2-15 ).When solar radiation passes through a transparent cover and impinges on the blackened absorber surface of high absorptivity, a large portion of this energy is absorbed by the plate and then transferred to the transport medium in the fluid tubes to be carried away for storage or use. The underside of the absorber plate and the side of casing are well insulated to reduce conduction losses. The liquid tubes can be welded to the absorbing plate, or they can be an integral part of the plate. The liquid tubes are connected at both ends by large diameter header tubes. The transparent cover is used to reduce convection losses from the absorber plate through the restraint of the stagnant air layer between the absorber plate and the glass. It also reduces radiation losses from the collector as the glass is transparent to the short wave radiation received by the sun but it is nearly opaque to long-wave thermal radiation emitted by the absorber plate (greenhouse effect). FPC is usually permanently fixed in position and requires no tracking of the sun. The collectors should be oriented directly towards the equator, facing south in the northern hemisphere and north in the southern. The optimum tilt angle of the collector is equal to the latitude of the location with angle variations of 10–15° more or less depending on the application [4].

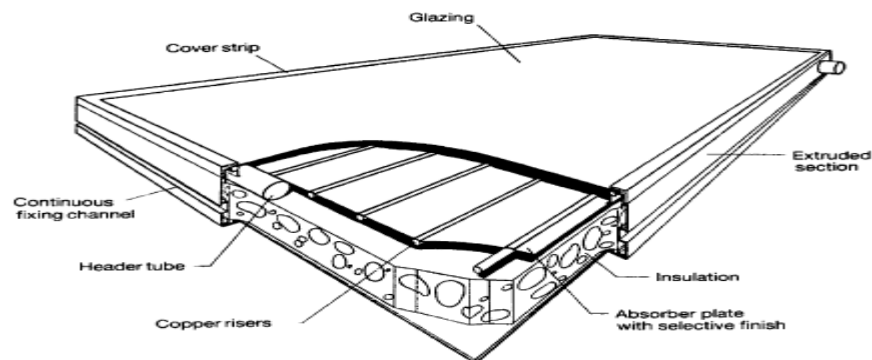


Figure2.15 pictorial view of a flat plate collector.

- Compound parabolic collectors (CPC)

CPC are non-imaging concentrators. These have the capability of reflecting to the absorber all of the incident radiation within wide limits. The necessity of moving the concentrator to accommodate the changing solar orientation can be reduced by using a trough with two sections of a parabola facing each other. Compound parabolic concentrators can accept incoming radiation over a relatively wide range of angles. By using multiple internal reflections, any radiation that is entering the aperture, within the collector acceptance angle, finds its way to the absorber surface located at the bottom of the collector. The absorber can take a variety of configurations [4].

It can be cylindrical or flat. In the CPC (see Figure2-16) the lower portion of the reflector (AB and AC) is circular, while the upper portions (BD and CE) are parabolic. As the upper part of a CPC contribute little to the radiation reaching the absorber, they are usually truncated thus forming a shorter version of the CPC, which is also cheaper. CPCs are usually covered with glass to avoid dust and other materials from entering the collector and thus reducing the reflectivity of its walls [4].

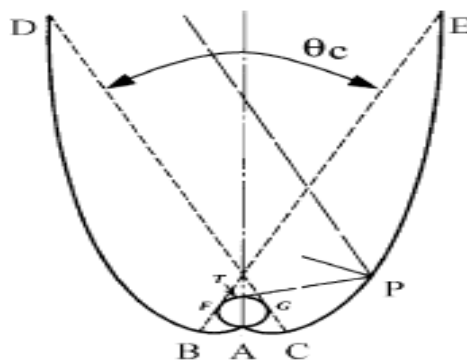


Figure2.16 Schematic diagram of a compound parabolic collector[4]

- **Evacuated tube collectors (ETC)**

Evacuated heat pipe solar collectors (tubes) operate differently than the other collectors available on the market. These solar collectors consist of a heat pipe inside a vacuum-sealed tube (see Figure 2-17). ETC has demonstrated that the combination of a selective surface and an effective convection suppressor can result in good performance at high temperatures. The vacuum envelope reduces convection and conduction losses, so the collectors can operate at higher temperatures than FPC. Like FPC, they collect both direct and diffuse radiation. However, their efficiency is higher at low incidence angles. This effect tends to give ETC an advantage over FPC in day-long performance. ETC use liquid vapour phase change materials to transfer heat at high efficiency. These collectors feature a heat pipe (a highly efficient thermal conductor) placed inside a vacuum-sealed tube. The pipe, which is a sealed copper pipe, is then attached to a black copper fin that fills the tube (absorber plate). Protruding from the top of each tube is a metal tip attached to the sealed pipe (condenser). The heat pipe contains a small amount of fluid (e.g. methanol) that undergoes an evaporating condensing cycle. In this cycle, solar heat evaporates the liquid, and the vapour travels to the heat sink region where it condenses and releases its latent heat. The condensed fluid returns back to the solar collector and the process is repeated. When these tubes are mounted, the metal tips up, into a heat exchanger (manifold). Water, or glycol, flows through the manifold and picks up the heat from the tubes. The heated liquid circulates through another heat exchanger and gives off its heat to a process or to water that is stored in a solar storage tank. The advantage of this design is that it is made entirely of glass and it is not necessary to penetrate the glass envelope in order to extract heat from the tube thus leakage losses are not present and it is also less expensive than the single envelope system [4].



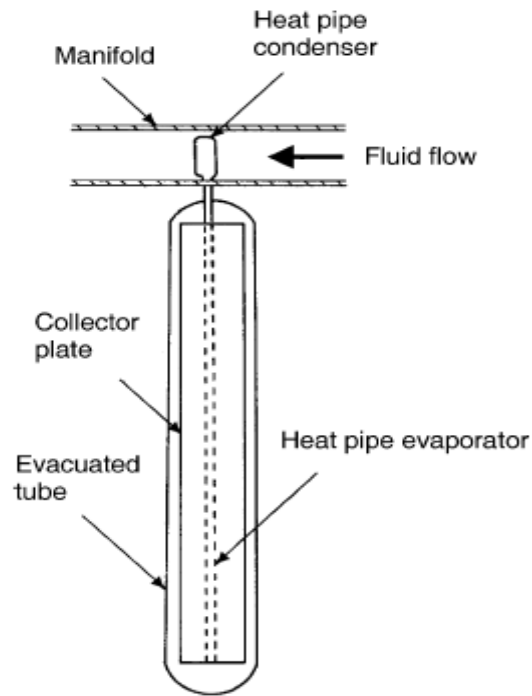


Figure 2.17 schematic diagram of an evacuated tube collector[4]

## 2.8.B Concentrating systems

In concentrating collectors solar energy is optically concentrated before being transferred into heat. Concentration can be obtained by reflection or refraction of solar radiation by the use of mirrors or lens. The reflected or refracted light is concentrated in a focal zone, thus increasing the energy flux in the receiving target. Concentrating collectors can also be classified into non-imaging and imaging depending on whether the image of the sun is focused at the receiver or not. The concentrator belonging in the first category is the CPC whereas all the other types of concentrators belong to the imaging type [4]. The collectors falling in this category are:

- linear Fresnel reflector (LFR)

LFR technology relies on an array of linear mirror strips which concentrate light on to a fixed receiver mounted on a linear tower. The LFR field can be imagined as a broken-up parabolic trough reflector large absorbers can be constructed and the absorber does not have to move (see Figure 2-18). The greatest advantage of this type of system is that it uses flat or elastically curved reflectors which are cheaper compared to parabolic glass reflectors. Additionally, these are mounted close to the ground, thus minimizing structural requirements [4].

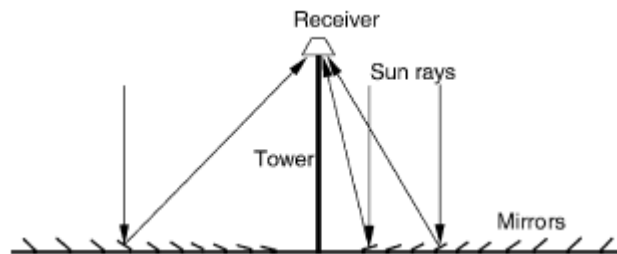


Figure 2.18 Schematic diagram of a downward facing receiver illuminated from an LFR field[4]

The first to apply this principle was the great solar pioneer Giorgio Francia who developed both linear and two-axis tracking Fresnel reflector systems at Genoa, Italy in the 60th. These systems showed that elevated temperatures could be reached using such systems but he moved on to two-axis tracking, possibly because advanced selective coatings and secondary optics were not available. One difficulty with the LFR technology is that avoidance of shading and blocking between adjacent reflectors leads to increased spacing between reflectors. Blocking can be reduced by increasing the height of the absorber towers, but this increases cost [4]. Compact linear Fresnel reflector (CLFR) technology has been recently developed at Sydney University in Australia. This is in effect a second type of solution for the Fresnel reflector field problem which has been overlooked until recently. In this design adjacent linear elements can be interleaved to avoid shading. The classical LFR system has only one receiver, and there is no choice

about the direction and orientation of a given reflector. However, if it is assumed that the size of the field will be large, as it must be in technology supplying electricity in the MW class, it is reasonable to assume that there will be many towers in the system. If they are close enough then individual reflectors have the option of directing reflected solar radiation to at least two towers (see Figure 2-20). This additional variable in the reflector orientation provides the means for much more densely packed arrays, because patterns of alternating reflector orientation can be such that closely packed reflectors can be positioned without shading and blocking. The interleaving of mirrors between two receiving towers is shown in Fig. 10. The arrangement minimizes beam blocking by adjacent reflectors and allows high reflector densities and low tower heights to be used [4].

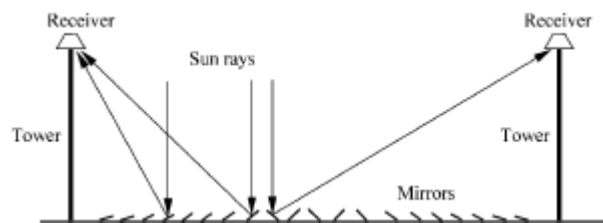


Figure 2.19 Schematic diagram showing interleaving of mirrors in a CLFR with reduced shading between mirrors[4]

- parabolic dish

A parabolic dish reflector is a point-focus collector that tracks the sun in two axes, concentrating solar energy onto a receiver located at the focal point of the dish. The dish structure must track fully the sun to reflect the beam into the thermal receiver, so as the collector is tracked in two axes (see Figure 2-20) [4].

The receiver absorbs the radiant solar energy, converting it into thermal energy in a circulating fluid. The thermal energy can then either be converted into electricity using an engine-generator coupled directly to the receiver, or it can be transported through pipes to a central power-conversion system. Parabolic-dish systems can

achieve temperatures in excess of 1500 C. Because the receivers are distributed throughout a collector field, like parabolic troughs, parabolic dishes are often called distributed-receiver systems [4].

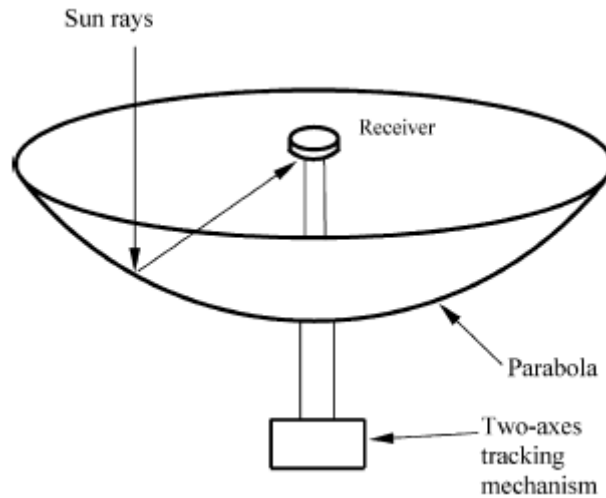


Figure 2.20 Schematic of a parabolic dish collector[4]

Parabolic dishes have several important advantages [4]:-

Because they are always pointing the sun, they are the most efficient of all collector systems;

They typically have concentration ratio in the range of 600–2000, and thus are highly efficient at thermal-energy absorption and power conversion systems;

They have modular collector and receiver units that can either function independently or as part of a larger system of dishes.

The main use of this type of concentrator is for parabolic dish engines. A parabolic dish-engine system is an electric generator that uses sunlight instead of crude oil or coal to produce electricity. The major parts of a system are the solar dish concentrator and the power conversion unit. Systems that employ small generators at the focal point of each dish provide energy in the form of electricity rather than as heated fluid. The power conversion unit includes the thermal receiver and the heat engine. The thermal receiver absorbs the concentrated beam of solar energy, converts it to heat, and transfers the heat to the heat engine. A thermal receiver can

be a bank of tubes with a cooling fluid circulating through it. The heat transfer medium usually employed as the working fluid for an engine is hydrogen or helium. Alternate thermal receivers are heat pipes wherein the boiling and condensing of an intermediate fluid is used to transfer the heat to the engine. The heat engine system takes the heat from the thermal receiver and uses it to produce electricity [4]. The engine-generators have several components; a receiver to absorb the concentrated sunlight to heat the working fluid of the engine, which then converts the thermal energy into mechanical work; an alternator attached to the engine to convert the work into electricity, a Waste heat exhaust system to vent excess heat to the atmosphere, and a control system to match the engine's operation to the available solar energy. This distributed parabolic dish system lacks thermal storage capabilities, but can be hybridized to run on fossil fuel during periods without sunshine. The Sterling engine is the most common type of heat engine used in dish-engine systems. Other possible power conversion unit technologies that are evaluated for future applications are micro turbines and concentrating photovoltaic [4].

- **Heliostat field collector**

For extremely high inputs of radiant energy, a multiplicity of flat mirrors, or heliostats, using altazimuth mounts, can be used to reflect their incident direct solar radiation onto a common target as (see Figure 2.21). This is called the heliostat field or central receiver collector. By using slightly concave mirror segments on the heliostats, large amounts of thermal energy can be directed into the cavity of a steam generator to produce steam at high temperature and pressure [4].

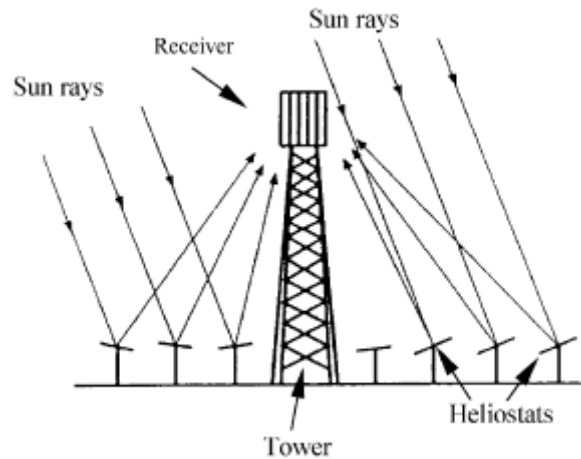


Figure 2.21 Schematic of central receiver system[4]

The concentrated heat energy absorbed by the receiver is transferred to a circulating fluid that can be stored and later used to produce power [4]. Central receivers have several advantages:

They collect solar energy optically and transfer it to a single receiver, thus minimizing thermal-energy transport requirements.

They typically achieve concentration ratios of 300–1500 and so are highly efficient both in collecting energy and in converting it to electricity;

They can conveniently store thermal energy;

They are quite large (generally more than 10 MW) and thus benefit from economies of scale.

Each heliostat at a central-receiver facility has from 50 to 150 m<sup>2</sup> of reflective surface. The heliostats collect and concentrate sunlight onto the receiver, which absorbs the concentrated sunlight, transferring its energy to a heat transfer fluid. The heat-transport system, which consists primarily of pipes, pumps, and valves, directs the transfer fluid in a closed loop between the receiver, storage, and power-conversion systems [4].

The average solar flux impinging on the receiver has values between 200 and 1000 kW/m<sup>2</sup>. This high flux allows working at relatively high temperatures of more than 1500 °C and to integrate thermal energy in more efficient cycles. Central receiver systems can easily integrate in fossil-fuelled plants for hybrid operation in a wide variety of options and have the potential to operate more than half the hours of each year at nominal power using thermal energy storage [4].

- parabolic trough collector

In order to deliver high temperatures with good efficiency a high performance solar collector is required. Systems with light structures and low cost technology for process heat applications up to 400 °C could be obtained with parabolic through collectors (PTCs). PTCs can effectively produce heat at temperatures between (50 and 400 °C). PTCs are made by bending a sheet of reflective material into a parabolic shape. A metal black tube, covered with a glass tube to reduce heat losses, is placed along the focal line of the receiver (see Figure 2-22) when the parabola is pointed towards the sun parallel rays incident on the reflector are reflected onto the receiver tube. It is sufficient to use a single axis tracking of the sun and thus long collector modules are produced. The collector can be orientated in an east–west direction, tracking the sun from north to south, or orientated in a north–south direction and tracking the sun from east to west. The advantages of the former tracking mode is that very little collector adjustment is required during the day and the full aperture always faces the sun at noon time but the collector performance during the early and late hours of the day is greatly reduced due to large incidence angles (cosine loss). North–south orientated troughs have their highest cosine loss at noon and the lowest in the mornings and evenings when the sun is due east or due west.

Over the period of one year a horizontal north–south trough field usually collects slightly more energy than a horizontal east–west one. Therefore the choice of orientation usually depends on the application and whether more energy is needed during summer or during winter [4].

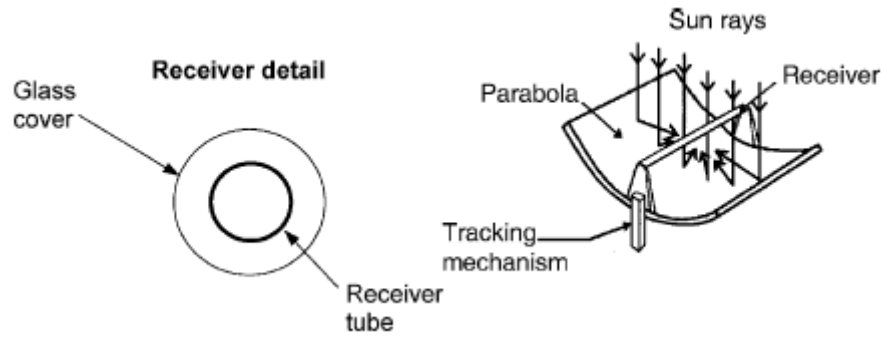


Figure 2.22 Schematic of a parabolic trough collector[4]

Parabolic trough technology is the most advanced of the solar thermal technologies because of considerable experience with the systems and the development of a small commercial industry to produce and market these systems. PTCs are built in modules that are supported from the ground by simple pedestals at either end. The biggest application of this type of system is the Southern California power plants, known as solar electric generating systems (SEGS) which have a total installed capacity of 354MW [4].

## 2.9 Definition of PTC

Parabolic trough collectors are made by bending a sheet of reflective material into a parabolic shape. A black metal tube, covered with a glass tube to reduce heat losses, is placed along the focal line of the receiver (see Figure 3.13). When the parabola is pointed toward the sun, parallel rays incident on the reflector are reflected onto the receiver tube. The concentrated radiation reaching the receiver tube heats the fluid that circulates through it, thus transforming the solar radiation into useful heat [9].



## 2.10 Power plant components

The energy flow in a parabolic trough power plant has the following structure: Direct solar radiation is concentrated and converted into thermal energy. The thermal energy is converted into pressure energy of vapour, which is converted into kinetic energy. The kinetic energy is finally transformed into electrical energy, the final product of the power plant. These energy conversion steps are realized in the respective power plant components: The parabolic trough collector and the tracking system are essential for the concentration process (see Figure 3.1). The receiver converts the radiation energy into thermal energy. Heat transfer medium and thermal storage are carriers of the thermal energy. The steam generator has the function to convert the thermal energy into pressure energy of a gaseous medium. This is done by the evaporation of water. The cooling system has the aim to complete the liquid/gaseous-cycle converting the steam back to water. The steam turbine converts the pressure energy in the steam into rotational energy. The electric generator, finally, converts the rotational energy into electric energy, which can be supplied to the electric grid [9].

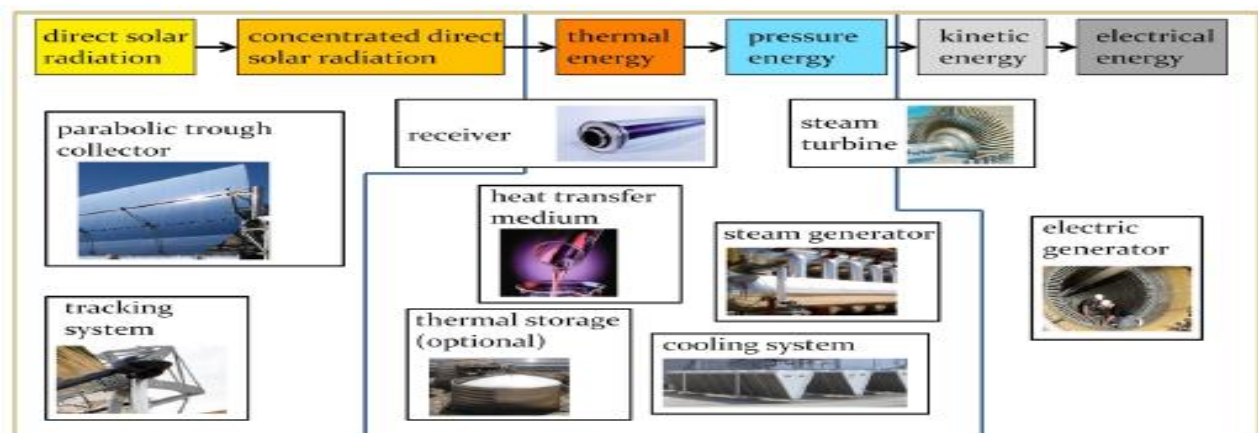


Figure 2.23 Energy conversion chain in a parabolic trough power plant and corresponding plant components[9]

## 2.11 parabolic trough collector

### 2.11.A Collector geometry

The collector, the parabolic trough, is a trough the cross-section of which has the shape of a part of a parabola. More exactly, it is a symmetrical section of a parabola around its vertex. Parabolic troughs have a focal line, which consists of the focal points of the parabolic cross-sections. Radiation that enters in a plane parallel to the optical plane is reflected in such a way that it passes through the focal line (see Figure 2.23-2.24). A proof of the existence of a focal point is presented in the annex. An appropriate analytic representation of a parabola is

$$Y = \frac{1}{4 \cdot f} \cdot x^2$$

Where  $f$  is the focal length the distance between the vertex of the parabola and the focal point [9].

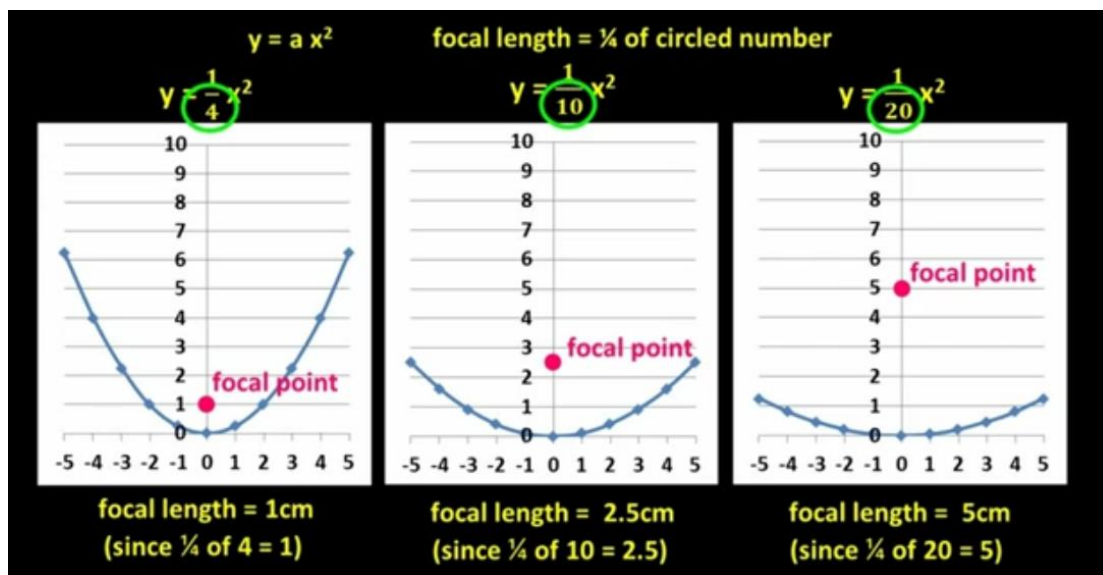


Figure 2.24 focal length of parabolic shape[9]

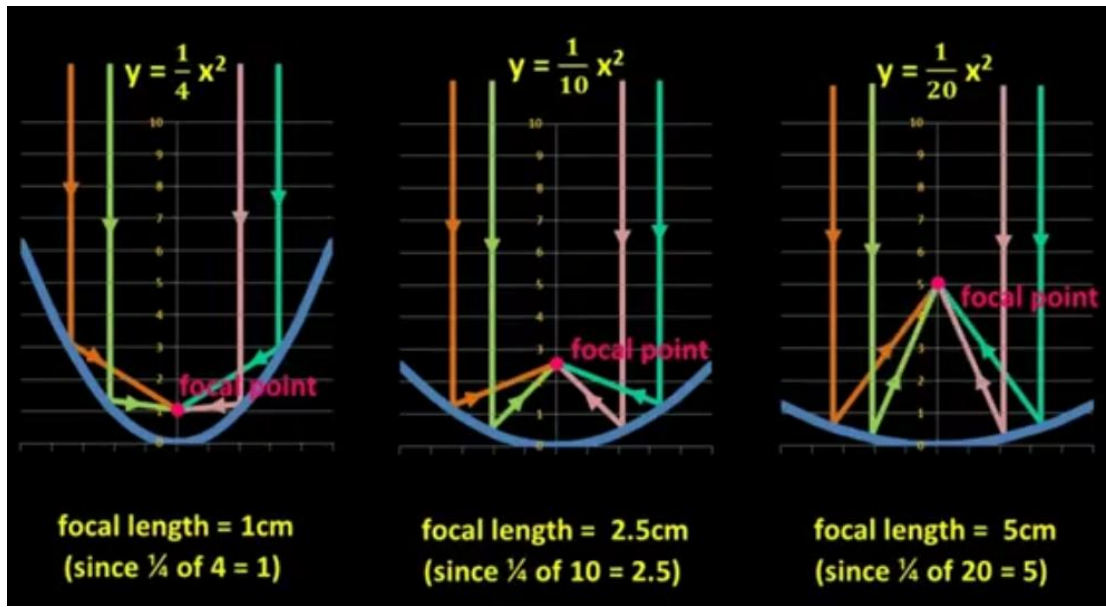


Figure 2.25 paths of parallel rays at a parabolic mirror[9]

## 2.11.B Parameters for the parabolic trough geometry

The following four parameters are commonly used to characterize the form and size of a parabolic trough (see Figure 3.4): trough length, focal length, aperture width which is the distance between one rim and the other, and rim angle which is the angle between the optical axis and the line between the focal point and the mirror rim [9].

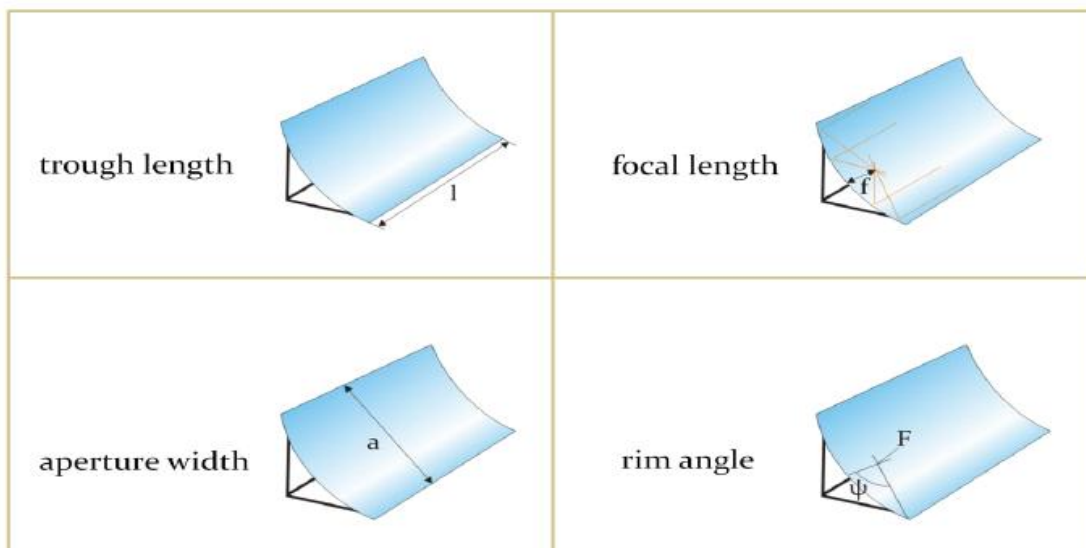


Figure 2.26 Geometrical parabolic trough parameters[9]

The rim angle is related to the distance between the different parts of the mirrors and the focal line (see Figure 2.26). The rim angle is a very important constructive trait of collectors. For instance, it has an effect on the concentration ratio and on the total irradiance per meter absorber tube [W/m].

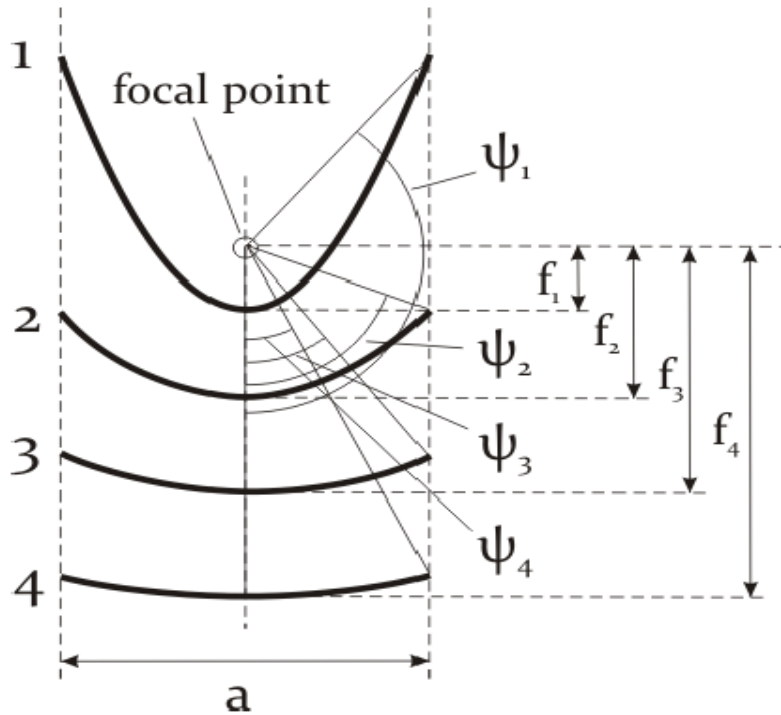


Figure 2.27 Relation between the focal length and the rim angle for a constant trough aperture width.

Qualitatively, we can understand in the following way that there must be some ideal rim angle range and that it should neither be too small nor too large. Taking a fixed aperture width will represent this relation:

If the rim angle is very small, then the mirror is very narrow and it is obvious that a broader mirror (with a larger rim angle) would enhance the power projected onto the absorber tube. If the rim angle is very big, then the way of the reflected radiation from the outer parts of the mirror is very long and the beam spread is very big, hence reducing the concentration ratio. A mirror with a smaller rim angle and the same aperture width would permit a higher concentration ratio.

Additionally, if we consider real mirrors with a certain degree of geometrical inexactness, then it is important to maintain a low distance to the absorber also because the effect of these geometrical mirrors errors. The larger distance to the absorber, the more weight carries the radiation aberration due to mirror slope errors (see Figure 2.28).

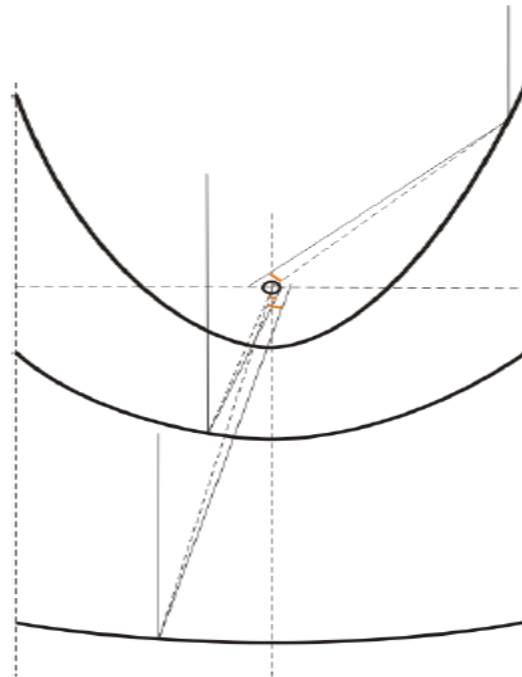


Figure 2.28 Effects of slope errors in dependence on the rim angle[9]

Last but not least there is an economical aspect that limits the reasonable rim angle:

At high rim angles the outer parts have a low contribution to the energy yield in relation to the mirror area. That means a high investment is necessary, which contributes only little to the energy yield [9].

### 2.11.C geometrical Concentration ratio

It is defined as the ratio of the collector aperture area to the receiver aperture area [9].

$$CG = \frac{A_{ap.c}}{A_{ap.r}}$$

CG	≡	geometrical Concentration ratio	
$A_{ap,r}$	≡	receiver aperture area	$m^2$
$A_{ap,c}$	≡	collector aperture area	$m^2$

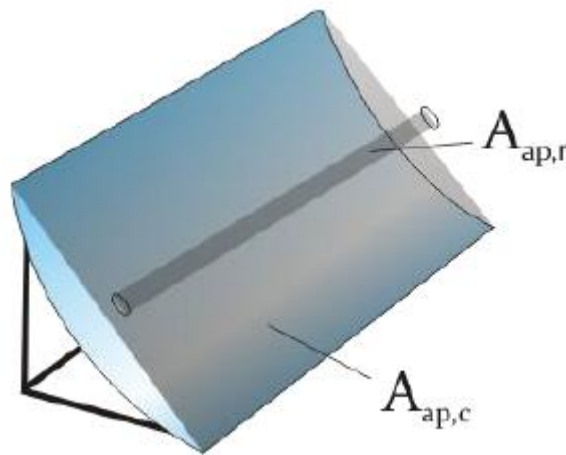


Figure 2.29 Collector aperture area and receiver aperture area[9]

### 2.11.D Mirror material

The main requirements for appropriate mirror materials are their reflective properties, which is a number that indicates the fraction of the incident radiation that is reflected by the surface. The reflectivity must be high. In general, the reflectivity is different for different wavelengths so that it has to be specified for a given wavelength or a given wavelength range, for instance for the visible light range. In the case of solar applications, the solar spectrum is of interest. There is a lot of type of mirrors used in power plants such as:

## 2.11.D1 Silver coated glass mirrors

The most common parabolic mirrors today consist of silver coated glass mirrors. Indeed, all realized commercial parabolic trough power plants use them. There are experiences with these mirrors since the first parabolic trough power plants were built in the 1980s. The mirrors have proven to be durable. Even after more than ten years of operation they hardly showed any decrease in specular reflectivity [9].



Figure 2.30 mounting of a parabolic trough with silver coated glass mirror[9]

The glass for the mirror facets is normally manufactured with the float glass method where the molten glass flows continuously on a bath of liquid tin. This method guarantees a very high evenness of the manufactured glass. Low-iron glass is used to increase the light transmission in the solar spectrum. After the glass is cut to the right size and got grinded, it is formed to the parabolic form in an oven. One possibility is to form the glass on a mould using its own weight. Another



possibility is to press it to achieve the desired parabolic form. (See Figure 2.31) it shows the high reflectivity of silver in the solar spectrum range [9].

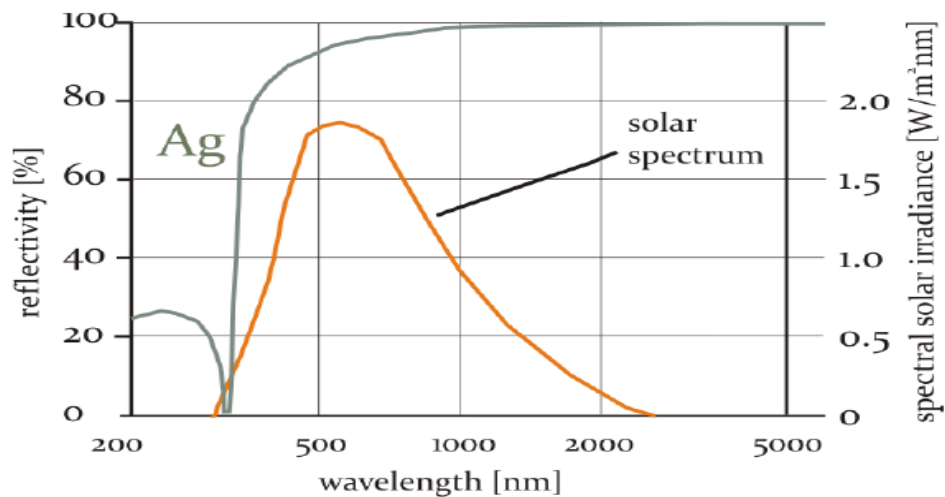


Figure 2.31 reflectivity of silver[9]

The mirrors have a multilayered structure. The first layer below the glass is the reflective layer. A protective copper layer is applied next to the silver layer, on which three epoxy varnishes are added: a prime coat, intermediate and protective top coat (see Figure 2.32). In most solar mirrors that were applied until now the first and second coat contain a certain percentage of lead, but protection layers without copper and lead are in development. The thickness of the complete mirror amounts to 4 to 5 mm. And the reflectivity of multilayered mirror is 93.5%

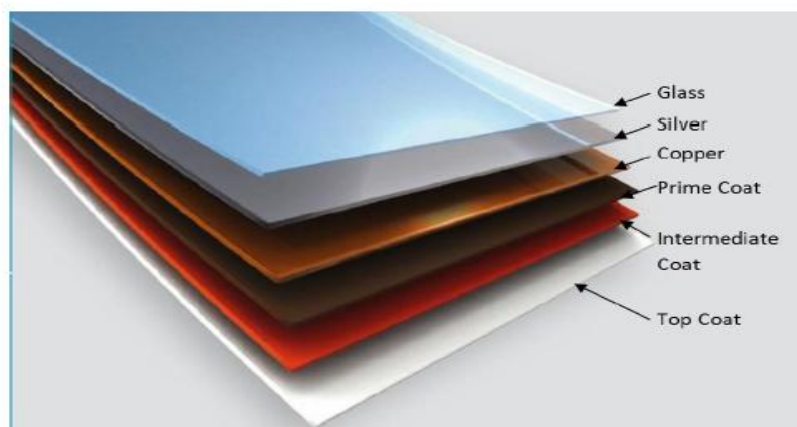


Figure 2.32 multilayered mirrors[9]



## 2.11.D2 silver coated polymer film

In the 1990s, NREL developed a silver coated polymer film as reflector material for solar applications. Its commercial name is now ReflecTech. It is a rollable reflective film that can be applied to any smooth non porous material. It is made out of multiple polymer layers with a reflective silver layer. Mirrors with ReflecTech have been tested since 2002 in the SEGS plants in California. Until now they did not show any decrease of reflectivity. It is claimed that ReflecTech offers a considerable economic advantage compared to glass mirrors. The mirror manufacturing process and the assembling process of the collector could be accelerated. Flexible facets could be put in a guide rail with a parabolic form (see Figure 2.34). An advantage is that the mirrors are not susceptible to breakage. The company Skyfuel, which commercializes the ReflecTech technology, indicates the reflectivity to be 94% [9].



Figure 2.33 reflectech film[9]

## 2.11.E Bearing structure

The bearing structure of a parabolic trough has the function to carry the mirrors in the right position, to give stability to the troughs and to allow an exact Sun tracking. In order to comply with these functions, the structures have to fulfill some construction requirements. In particular, the stiffness requirements are very high, because any deviation from the ideal parabolic collector shape causes losses in the optical efficiency of the system. It is important that the parabolic troughs are neither deformed by their own weight nor by wind loads. The aperture area represents a large area that is exposed to the wind so that the resulting wind loads are considerable. The collector has to be constructed in such a way that it withstands these loads with only very small geometrical deviations [9]. Additionally, a high stiffness allows longer troughs so that the number of pylons and tracking units can be reduced, which reduces costs. The stiffness must be combined with lightweight constructions, which allow the usage of weaker foundations and tracking mechanisms. A light construction is also less prone to deformations due to the own weight. Also light structures reduce the energy demand for the collector tracking. Generally, the bearing structure of a collector consists of a main body, which in most cases is a space frame or tube structure made out of steel or aluminum [9]. Only in the case of the mentioned Solarlite collector, the central body is made out of non-metallic materials. Further elements of the bearing structure are:

Mirror support points on the space frame structure or on special cantilever arms.

Receiver support, also called heat collection element (HCE) support.

Structure for the mounting to the pylons.

These elements are found, for example, in the Euro trough collector (see Figures 2.35-2.36) it show a photo of the main collector body and a schematic representation of the collector components.



Figure 2.34 Space frame structure of a Euro trough collector module [9]

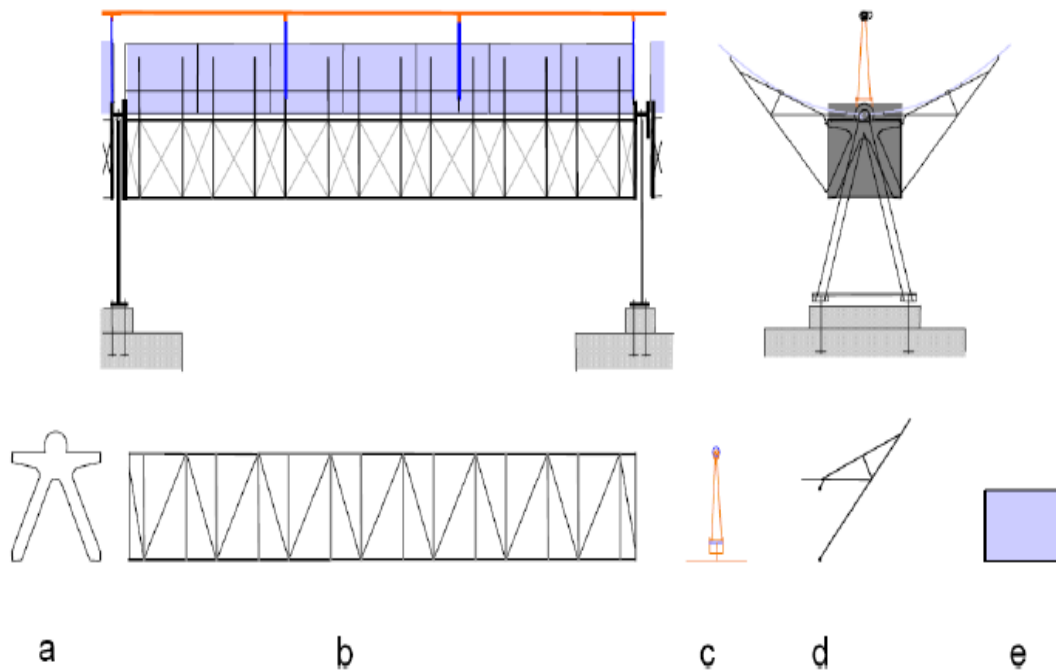


Figure 2.35 schematic of Euro trough module structural elements: (a) front and rear endplates for mounting to the pylons, (b) space frame structure, (c) receiver supports, (d) cantilever arm, (e) mirror facet [9]

An overview of some types of parabolic trough collectors and their technical data is given in the following table [9]:

Table 2.3 types of parabolic trough collectors and their technical data[9]

Collector	LS-2	LS-3	Euro trough	ENEA	SGX-2	Sener trough	Helio trough	Skytrough
<b>Bearing structure</b>	Torque tube	V-truss	Torque box	Torque tube	Aluminum space frame	Torque tube	Torque tube	Aluminum space frame
<b>Year</b>	1985	1989	2002	2004	2005	2005	2009	2010
<b>Aperture [m]</b>	5	5.7	5.76	5.76	5.77	5.76	6.77	6
<b>Module length [m]</b>	12	12	12	12.5	12	12	19.1	14
<b>Rim angle [°]</b>	80	80	80	77	80	80	89.5	82.5
<b>Focal length [m]</b>	1.49	1.71	1.71	1.8	-	1.7	1.71	1.71
<b>Geometric concentration ratio</b>	71	82	82	75-80	82	80	76	75
<b>Absorber tube diameter [m]</b>	0.07	0.07	0.07	0.07	0.07	0.07	0.09	0.08
<b>References</b>	SEGS	SEGS	SEGS 5, Andasol 1	Archimedes power plant/ Italy	Nevada	Extresol 1,2	Test loop SEGS	Test loop SEGS

## 2.11.F Receiver

Receivers for parabolic trough power plants have the task to convert the radiation into heat and to transport the heat to the pipes, which leads it further to the power block [9]. A constructive challenge is the heat expansion of the receiver due to the changing temperatures between operation and non-operating state. It has also to be taken into account that the receivers in a parabolic trough power plant are moveable parts which require flexible pipe connections. The receiver has to fulfill several geometrical and physical requirements. The reflected radiation has to hit the absorber surface, which implies geometric constraints. The radiation has to be converted as completely as possible into heat and the optical and thermal losses at the surfaces of the receiver components should be as small as possible [9].

Parabolic trough power plant receivers are produced by the German Schott AG, the Italian Archimede Solar Energy (ASE) and the German Siemens AG, which acquired in 2009 the Israeli company Solel Solar Systems that had developed a receiver. Schott and Siemens receivers use thermo oil as heat transfer fluid (see Figure 2.37-2.38). Therefore the receivers are designed for an operation temperature of 400°C. Siemens receivers are also used in the first direct steam generating plants. Archimede, on the other hand, developed a receiver for molten salt as heat transfer fluid (see Figure 2.39). It is designed for a maximum operation temperature of 580°C [9].



Figure 2.36 Schott PTR 70 [9]



figure 2.37 Siemens UVAC 2010[9]

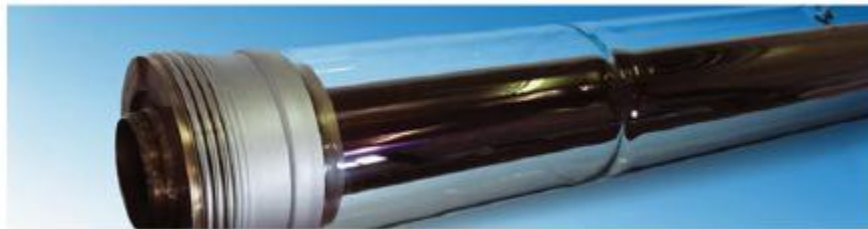


Figure 2.38 Archimede HEMS08[9]

## 2.11.F1 Receiver components

The receiver has to be constructed in such a way that high radiation absorption and low thermal losses are realized. Low thermal losses refer to low irradiative losses as well as low convective and conductive losses. In the following we will describe how and with which components the receiver fulfils these functional requirements (see Figure 3.17). We will refer to the absorber tube, the evacuated glass tube and a group of further specific constructive elements [9].



Figure 2.39 Structure of a parabolic trough receiver[9]

## 2.11.F2 Absorber tube

In order to reach high radiation absorption and a low heat loss at the absorber tube, its absorptance must be high in the visible light range and its emissivity must be low in the infrared range. Remember that the absorptance and the emissivity of a body for a specific spectral range are always identical from (Kirchhoff's law):

$$\alpha_{\lambda} = \varepsilon_{\lambda}$$

$\alpha_{\lambda} \equiv$  spectral absorptance

$\varepsilon_{\lambda} \equiv$  emissivity (in specific spectral range)

$\lambda \equiv$  wavelength

For different spectral ranges, absorptance and emissivity can be (and normally are) different. In the case of the absorber tube, the absorptance must be high for one spectral range, the solar spectral range ( $250\text{nm} \leq \lambda \leq 2500\text{nm}$ ), and the emissivity must be low for another spectral range, the infrared range ( $3000\text{nm} \leq \lambda \leq 50000\text{nm}$ ). This is physically possible so special selective coatings have been developed to reach this. Selective coatings for the absorber tubes are made of cermet, which is a material that consists of metallic nano-particles that are embedded in a ceramic matrix. (The combination of ceramic (cer) and metallic materials (met) motivates the name “cermet”.)

More exactly, the coating consists of different layers. First, there is a reflection layer made out of a metal that is highly reflective in the infrared range, for instance copper, aluminum or molybdenum. Second there is the cermet layer, which itself can be divided into different layers with higher and lower metal content (see Figure 2.41). The cermet layer consists of an oxide like  $\text{Al}_2\text{O}_3$  or  $\text{SiO}_2$  and a metal like molybdenum. The antireflection ceramic layer consists of oxides like  $\text{Al}_2\text{O}_3$  or  $\text{SiO}_2$  [9].

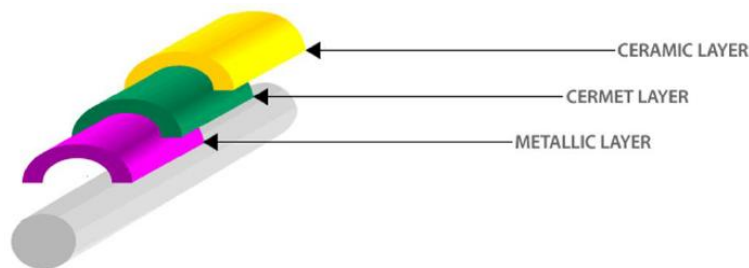


Figure 2.40 Multi-layer coating of the absorber tube[9]

An absorptance of 0.95 (Schott, Archimede) or even 0.96 (Siemens) for the solar radiation have been reached, and an emissivity of 0.1 (Schott, Archimede) or even 0.09 (Siemens) for the thermal radiation at  $400^\circ\text{C}$ . Archimede indicates additionally an emissivity of less than 0.15 at  $580^\circ\text{C}$  for the molten salt receivers, which are designed to resist higher temperatures than the therm0 oil systems of Schott and Siemens [9].

## 2.11.F3 Glass tube

In order to reach a low convective (and also conductive) heat loss, the absorber tube is protected with a glass sheath around it, which hinders the air to flow around the hot absorber tube. Additionally, the glass body is evacuated so that the convective and conductive heat loss is reduced further. Schott indicates a remaining gas pressure of  $\leq 10^{-3}$  mbar, Archimede even of  $\leq 10^{-4}$  mbar. The transmittance of the glass tubes, which are made out of borosilicate glass, is indicated to be at least 0.96 for the solar radiation. A special antireflective coating guarantees a low reflectivity of the glass sheath. Archimede indicates that this coating increases the transmittance by 0.04 (from 0.92 without coating to the mentioned 0.96 with coating) [9]. The glass material has quite a low transmittance in the infrared range. This also contributes slightly to the insulation effect because a part of the emitted thermal radiation of the absorber tube is maintained in the system: It heats the glass, reduces thereby the convective heat loss from the absorber to the glass tube and generates additional thermal radiation back onto the absorber tube (see Figure 2.42). It illustrates the transmittance of borosilicate glass [9].

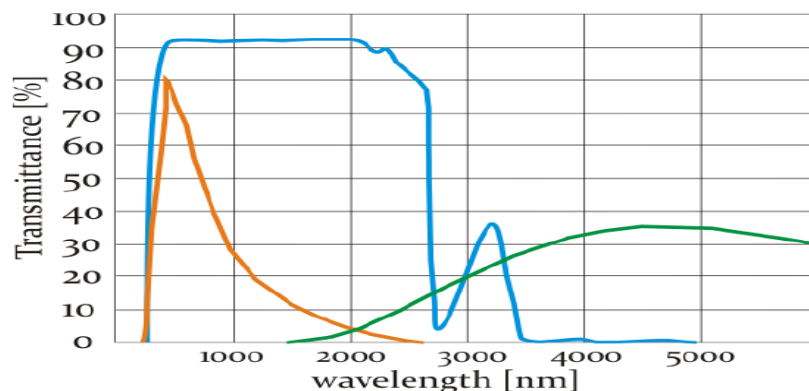


Figure 2.41 Transmittance of borosilicate glass without antireflective coating (blue line)

Solar spectrum (orange line)

Thermal radiation at about 380 °C (green line) [9]



## 2.11.F4 Further important receiver components

The temperature changes of the absorber tube require that it is connected in a flexible way with the glass tube. This is guaranteed with the bellows at the receiver ends [9]. Additionally, the temperature changes of the glass tube and the metallic elements at the receiver ends imply a specific constructive challenge: The thermal expansion coefficients of the glass near the compensator and the compensator itself have to coincide in order to reduce tension forces. This is necessary especially for the durability of the vacuum in the glass tube. Furthermore, a getter is integrated into the receiver in order to maintain the vacuum. Especially hydrogen, which emerges in smaller quantities due to cracking processes in the thermo oil, can traverse the absorber tube and diminish the vacuum quality. The getter absorbs the hydrogen and avoids thereby the deterioration of the thermal insulation properties of the receiver [9]. The receivers have to resist certain pressure. Maximal operating pressures are indicated to be 20 bars for the Archimede receiver and 40 bars for the Schott receiver. This is important for their use in direct steam generating power plants where they limit the steam pressure. The Solarlite direct steam generation power plant projects limit the steam pressure to 30 bars. Novatec's Fresnel power plants PE 1 and PE 2, however, are operated with 55 bars [9].

## 2.12 Heat transfer fluid

The heat transfer fluid (HTF) has the task to accumulate the thermal energy in the collectors and to transport it to the power block. There are two fundamental manners how the heat can be transferred to the power block: First, a special HTF is applied, from which the heat is transferred to the Rankine cycle working fluid (water), or, second, the steam for the Rankine cycle is generated directly in the

absorber tubes of the parabolic troughs and transported to the turbine. The first version is called indirect steam generation and the second one called direct steam generation. Indirect steam generation power plants contain two fluid cycles, a heat transfer fluid cycle and the Rankine cycle working fluid. The thermal connection between them is consists of an economizer (feed water preheating), an evaporator and a superheated. Direct steam generation power plants, on the contrary, contain only one fluid cycle, the steam cycle. Preheating, steam generation and (if included) superheating is realized directly within the solar field [9].

Indirect steam generation systems use a liquid heat transfer fluid. The heat transfer medium in direct steam generation systems is the water/steam of the Rankine cycle itself.

### 2.12.A Heat transfer fluid in indirect steam generation power plants

A HTF has to fulfill certain requirements: It must be liquid. That means that it should have a sufficiently high evaporation temperature (under manageable pressures) so that it is not evaporated under the high temperatures that are reached in the solar field. Additionally, low freezing temperatures are an advantage so that no freezing protection measures are necessary if the temperatures in the solar field get low. It is also important that its thermal stability is sufficient to stand the high operation temperatures (no thermal cracking, for instance). Evaporation temperature and thermal stability determine the maximum operation temperature of a HTF [9]. In order to store and transport high amounts of thermal energy, a high specific heat capacity is useful. Also high heat conductivity is advantageous for quick heat transfer processes. Low viscosity is important to reduce pumping energy. Also of course, low investment costs and a sufficient availability are also

important criteria. Finally, environmentally friendly materials are preferable as well as materials with low inflammability and low explosively (see Figure 2.43).



Figure 2.42 HTF selection criteria [9]

The following table gives an overview over some properties of some materials that are considered as appropriate candidates for a usage as HTF in parabolic trough power plants [9].

Table2.4 Nearly all parabolic trough power plants use synthetic thermo oil as HTF [9]

Medium	Max. temperature [°C]	Heat capacity [J/kg/K]	Heat conductivity [W/m/K]
Mineral oil	300	2600	0.12
Synth. oil	400	2300	0.11
Silicon oil	400	2100	0.1
Nitride salt	450	1500	0.5
Nitrate salt	565	1600	0.5
Carbonate salt	850	1800	2.0
Sodium (liquid)	850	1300	71.0

Mineral oil was used in an early commercial power plant in the 1980s. Currently efforts are done to use molten salt as HTF. However, synthetic thermo oil is still the standard HTF.

### 2.12.A1 Mineral oil

Mineral oil was used in the first SEGS plant, which started operation in 1985. It had the advantage that a direct storage system could be implemented, i.e. a storage system that uses the HTF directly as storage medium, because mineral oil can be used as thermal storage medium as well. However, the main disadvantage of mineral oil, which motivated its substitution by thermo oil, is its operation temperature limit. At temperatures above 300°C it gets unstable [9].

### 2.12.A2 Synthetic thermo oil

Synthetic thermo oil (or simply “thermo oil”) is a eutectic mixture of biphenyl/diphenyl oxide. There are more than 25 years of experience with this HTF in parabolic trough power plants. It has been proven that the technology is reliable, which is also an important argument for investors and operators to go on using it. Synthetic thermo oil satisfies quite well the mentioned requirements. It is liquid until 12°C, which means that freeze protection is quite easy or even unnecessary. It has quite a high specific heat capacity and it can be acquired in large quantities [9]. However, it has also some disadvantages and limitations:

The maximum operation temperature is about 400°C. Beyond this temperature, thermal cracking happens, which destroys the thermo oil. It resists higher temperatures than mineral oil. However, live steam temperature is limited to about 370°C, which limits the power block efficiency. Thermo oil has to be replaced periodically because of aging processes (The chemical structure changes over

longer time spans). Thermo oil is quite expensive. About 5% of the investment costs for the Andasol power plants must be afforded for the HTF. The high costs and also high vapour pressures at the operation temperatures impede that thermo oil is used as storage medium. Thermo oil is environmentally less friendly than some other possible media. Leakages are not only a problem for the plant operation but also for the environment [9].

### 2.12.A3 Molten salt

Today, the usage of molten salts as HTF is still under investigation. The pioneer in this field is the Italian company Archimede Solar Energy (ASE). The used molten salt mixture is the eutectic mixture of 60%  $\text{NaNO}_3$  and 40%  $\text{KNO}_3$  [9].

The most important advantage of these molten salts as HTFs is that the output temperature of the solar field can be increased to 450-550°C, which allows a higher Rankine cycle efficiency than in thermo oil systems. Molten salts are cheaper than thermo oil. They are used in agriculture as fertilizer and are available in large quantities. Additionally, they are environmentally friendlier. They are non-toxic and also non-inflammable [9]. An important disadvantage of molten salts is the high freezing point, which is between 120 and 220°C for binary<sup>43</sup> and ternary<sup>44</sup> molten salts. That means that strategies have to be developed to avoid the freezing of the molten salts. Different solutions are conceivable: The piping system could be heated or the HTF could be stored in a sufficiently insulated tank during the night. The higher temperature and the more aggressive characteristics of salt may also imply that superior and more expensive materials have to be used [9].

## 2.13 Direct steam generation

The heat transfer medium that flows through the receivers of the solar field is the working fluid of the Rankine cycle itself. Of course, this working fluid is normally water. Water is, indeed, quite an ideal HTF if we consider the suitability criteria for HTFs mentioned above. Only the criterion of the high evaporation temperature does not apply, but this criterion is of no importance in the case of direct steam generation, because evaporation is just intended (see Figure 2.44). For small systems and temperature levels below 400°C, however, organic working media may be an alternative; they allow acceptable plant efficiencies also at low operation temperatures [9].

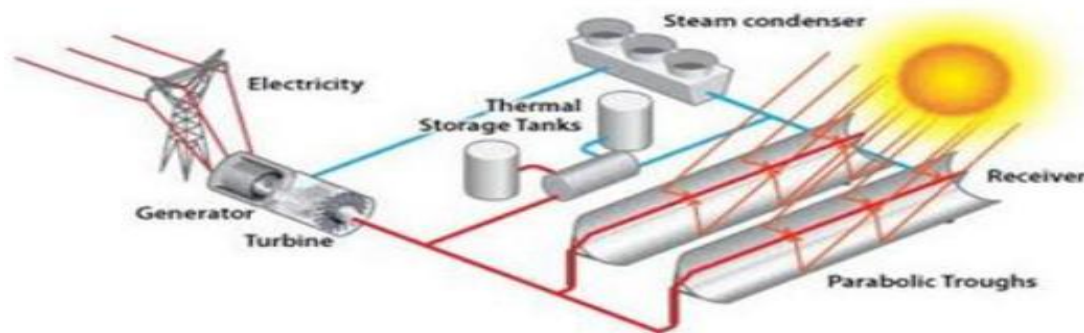


Figure 2.43 Direct steam generation systems[9]

DSG is the standard solution in Fresnel power plants, while parabolic trough power plants until now were constructed as indirect steam generation systems. However, there are continuous efforts to develop also DSG for parabolic trough power plants. Currently, the first commercial parabolic power plant with DSG is under construction in Kanchanaburi, Thailand [9].

## 2.14 Advantages and challenges of DSG

- Advantages

1. Steam as heat transfer fluid allows higher temperatures because there is no danger of thermo oil cracking. This allows higher steam cycle efficiencies. The aspired steam parameters go up to 550°C and 120 bars<sup>45</sup> (thermo oil systems: 400°C and 100 bars). In 2011, a DSG test loop was integrated by DLR in a conventional Endesa power plant in Carboneras (Spain). In this test loop, temperatures of up to 550 °C are reached [9].
2. The number of construction components can be reduced because no heat exchange has to be realized between a solar field heat transfer fluid and Rankine cycle working fluid.
3. The usage of steam as a heat transfer fluid may reduce the mean heat transfer fluid temperature in the absorber tube (even at higher final temperatures) and reduce, hence, thermal losses. This reduction is possible because in a large part of the receivers the boiling process is realized, which takes place at a reduced temperature. Only in the small part, where the superheating of the steam is realized (if there is superheating), high temperatures are reached.
4. The thermo oil itself is an expensive component of CSP plants so that the lack of thermo oil is a direct economic advantage.
5. As there is no heat transfer between two heat transfer fluids, there is one thermal loss factor less.
6. Water has further advantages in comparison to other HTFs: It is environmentally friendlier than thermo oil so that leakages in a directly steam generating plant does not imply environmental dangers. It is less

corrosive than salt. Its freezing temperature is much lower than the freezing temperature of salt and even slightly lower than of thermo oil. The effort required to ensure adequate anti-freeze protection is reduced significantly.

According to studies, the level zed electricity costs with a directly steam generating system can (under certain boundary conditions) be lower by more than 10% in relation to the conventional indirect steam generation technology [9].

## 2.15 Challenges

An important challenge of the DSG technology is the high pressure of the water/steam in the absorber tubes. As there is no separation between solar field HTF fluid cycle and power block steam cycle, the water/steam in the solar field has the pressure of the live steam. This was the main problem why DSG was not applied in parabolic trough power plants for a long time. Especially the fact that the receivers must be moveable and need flexible connections was an obstacle for the application of DSG in parabolic trough power plants. This problem does not exist in Fresnel solar fields, where the receivers are fixed; therefore DSG is the standard solution in Fresnel power plants [9]. There are still no commercially available large storage systems for DSG systems. Until now, only short time steam storages for DSG systems with saturated steam generation are commercially applied. The solar field control is more difficult than in indirect steam generation systems. This holds especially for superheated steam generating systems. In the test loop at the PSA (see below “Experiences”), three different loop operation concepts for the generation of superheated steam - continuous flow concept, injection concept and recirculation concept - were compared and evaluated (see Figure 2.45) [9].



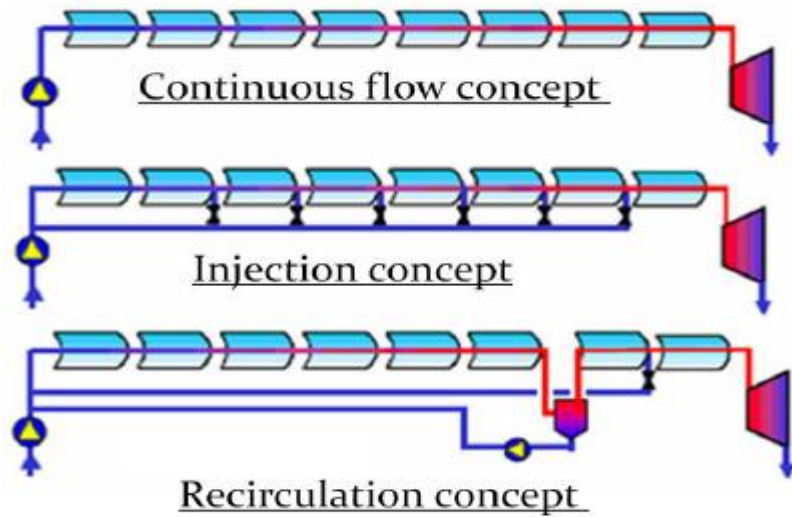


Figure 2.44 operation concepts[9]

The recirculation mode was demonstrated to be the most appropriate for direct steam generation. A steam separator in the collector field separates the evaporation zone from the superheating section. This implies the advantage that the shifting of the evaporation and overheating zones in the collector is avoided. Stable evaporation and superheating sections reduce the thermal stress in the receivers and allow a safer collector operation. The water that is not evaporated is pumped back to the beginning of the loop (recirculation). The recirculation concept can be applied also to generate saturated steam. In this case there is no superheating section; the steam separator is located directly between the solar field and the power block [9]. An important step in the development of the DSG technology was the installation of a 700m long experimental DSG loop in 1999 at the Plataforma Solar de Almería. During more than 10,000 operation hours the feasibility of the direct steam generation in parabolic trough collectors was demonstrated. Steam conditions of 100 bars and 400 °C were reached. New absorber tubes and flexible receiver connections had to be developed in order to withstand the high pressures [9].



Figure 2.45 DISS test facility at Plataforma Solar de Almería[9]

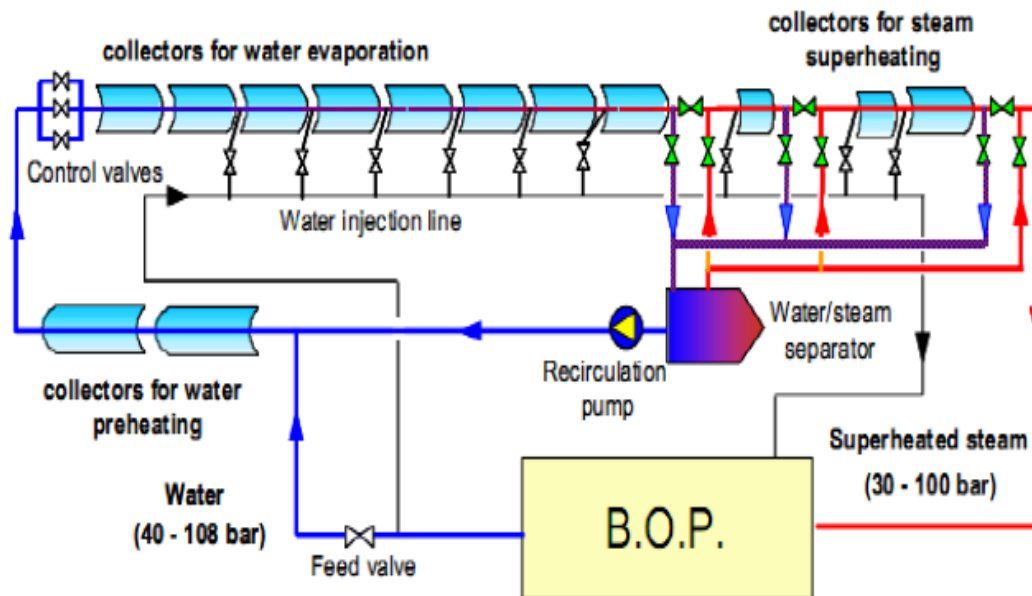


Figure 2. 46Schema of DISS test facility[9]

The first commercial parabolic power plant with direct steam generation is under construction in Kanchanaburi, Thailand.<sup>51</sup> The German company Solarlite constructs a 5 MW plant, which will be extended in a second step to a 9 MW plant. The generated electricity is delivered to the public grid. The solar field produces superheated steam. It contains 12 evaporator loops and 7 superheated loops [9]. A combination of recirculation and injection concept is applied for the generation of the superheated steam. It is claimed that the advantage of combining these two concepts is a better controllability of the process parameters even during

fluctuating DNI conditions. The recirculation mode ensures that the receivers in the evaporator solar field are well cooled and the system pressure is maintained. The injection concept enables better temperature stability of the superheated steam. Wet cooling is applied. The operating parameters are 330°C and 30 bars. At these conditions the power block reaches an efficiency of 26 %. The receivers have a slightly stronger wall thickness than the receivers in indirect steam generation systems in order to withstand the higher pressures [9].

## 2.16 Solar field orientation

Theoretically, the parabolic troughs in the solar field of a CSP plant can have any orientation. It is always possible to track the Sun. However, there is a preferred orientation, which is the north-south alignment with the respective east-west tracking. East-west alignment with the respective north-south tracking was applied for experimental purposes only [9].

East-west alignment has the following advantages and disadvantages:

- The collector performance over the day is quite uneven. Due to large incidence angles, the collector performance is reduced considerably in the hours after sunrise and the hours before sunset. At noon, the full aperture always faces the Sun, i.e. the incidence angle is zero. This means that the highest possible thermal peak power of the solar field at a given direct irradiance is always reached [9].
- Energy yield differences between summer and winter are smaller than for north-south alignment. Contrary to north-south alignment, incidence angles on the collector are not larger in winter than in summer [9].
- Quite small tracking movements are required during the day.
- The annual energy yield is lower than for north-south alignment.

North-south alignment has the corresponding advantages and disadvantages:

- The collector performance over the day is quite even.
- Due to incidence angle differences between summer and winter, the seasonal energy yield differences are larger than for east-west alignment [9].

The annual energy yield is higher than for east-west alignment

# CHAPTER THREE

# Modeling of Hourly Solar Radiation on Horizontal and Inclined Surfaces for Khartoum/ Sudan:-

## 3.1 Introduction

The incoming solar radiation on the outer surface such as the surface of buildings, Factories and hospitals are important matters, especially in the areas of air conditioning. For example, in the cooling purposes, solar radiation affects the space cooling load calculations, because it has an effect in calculations of solar- air temperature. It is important temperature in calculations of solar heat gain by conduction through the outer surfaces. As well as enter into direct solar heat gain through windows and translucent surfaces. The effect of solar radiation and appears larger in calculations relating to solar systems which are used, for example, in the heating fluid operations, particularly air and water in the solar collectors used for solar heating, lighting and solar drying. Also in the field of electricity generation using solar radiation or solar energy to generate electricity in direct or indirect ways by solar cells or solar collectors. The solar radiation falling on earth's surface process is not simple, because solar radiation depends on a lot of factors and variables of these factors are the amount of solar energy out of the atmosphere, solar scattered due to the collision of solar radiation and atmosphere atoms and the effect of the layer of the atmosphere and solar angles and changes real-time with the time and location and climate ... etc. For many developing countries solar radiation measurements are only available for selected stations due to the cost of the measurement equipment and techniques involved. It is rather important to elaborate <sup>[10]</sup> mathematical methods to estimate the solar radiation on the basis of sun position geometry and more readily meteorological data. In this research a simple model was developed to estimate the direct, diffuse, and total solar radiation on horizontal and Inclined surfaces.

### 3.2 Location of study

This study is based on the geographical location of Khartoum which located at  $15.9667^{\circ}\text{N}$  latitude. And  $32.8667^{\circ}\text{E}$  Longitude .Khartoum is situated at an altitude of 382 meters (1.253.28 feet) above sea level above the plain flat ground surface with a slight decline. Khartoum is one of the hottest cities in the world.

Where the temperature may exceed more than  $48^{\circ}\text{C}$   $118.4^{\circ}\text{F}$  in the middle of summer but the annual average maximum temperature of about  $37.1^{\circ}\text{C}$   $98.78^{\circ}\text{F}$ .



Figure 3.1 location of study[14]

### 3.3 Estimation of Hourly Solar Radiation in horizontal surface Using Mathematical Model

The total radiation received on the horizontal is a summation of the direct and diffuse radiation. developed to estimate the amount of global solar radiation on horizontal surfaces using various climatic parameters ,such as sunshine duration, cloud cover, humidity, maximum and minimum ambient temperatures wind speed...etc <sup>[10]</sup>.

- Solar constant this is the flux of solar radiation on a surface normal to the sun's rays beyond the earth's atmosphere at the mean earth-sun distance. The currently accepted value of solar constant is 1370 W/m<sup>2</sup>. [11].
- Air mass ratio Is the ratio of mass of atmosphere in the actual sun-earth path to that which would exist if the sun were directly overhead at sea level The expression for solar air mass ratio is given by:

$$M = \frac{1}{\sin \beta} \quad [11] .$$

Where: -

$\beta$  : altitude angle which depends on the location, time of the day and day of the year. Thus smaller the altitude angle, larger will be the depletion of radiation .



- reflectivity of the ground it is a horizontal surface from where the solar radiation is reflected on to a given surface. Table 3.1 below shown the percentage of the ground reflectivity [12].

**Table 3.1** percentage of the ground reflectivity

Earth ground	reflectivity %
Hardscrabble	20
Sods	30
Geest	45-35
Oceans	10-2
Forests	18-6
Glacial	70-20
Ciest	80-70

- Solar angles

1. Latitude (L)

It is the angle between the lines joining O and P and the projection of OP on the equatorial plane.

$$\text{Latitude angle } I = \text{angle POA}$$

Thus the latitude along with the longitude indicates the position of any point on earth and it varies from 00 at equator to 900 at the poles.

2. Hour angle (h)

It is the angle between the projection of OP on the equatorial plane . the line OA and the projection of the line joining the center of the earth to the center of the sun .

$$\text{Hour angle } h = \text{angle AOB}$$

$$h = (12 - \text{LST}) \cdot 15 \quad [10].$$

LST: local solar time, for any location is given by :

$$LST = LStT + EOT + 4(LON - LSM) \quad [11].$$

Where :

LStT : local standard time.

EOT: equation of time which given by :

$$EOT = 0.2292(0.075 + 1.868 \cos N - 32.077 \sin N - 4.615 \cos 2N - 40.89 \sin 2N)$$

$$N = (n - 1) \cdot \frac{360}{365} \quad [11].$$

n is the day of the year counted from January 1st.

LON: local longitude of the location.

LSM : local standard time meridian.

Declination (d)

The declination angle is the angle between the line joining the center of the earth and sun and its projection on the equatorial plane angle between line OO' and line OB .

$$\text{Declination } d = \text{angle } O'OB$$

$$d = 23.47 \sin \left[ \left( \frac{284+n}{365} \right) \cdot 360 \right] \quad [11].$$

(n) Is the day of the year counted from January 1ST .

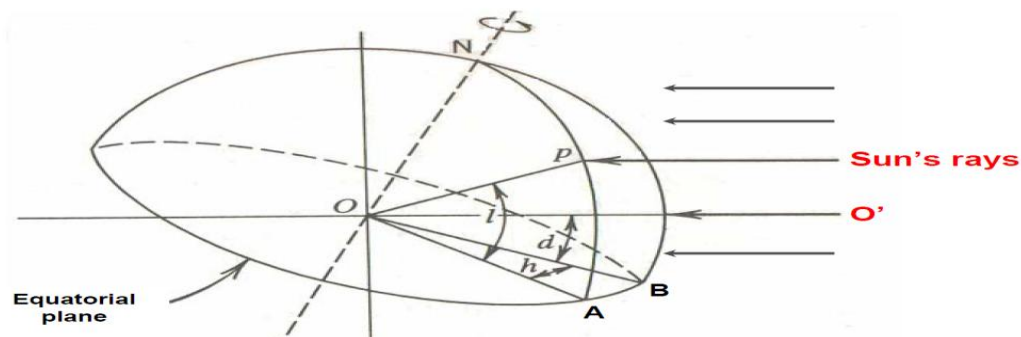


Figure 3.2 Definition of Latitude l, Hour angle h and Declination d angles [11]

In addition to the three basic solar angles the latitude, hour angle and declination several other angles have been defined (in terms of the basic angles) which are required in the solar radiation calculations. Figure 3.3 shows a schematic of one apparent solar path and defines the altitude angle ( $\beta$ ) zenith angle ( $\psi$ ) and solar azimuth angle ( $\gamma$ ).

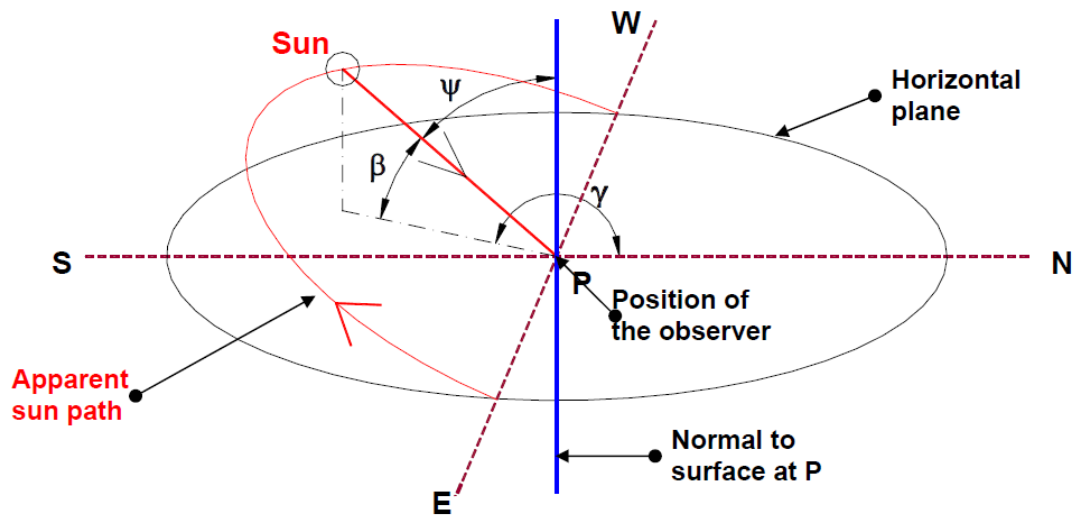


Figure 3.3 Definition of altitude ,zenith and azimuth angles [11 ]

### 3. Altitude angle ( $\beta$ )

It is the angle between the sun's rays and the projection of sun's rays onto a horizontal plane. The expression for altitude angle is given by :

$$\beta = \sin^{-1}(\cos I \cdot \cos h \cdot \cos d + \sin I \cdot \sin d) \quad [11].$$

where :

I: latitude angle.

h: hour angle.

d: declination angle.

### 4. Zenith angle ( $\psi$ )

It is the angle between sun's rays and the surface normal to the horizontal plane at the position of the observer. The expression for zenith angle is given by :

$$\Psi = \frac{\pi}{2} - \beta \quad [11].$$

Where :

$\beta$ : Altitude angle.

### 5. Solar azimuth angle $\gamma$ :

It is the angle in horizontal plane measured from north to horizontal projection of the sun's rays. The expression for solar azimuth angle is given by :

$$\gamma = \sin^{-1} \left( \frac{\cos d \cdot \sin h}{\cos \beta} \right) \quad [11].$$

where:

d: declination angle.

h: hour angle.

The solar azimuth angle ( $\gamma$ ) is measured in a horizontal plane between a south line and the direction from the site to the sun as projected onto a horizontal plane. The solar altitude angle ( $\beta$ ) and solar azimuth angle ( $\gamma$ ) are related to the fundamental angles of latitude ( $I$ ) solar declination ( $d$ ) and hour angle ( $h$ )

### 6. Incident angle of sun's rays ( $\theta$ )

The solar incidence angle  $\theta$  is the angle between the sun's rays and the normal on a surface. For a horizontal plane, the incidence angle  $\theta$  and the zenith angle  $\gamma$  are the same for horizontal surface calculation. As shown in **figure 3.4** The expression for solar incidence angle is given by:

$$\theta = \psi = \frac{\pi}{2} - \beta \quad [11].$$

$\theta$ : Angle of incidence. As shown in **figure 3.5** the angle of incidence is equal to the zenith angle for horizontal surface calculations.

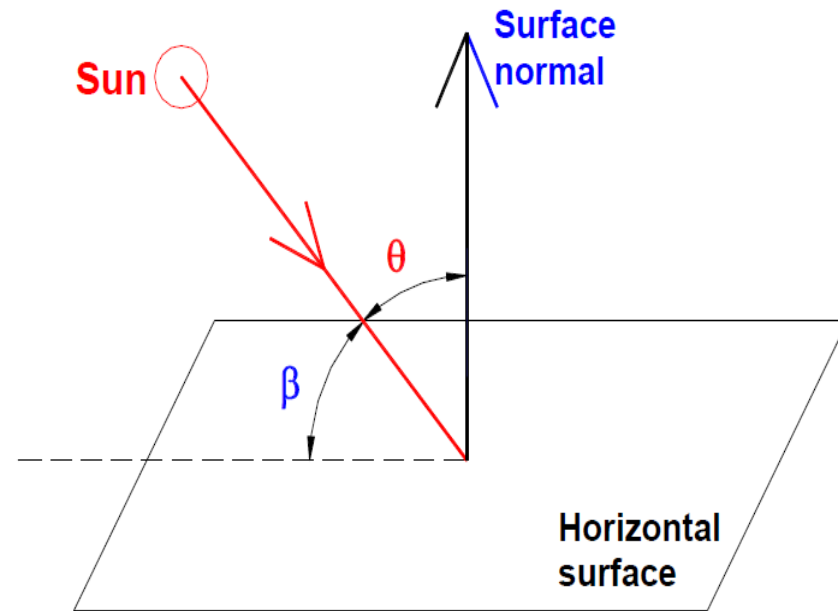


Figure 3. 4incidence angle in horizontal surface[11 ]

- **Direct radiation from the sun : -**

$$Idn = A \cdot \exp\left(\frac{-B}{\sin \beta}\right) \quad [11].$$

Where : -

$Idn$  : Direct radiation from the sun (  $\text{W/m}^2$  ) .

$A$  : is the apparent solar irradiation which is taken as  $1230 \text{ W/m}^2$  for the months of December and January and  $1080 \text{ W/m}^2$  for mid-summer.

$B$  : is the atmospheric extinction coefficient which takes a value of 0.14 in winter and 0.21 in summer .<sup>[11]</sup>.

$\beta$  : altitude angle .

- **Beam radiation : -**

$$Ib = Idn \cdot \cos \psi \quad [11].$$

Where : -

Ib : Beam radiation ( $\text{w/m}^2$ ) .

Idn: Direct radiation from the sun ( $\text{w/m}^2$ ) .

$\psi$  : Zenith angle .

- **Diffuse radiation from sky : -**

$$Id = C \cdot Idn \cdot Fws \quad [11].$$

Where :-

Id : Diffuse radiation from sky .

C: The value of C is assumed to be constant for a cloudless sky for an average day of a month. Its average monthly values have been computed and are available in tabular form. The value of C can be taken as 0.135.

Idn : Direct radiation from the sun ( $\text{w/m}^2$ ) .

Fws : the factor Fws is called as view factor or configuration factor and is equal to the fraction of diffuse radiation that is incident on the surface . for diffuse radiation FWS is a function of the orientation of the surface only . it can be easily shown that this is equal to:

$$Fws = \frac{1 + \cos \Sigma}{2} \quad [11].$$

Where  $\Sigma$  is the tilt angle obviously for horizontal surfaces ( $\Sigma = 0^\circ$ ) the factor  $F_{ws}$  is equal to 1

- **Total solar radiation** the total radiation received on the horizontal is a summation of the direct and diffuse radiation. According to ASHRAE model total solar irradiation on horizontal surface is given by:

$$I_t = I_b + I_d \quad [11].$$

Where: -

$I_t$ : total solar radiation. ( $\text{w/m}^2$ )

$I_b$ : Beam radiation. ( $\text{w/m}^2$ )

$I_d$ : Diffuse radiation from sky. ( $\text{w/m}^2$ )

### 3.4 The algorithm of horizontal surface

The flowchart in **figure3.6** shows in detail the calculation of potential solar radiation in horizontal surface.

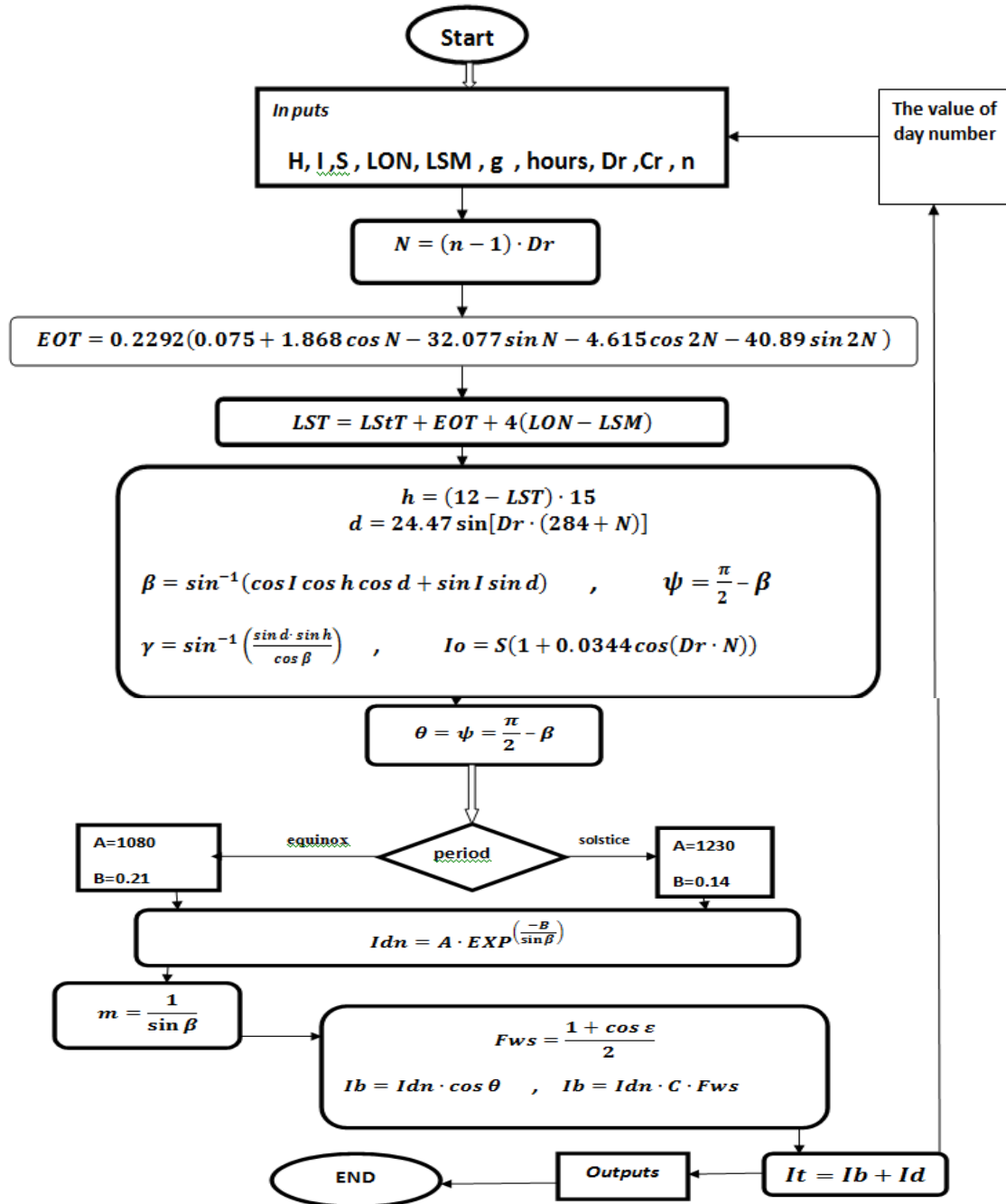


Figure 3.5 flowchart to calculate the potential solar radiation in horizontal surface.



### 3.5 Estimation of Hourly Solar Radiation in Inclined surface Using Mathematical Model:

The total radiation received by an inclined surface consists of beam, diffuse, and reflected radiation. The reflected radiation here is the radiation reflected from the surrounding ground. Different models for estimating the total solar radiation on inclined surfaces had been proposed and evaluated. The total radiation received on an inclined can be calculated in a similar way as the sum of the direct (beam), diffuse and reflected radiation.

The general form of total hourly solar radiation energy incident on an inclined surface  $Q_t$  is given by:

$$Q_t = Q_b + Q_d + Q_r \quad [10]$$

Where:

$Q_t$ : total radiation received by an inclined surface ( $\text{w/m}^2$ ).

$Q_b$ : direct (beam) radiation in an inclined surface ( $\text{w/m}^2$ ).

$Q_d$ : diffuse radiation in an inclined surface ( $\text{w/m}^2$ ).

$Q_r$ : reflected radiation from the surrounding ground ( $\text{w/m}^2$ ).

Direct (beam) radiation in an inclined surface is given by:

$$Q_b = I_b \cdot R \quad [10]$$

Where  $I_b$  is the direct radiation in horizontal surface and  $R$  is the hourly geometric factor given by:

$$R = \frac{\cos \psi}{\cos \theta} \quad [10]$$

Where  $\psi$  is the solar zenith angle and  $\theta$  is the incidence angle the angle between The beam radiation on a surface and the normal to that surface and it is given by:

$$\cos \theta = \sin d \cdot \sin I \cdot \sin \varepsilon - \sin d \cdot \cos I \cdot \sin \varepsilon \cdot \cos \gamma_s + \cos d \cdot \cos I \cdot \cos \varepsilon \cdot \cos h + \cos d \cdot \sin I \cdot \sin \varepsilon \cdot \cos \gamma_s \cdot \cos h + \cos d \cdot \sin \varepsilon \cdot \sin \gamma_s \cdot \sin h$$

[10]

Where  $\gamma_s$  is the surface azimuth angle defined as the deviation of the projection on a horizontal plane of the normal to the surface from the local meridian, with zero due south's, east negative, and west positive. and  $\varepsilon$  surface tilt angle from the horizontal.

Among the methods available for prediction of radiation fluxes on tilted surfaces is the method of (Liu and Jordan 1962). This is a simple isotropic model that had been tested by many investigators and found to give good results. In this method the diffuse radiation on the tilted surface is given by:

$$Q_d = I_d \cdot \left( \frac{1 + \cos \varepsilon}{2} \right) \quad [10]$$

Where  $I_d$  is the diffuse radiation in horizontal surface and  $\varepsilon$  surface tilt angle from the horizontal .

The radiation reflected from the surrounding ground in an inclined surface  $Q_r$  is given by :

$$Q_r = \rho \cdot I_t \cdot \left( \frac{1 - \cos \varepsilon}{2} \right) \quad [10]$$

Where  $\rho$  : the ground reflectivity or surrounding diffuse reflectance for the total solar radiation, It is the total solar radiation in horizontal surface and  $\varepsilon$  surface tilt angle from the horizontal.

### 3.6 the algorithm of tilted surface

The flowchart in **figure3.7** shows in detail the calculation of potential solar radiation in Inclined surface:-

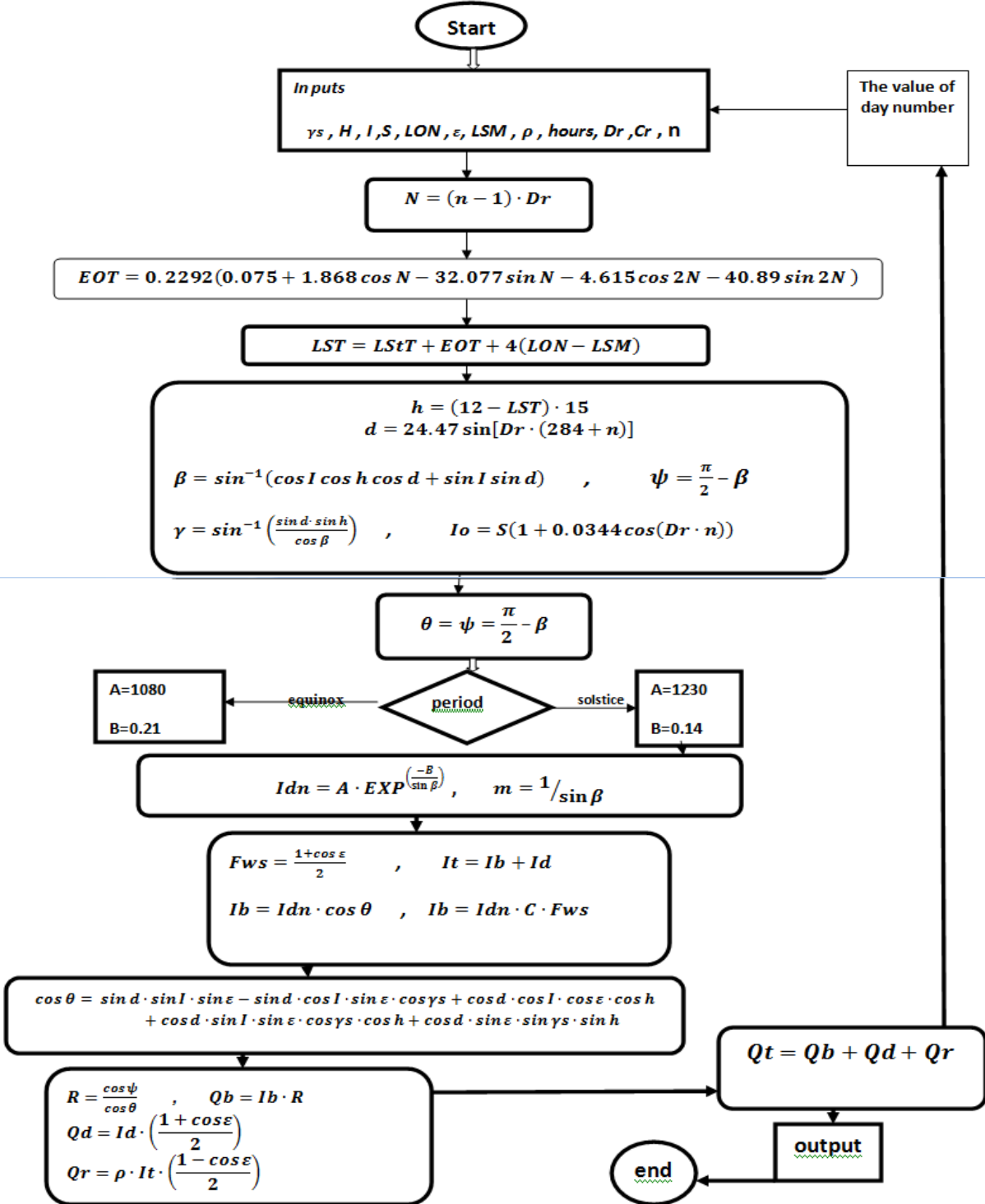


Figure 3.6 flowchart to calculate the potential solar radiation in Inclined surface.

### 3.7 Computational procedures

The intensity of solar radiation is a function of the solar direction relative to the Local plane of the Earth's surface at that instance. Variables such as solar azimuth angle and solar altitude angle change continuously throughout the day, and so have to be calculated every time the intensity of solar radiation is computed. Solar declination may be assumed to be constant and is calculated only once per day. to simplify the explanations, the Ptolemaic view of the Sun's motion around the Earth will be used in other words the site is fixed. The fundamental equations mention above will used to calculate the solar radiation.

The Sun's position in the sky is described by the solar altitude  $\beta$  and solar azimuth  $\gamma$  angles. The solar altitude angle  $\beta$  is the angular elevation of the Sun above the horizontal . It is measured from the local horizontal plane upward to the centre of the sun. The solar altitude angle changes continuously that is daily and seasonally. It is zero at sunrise each day, increases as the Sun rises and reaches a maximum at solar noon and then decreases again until it reaches zero at sunset .The noon solar altitude angle varies seasonally the seasonal change being due to the declination angle changing daily.

The steps to calculate solar radiation as shown in flowchart the first step is define the parameters supplied by the user such as: altitude of the site **H** Khartoum is situated at an altitude of 382 meters above sea level , latitude of site **I** , standard and local Longitude of the site **LON, LSM** .

Khartoum located at  $15.9667^{\circ}\text{N}$  latitude,  $32.8667^{\circ}\text{E}$  local Longitude and  $30^{\circ}\text{E}$  standard longitude , the ground reflectivity of the site  $\rho$  assume the ground of Khartoum hardscrabble than the percentage of the ground reflectivity is equal to 20% , hours to calculate the solar flux and the tilt angles like surface azimuth angle  $\gamma_s$  and surface tilt angle  $\epsilon$  .After defined parameters and from equations

**2,5,6,7,8,9,18** calculate hour, declination , altitude , zenith ,solar azimuth, incident angle of sun's rays for horizontal and tilt surfaces respectively. Then from equation **3,4** calculate local solar time . and from equation **1** calculate air mass ratio . after that apply in equation **10** to find Direct radiation from the sun and from equation **11,12** calculate beam and diffuse radiation in horizontal surface to find total solar radiation in horizontal surface we apply in equation **14**.After finding solar radiation in horizontal surface apply in equations **16,19,20** to calculate beam , diffuse and reflected radiation for incident surface respectively. Then apply in equation **15** to find total solar radiation in an inclined surface.

### 3.8 Model Parameters

They are model inputs and can be divided into two groups. The first group includes parameters supplied by the user such as: the simulation time (**LStT**), latitude angle, surface azimuth, tilt angle for the inclined surface, day and month number which were used to calculate the solar radiation at the surface , the ground reflectivity, standard and local Longitude .The second group includes parameters taken from the literature such as: sea level, solar constant and the constants which are used to calculate the atmospheric transmittance for beam and diffuse radiation.

### 3.9 Software Tools

The models were designed by using MATLAB R2010b which is an interactive tool for modeling, simulating and analyzing dynamic systems. MATLAB R2010b provides a complete set of modeling tools that can be used to quickly develop detailed program of the systems. providing the user with immediate access to an extensive range of analysis. MATLAB

R2010b enables the building of program and graphical block diagrams, to simulate dynamic systems, evaluate system performance and refine the designs <sup>[14]</sup> .

### 3.10 Theoretical Study of a Parabolic Trough Solar Collector using Mathematical Model

#### 3.10.A Introduction

Theoretical study has been conducted to determine the thermal efficiency of a parabolic trough solar collector. The study has been performed during winter and summer at Khartoum. The solar radiation of Khartoum was calculated theoretically and a theoretical study was performed by using MATLAB R2010b program. The dimensions and specifications of the collector were entered to the program to determine the theoretical thermal efficiency of parabolic trough solar collector.

#### 3.10.B Solar Parabolic Trough Performance

The parabolic trough is also referred to as a cylindrical parabolic collector or a linear parabolic collector. The basic elements making up conventional collector are:

- (1) The absorber tube located at the focal axis through which the liquid to be heated flows.
- (2) The concentric transparent cover.
- (3) The reflector.
- (4) The support structure and Elements.

(1) And (2) together constitute the receiver, while elements (3) and (4) constitute the concentrator. Energy delivery temperatures can be increased by decreasing the area from which heat losses occur, Increase the concentration ratio. For maximum high flux intensity tracking is done to track the sun so that beam radiation will be directed onto the absorbing surface. There are also requirements for maintenance, particularly to retain the quality of optical systems for long periods of time in the presence of dirt, weather, and oxidizing or other corrosive atmospheric components [12].

### 3.10.C Definitions

#### The aperture (W)

Aperture is the plane opening of the concentrator through which the solar radiation passes. It is characterized by the diameter or width of the opening.

#### Concentration ratio (C)

The ratio of the effective area of the aperture to the surface area of the absorber. Values of the concentration ratio vary from unity to a few thousand. This quantity is also referred to as the geometric concentration ratio or simply concentration ratio [12].

#### Intercept factor ( $\gamma$ )

The fraction of the radiation, which is reflected or refracted from the concentrator and is incident on the absorber. The value of the intercept factor is generally close to unity [12].

## Acceptance angle ( $2\theta$ )

The angle over which beam radiation may deviate from the normal to the aperture plane and yet reach the absorber . Collectors with large acceptance angles require only occasional adjustments, while collectors with small acceptance angles have to be adjusted continuously [12].

### 3.10.D Assumption

1. Considered heat transfer take place under steady state conditions.
2. The Heat flow is unidirectional.
3. There is no internal heat generation.
4. The material of receiver and reflector is stainless steel.
5. Mass flow rate is constant.

### 3.10.E Theory

- Parabolic equations:

Geometrical concentration ratio ***Cr*** is defined as the area of the collector aperture ***Ap*** divided by the surface area of the receiver ***Ar.ext***.

$$Cr = \frac{Ap}{Ar.ext} = \frac{W \cdot Dr.ext}{\pi \cdot Dr.ext} \quad [12]$$

The parabolic equation shows the x and y displacements of the parabolic collector with its width, ***W*** and depth, ***d*** and used to obtain the right curvature of the parabolic trough.

$$y = \frac{d}{(0.5 \cdot W)^2} \cdot x^2 \quad [12]$$



focus length is calculate as:

$$f = \frac{w}{16 \cdot d} \quad [12]$$

The rim angle of a parabolic collector is calculated by using next equation with inputs for the focal length, width and depth.

$$\text{rim angle} = \frac{2 \cdot f}{\sqrt{(0.5 \cdot W)^2 + (d - f)^2}} \quad [12]$$

The concentrator height is given by:

$$h = \frac{0.5 \cdot W}{\sqrt{2 \cdot \sigma}} \quad [12]$$

Where:

$\sigma$  is the standard deviation of the normally distributed radiation that is intercepted by the receiver.

- **Calculation of Solar Radiation**

The above section has been discussed Calculation of Solar Radiation in horizontal and tilted surface the value of solar radiation striking the ground is very important to calculate the efficiency and performance of parabolic trough solar collector which present the input energy of solar collector.

The energy gain(input) to parabolic trough solar collector is given by:

$$qi = Ib \cdot Rb \cdot W \cdot L \quad [13]$$

Where ***qi*** is the energy input to collector by  $\text{w/m}^2$ , ***Ib*** is the beam(direct) solar radiation striking the solar collector by  $\text{w/m}^2$ , ***L*** is the Length of parabolic collector and ***W*** Aperture width of parabolic collector by meter.

**Rb** is geometric factor or tilt factor for beam radiation is the ratio of the beam radiation flux falls on a tilted surface to that falling on a horizontal surface and is given by:

$$Rb = \frac{\cos \psi}{\cos \theta} [13]$$

Where  $\psi$  is Zenith angle and  $\theta$  Incident angle of sun's rays is given by

$$\cos \theta = \sin d \cdot \sin I \cdot \sin \varepsilon - \sin d \cdot \cos I \cdot \sin \varepsilon \cdot \cos \gamma_s + \cos d \cdot \cos I \cdot \cos \varepsilon \cdot \cos h + \cos d \cdot \sin I \cdot \sin \varepsilon \cdot \cos \gamma_s \cdot \cos h + \cos d \cdot \sin \varepsilon \cdot \sin \gamma_s \cdot \sin h [13]$$

$$\Psi = \frac{\pi}{2} - \beta [13]$$

Where  $\beta$  is Altitude angle given by:

$$\beta = \sin^{-1}(\cos I \cdot \cos h \cdot \cos d + \sin I \cdot \sin d) [13]$$

$I$  is latitude angle

$h$  is hour angle

$d$  is declination angle

- Calculation of Thermal Efficiency

The theoretical useful energy from parabolic trough solar collector calculated by equation

$$q_o = Ap \cdot Fr \left[ H_{ap} - \frac{Ar_{ext}}{Ap} \cdot U_l \cdot (T_{f,i} - T_{amb}) \right] [13]$$

Where aperture area of parabolic trough solar collector which given by:

$$Ap = (W - Dr_{ext}) \cdot L [13]$$

$W$  is collector width [m]

$Dr_{ext}$  is external diameter of receiver. [m]

$L$  is collector length.  $[m]$

absorbed radiation is given by:

$$H_{ap} = I_b \cdot \alpha \cdot \rho \quad [13]$$

$I_b$  is beam solar radiation.  $[w/m^2]$

$\alpha$  is Absorptivity.  $[\text{dimensionless}]$

$\rho$  is reflectivity.  $[\text{dimensionless}]$

external surface area of receiver given by:

$$Ar_{ext} = \pi \cdot Dr_{ext} \cdot L \quad [13]$$

$Dr_{ext}$  is internal diameter of receiver.  $[m]$

$L$  is collector length.  $[m]$

internal surface area of receiver given by:

$$Ar_{int} = \pi \cdot Dr_{int} \cdot L \quad [13]$$

$Dr_{int}$  is internal diameter of receiver.  $[m]$

$L$  is collector length.  $[m]$

The heat removal factor of collector is given by:

$$Fr = \frac{M \cdot Cp}{Ar_{int} \cdot Ul} \cdot \left[ 1 - \exp\left(-\frac{Ar_{int} \cdot Ul \cdot Z}{M \cdot Cp}\right) \right] \quad [13]$$

overall heat loss coefficient is given by:

$$Ul = hw + hr \quad [13]$$

**hw** is convective heat transfer coefficient between receiver and ambient which given by:

$$hw = \frac{NUa \cdot Ka}{Dr.ext} \quad [13]$$

**Ka** is conductivity of air.

**Dr.ext** is internal diameter of receiver.  $[m]$

**NUa** is Nusselt number of air given by:

$$NUa = 0.4 + 0.54 \cdot Re.a^{0.53} \quad \text{for } 0.1 < Re.a < 1000$$

$$NUa = 0.3 \cdot Re.a^{0.6} \quad \text{for } 1000 < Re.a < 50000$$

**Re.a** is Reynolds number of air given by:

$$Re.a = \frac{V \cdot Dr.ext}{\nu_a} \quad [13]$$

**hr** is radiation heat transfer coefficient between receiver and ambient given by:

$$hr = \sigma \cdot \varepsilon \cdot (T.r - T.amb) \quad [13]$$

**ε** is Emissivity of receiver tube surface

**σ** is Stefan–Boltzman constant.

**T.r** is receiver temperature.  $[^{\circ}C]$

**T.amb** is ambient temperature.  $[^{\circ}C]$

Efficiency factor of parabolic trough solar collector is given by:

$$Z = \left[ \frac{\frac{1}{U_l}}{\frac{1}{U_l} + \frac{Dr.ext}{Dr.int \cdot hw} + \frac{Dr.ext \cdot \ln \frac{Dr.ext}{Dr.int}}{2Ka}} \right] \quad [13]$$

The theoretical thermal efficiency is writing as:

$$\eta.th = \frac{q_o}{q_i}$$

$$\eta.th = \frac{Ap \cdot Fr \left[ Hap - \frac{Ar.ext}{Ap} \cdot Ul \cdot (Tf.i - T.amb) \right]}{Ib \cdot Rb \cdot W \cdot L} \quad [13]$$

### 3.11 the algorithm of theoretical efficiency

The flowchart in **figure 3.7** shows in detail the calculation of Thermal Efficiency of parabolic trough solar collector.

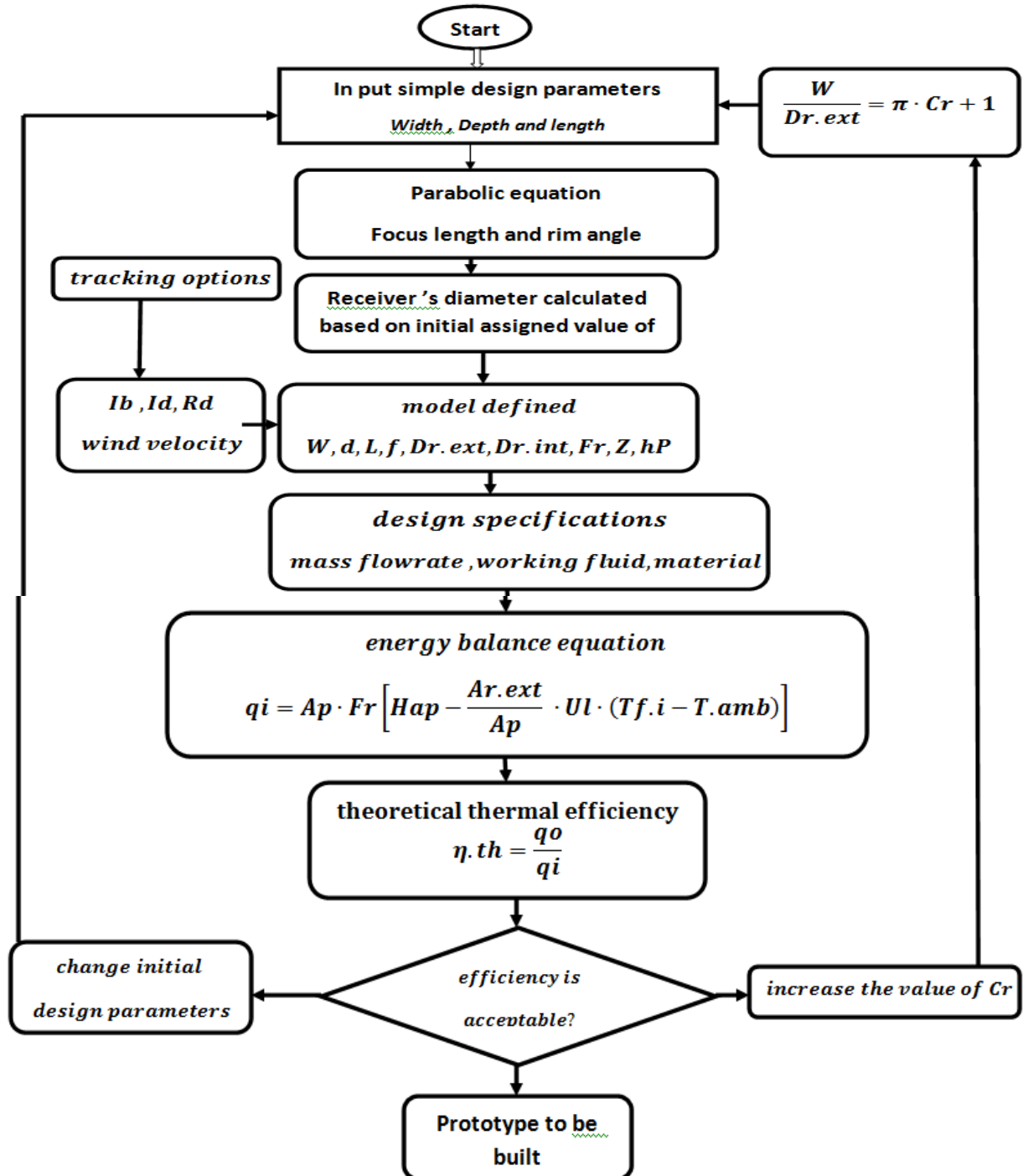


Figure 3.7 flowchart to calculate Thermal Efficiency of parabolic trough solar collector.

### 3.12 Simulation and analyzing the flow inside the tube

A (2-D) mesh of a Z shape tube had been built using GAMBIT 2.3.16. It had been exported to FLUENT 6.3.26 to study and analyze the flow of fluid and heat transfer through the tube.

### 3.13 TUBE in GAMBIT:

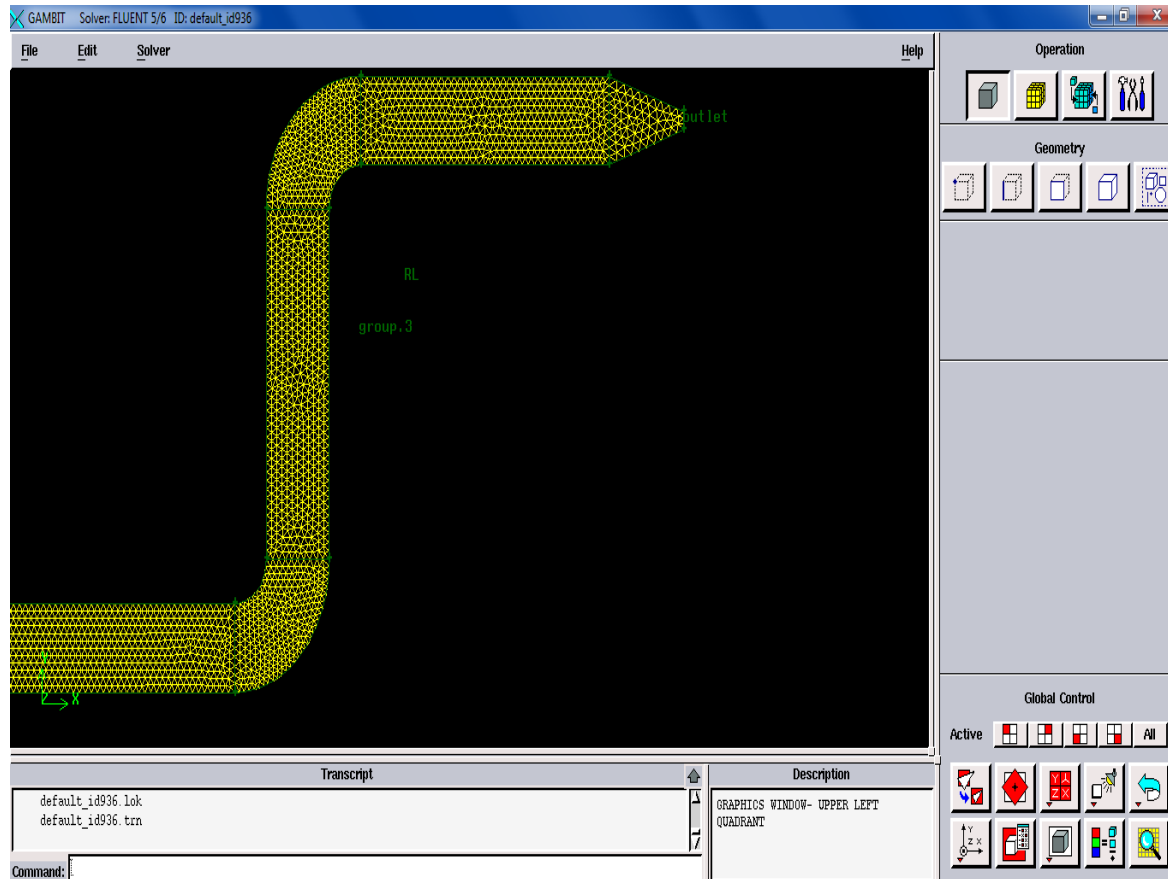
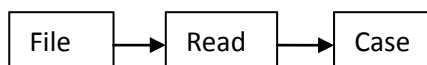


Figure 3.8 Design the tube in gambit.[15]

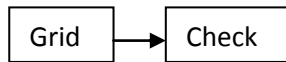
### 3.14 Steps of solution in FLUENT

#### Step1: Grid

- 1- Read the mesh file, TUBE2D.msh.



- 2- Check the grid.



3- Scale the grid.

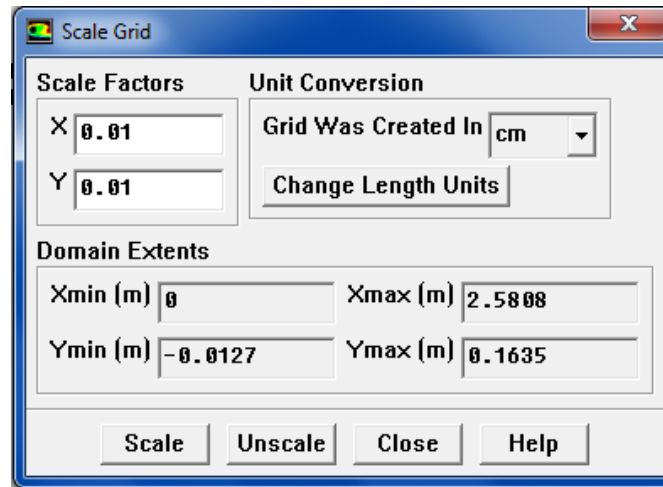
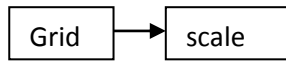


Figure 3.9 Scale grid. [15]

4- Display the grid.

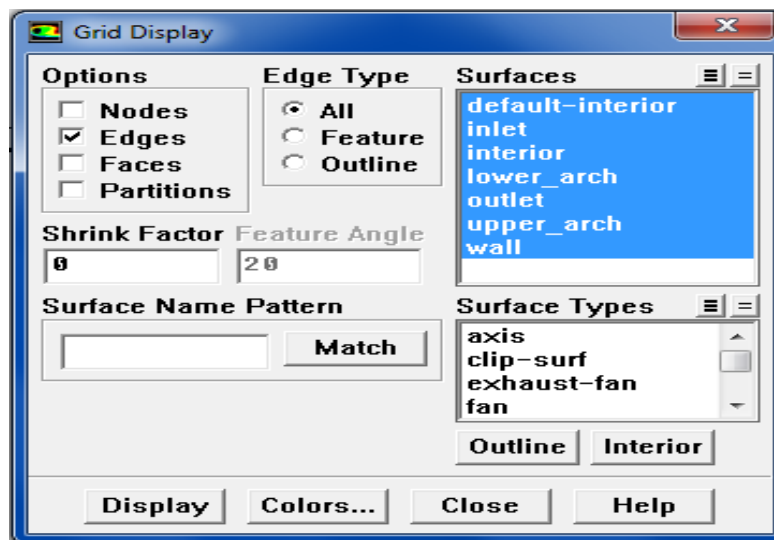


Figure 3.10Grid Display[15]



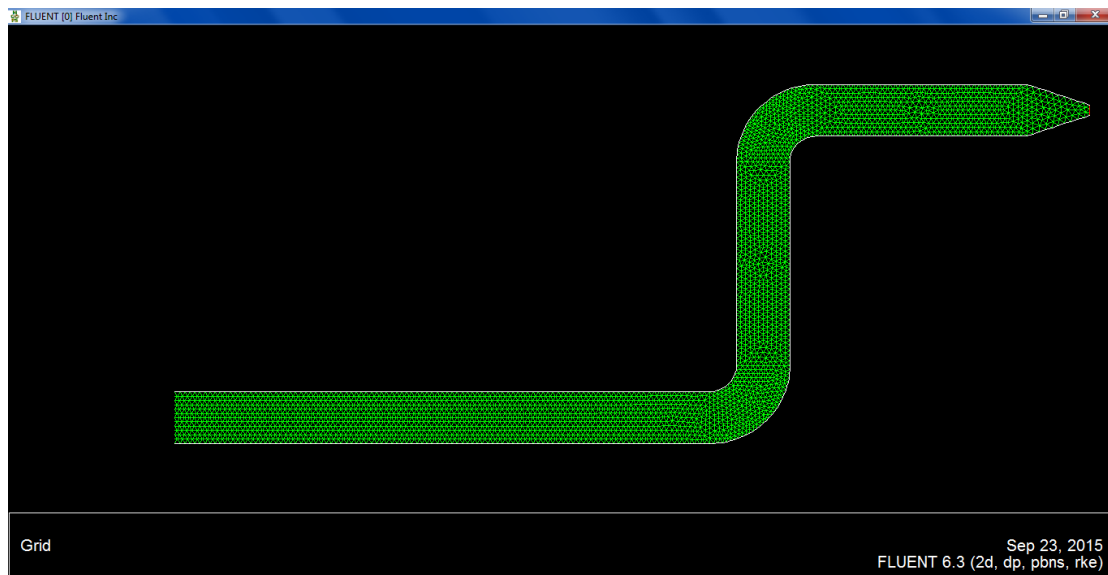


Figure 3.11 Grid [15]

## Step2: Models

1- Set the Solver settings.

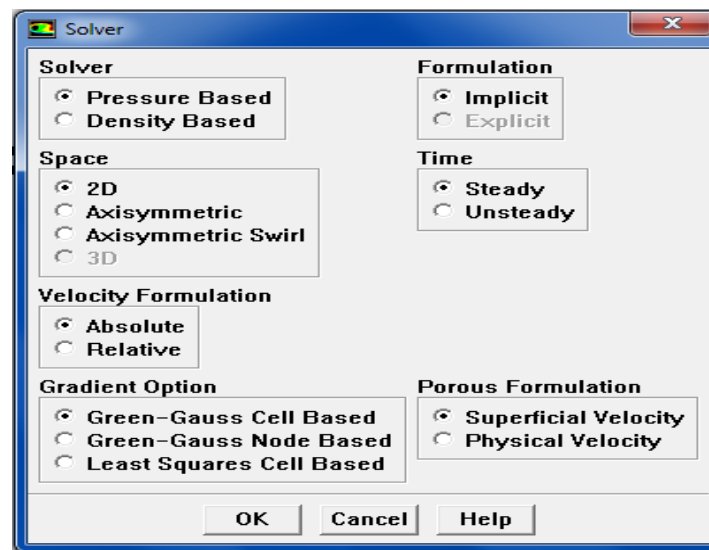
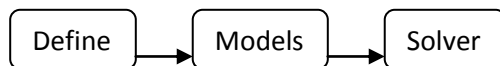


Figure 3.12 Solver[15]

2- Enable the energy equation.

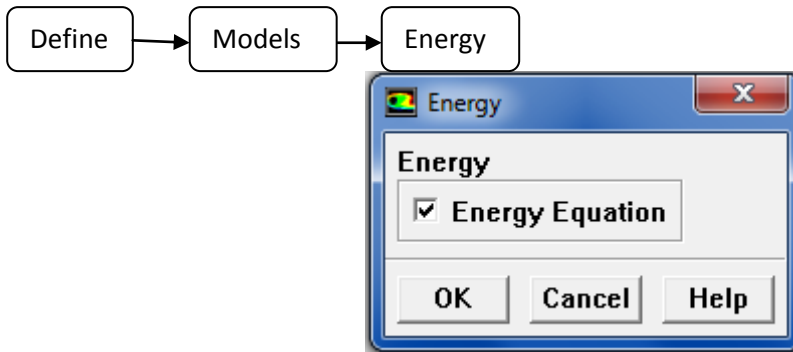


Figure 3.13 Energy[15]

3- Enable the K-epsilon turbulence model.

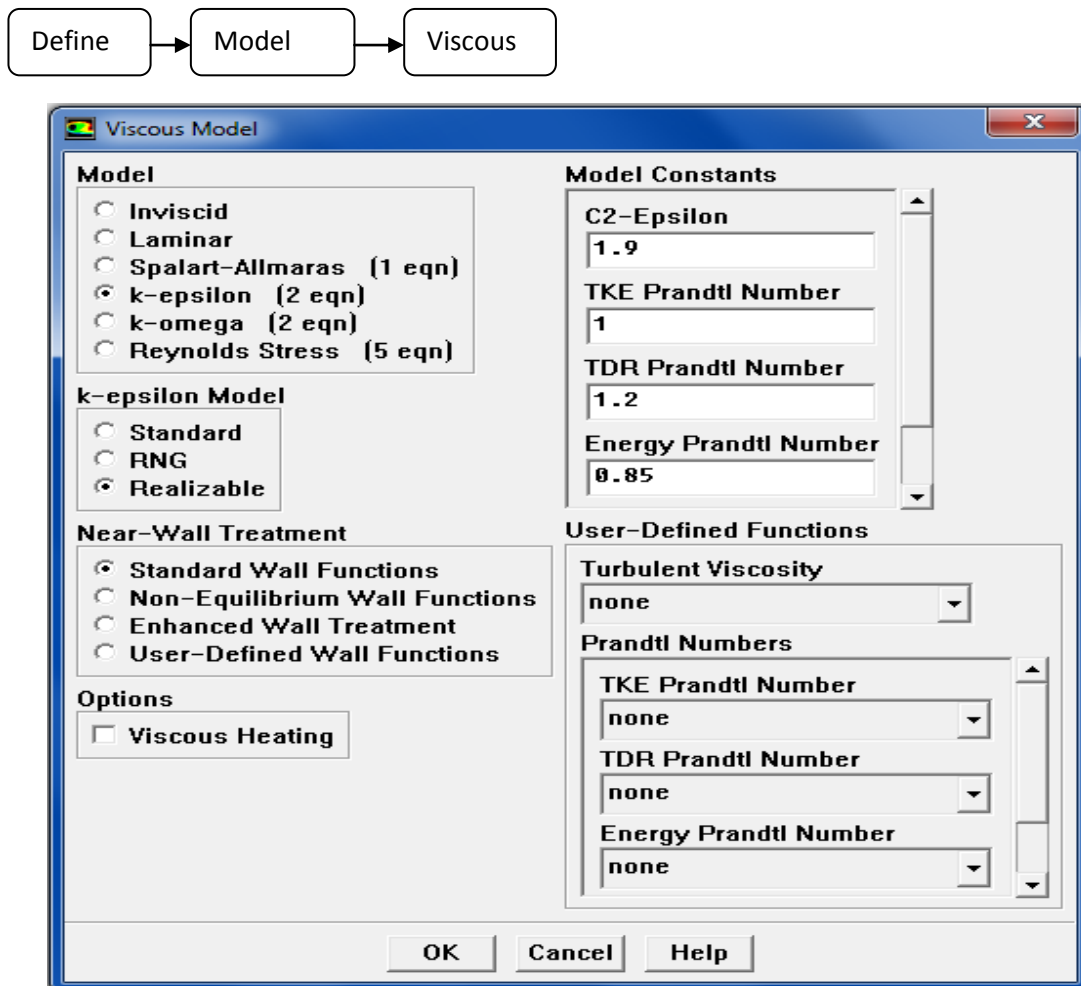
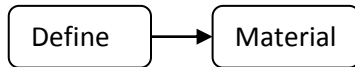


Figure 3.14 Viscous Model[15]

### Step3: Materials

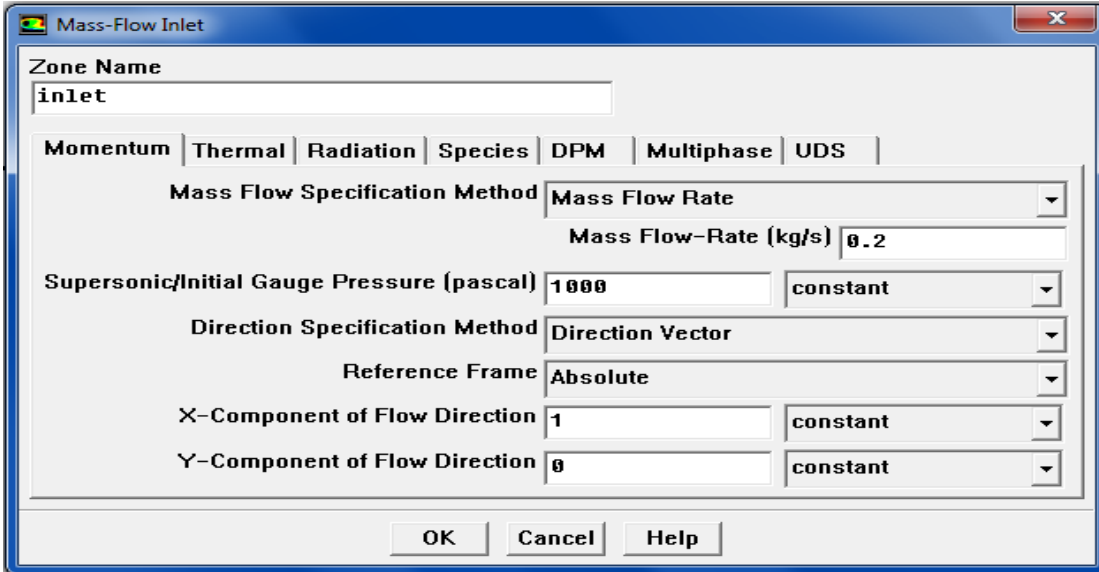
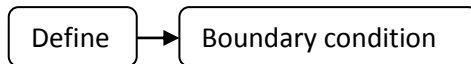
The default working fluid material is water vapour. The default settings need tube modified to account for compressibility and variations of the thermo physical properties with temperature.



The screenshot shows the 'Materials' dialog box in ANSYS Fluent. The 'Name' field is 'water-vapor' and the 'Chemical Formula' is 'h2o'. The 'Material Type' is 'fluid', and the 'Fluent Fluid Materials' dropdown is set to 'water-vapor (h2o)'. The 'Mixture' dropdown is set to 'none'. The 'Order Materials By' section has 'Name' selected. The 'Properties' section shows the following values: Density (kg/m3) is 'constant' with a value of '0.5542'; Cp (J/kg-K) is 'constant' with a value of '2014'; Thermal Conductivity (W/m-K) is 'constant' with a value of '0.0261'; and Viscosity (kg/m-s) is 'constant' with a value of '1.34e-05'. The 'Fluent Database...' and 'User-Defined Database...' buttons are visible on the right. At the bottom are 'Change/Create', 'Delete', 'Close', and 'Help' buttons.

Figure 3.15 Materials[15]

## Step4: Boundary condition



Mass-Flow Inlet

Zone Name: inlet

Momentum | Thermal | Radiation | Species | DPM | Multiphase | UDS

Mass Flow Specification Method: Mass Flow Rate

Mass Flow-Rate (kg/s): 0.2

Supersonic/Initial Gauge Pressure (pascal): 1000 constant

Direction Specification Method: Direction Vector

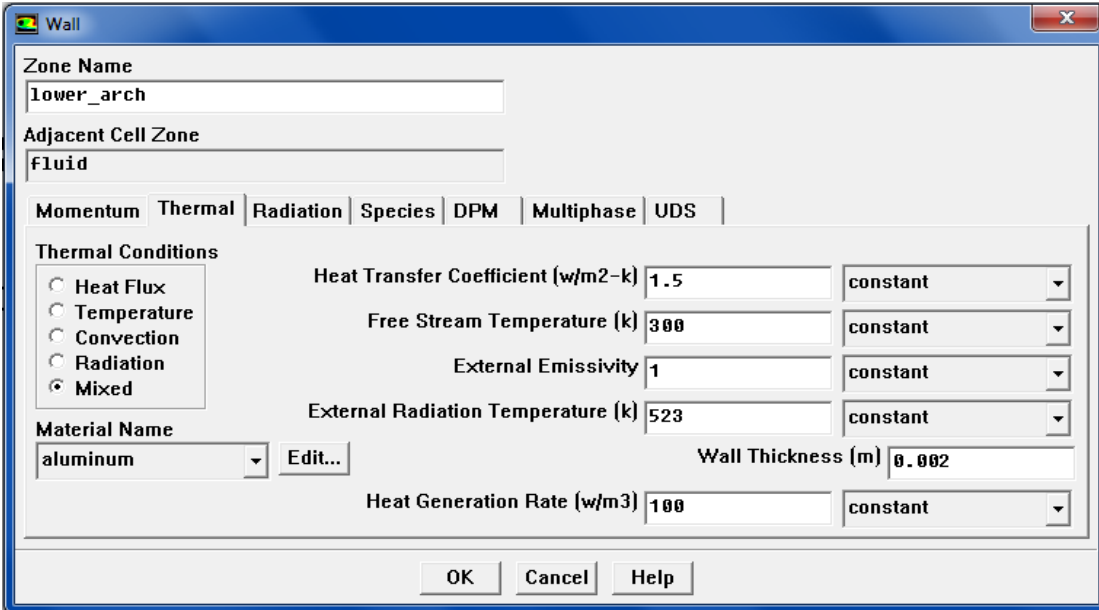
Reference Frame: Absolute

X-Component of Flow Direction: 1 constant

Y-Component of Flow Direction: 0 constant

OK Cancel Help

Figure 3.16 Boundary Condition for inlet [15]



Wall

Zone Name: lower\_arch

Adjacent Cell Zone: Fluid

Momentum | Thermal | Radiation | Species | DPM | Multiphase | UDS

Thermal Conditions

- ☐ Heat Flux
- ☐ Temperature
- ☐ Convection
- ☐ Radiation
- ☒ Mixed

Heat Transfer Coefficient (w/m2-k): 1.5 constant

Free Stream Temperature (k): 300 constant

External Emissivity: 1 constant

External Radiation Temperature (k): 523 constant

Material Name: aluminum Edit...

Wall Thickness (m): 0.002

Heat Generation Rate (w/m3): 100 constant

OK Cancel Help

Figure 3.17 Boundary Condition for lower arch [15]

Wall

Zone Name  
wall

Adjacent Cell Zone  
fluid

Momentum Thermal Radiation Species DPM Multiphase UDS

Thermal Conditions

☐ Heat Flux  
☐ Temperature  
☐ Convection  
☐ Radiation  
☒ Mixed

Heat Transfer Coefficient (w/m<sup>2</sup>-k) 1.5 constant

Free Stream Temperature (k) 300 constant

External Emissivity 1 constant

External Radiation Temperature (k) 350 constant

Material Name  
aluminum Edit...

Wall Thickness (m) 0.002

Heat Generation Rate (w/m<sup>3</sup>) 100 constant

OK Cancel Help

Figure 3.18 Boundary Condition for wall [15]

Wall

Zone Name  
upper\_arch

Adjacent Cell Zone  
fluid

Momentum Thermal Radiation Species DPM Multiphase UDS

Thermal Conditions

☐ Heat Flux  
☐ Temperature  
☐ Convection  
☐ Radiation  
☒ Mixed

Heat Transfer Coefficient (w/m<sup>2</sup>-k) 1.5 constant

Free Stream Temperature (k) 300 constant

External Emissivity 1 constant

External Radiation Temperature (k) 350 constant

Material Name  
aluminum Edit...

Wall Thickness (m) 0.002

Heat Generation Rate (w/m<sup>3</sup>) 100 constant

OK Cancel Help

Figure 3.19 Boundary Condition for upper arch [15]

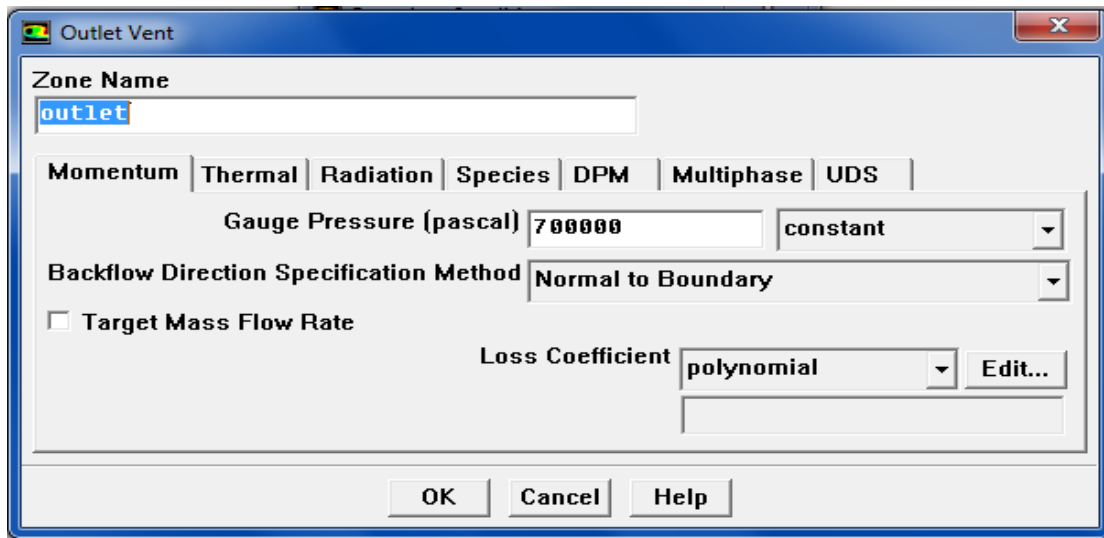


Figure 3.20 Boundary Condition for outlet [15]

## Step5: Solution

- 1- Enable the plotting of residuals during the calculation

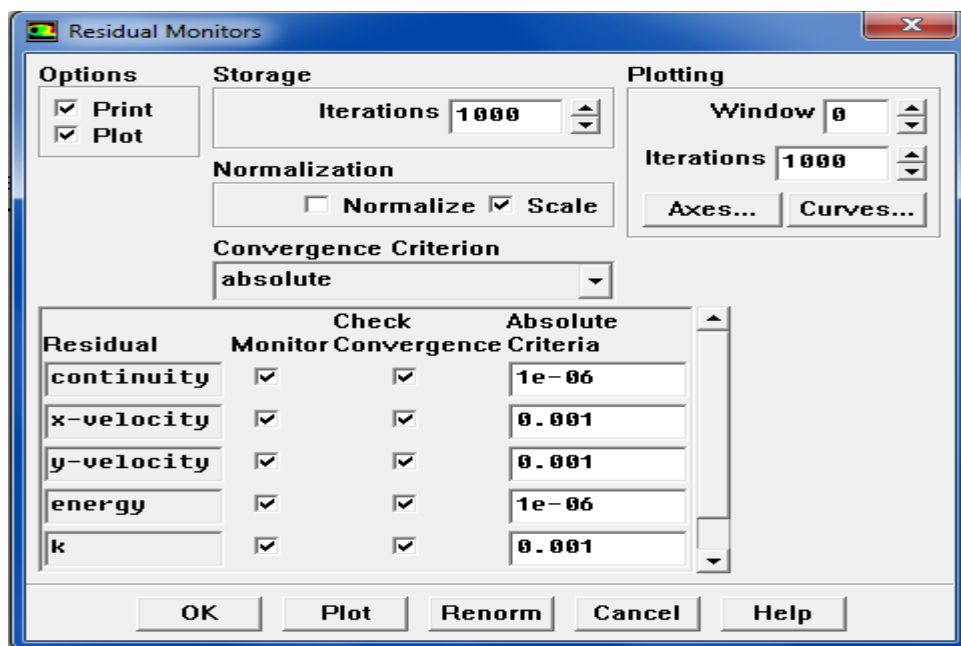


Figure 3.21Residual Monitors [15]

2- Initialize the flow.

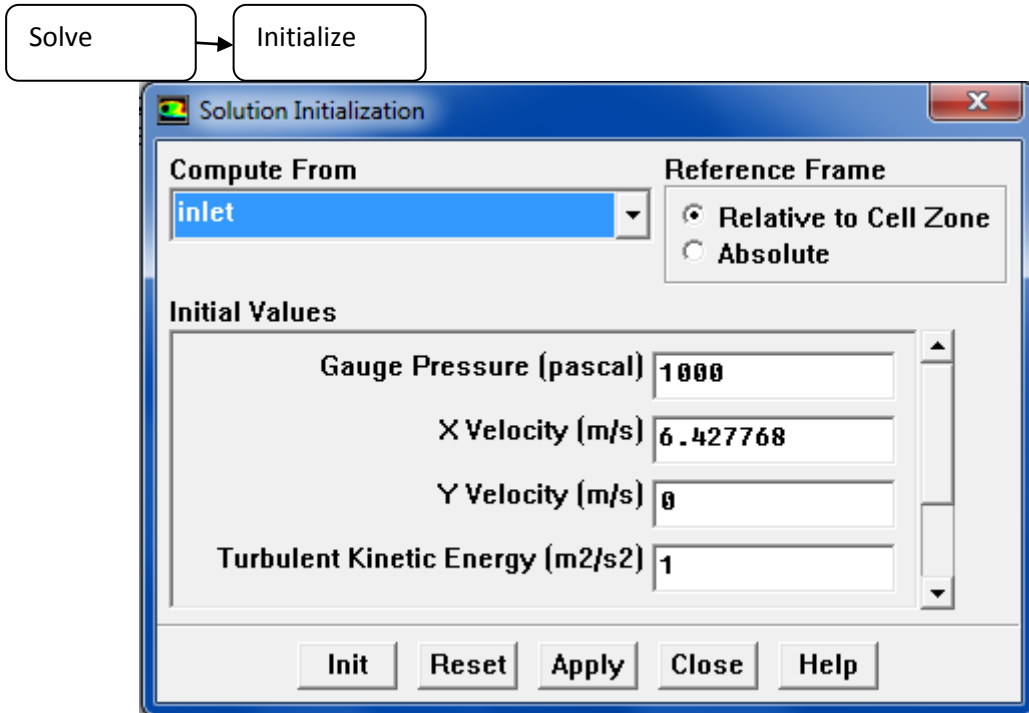


Figure 3.22 Initialize the flow [15]

3- Start the calculation by requesting 600 iterations.

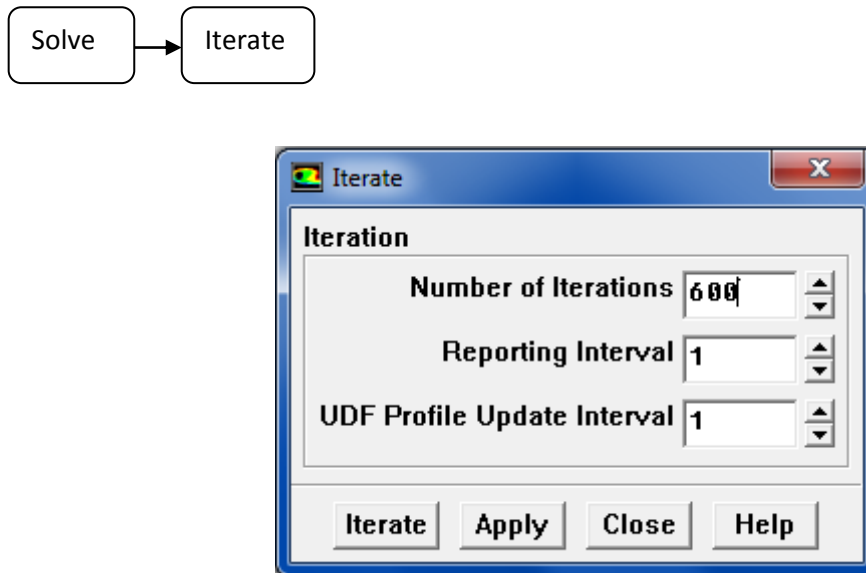


Figure 3.23 Iterate [15]

**Note:** The solution had been converged after 543 iterate.

### 3.15 experimental model

#### 3.15.A Design of experimental model

The shape of the parabolic had been studied and designed numerically with the following equation:

$$Y = \frac{X^2}{A}$$
$$A = 4 \cdot (F \cdot L)$$

Where:

Y: distance in y direction.      X: distance in x direction.

A: area of parabolic.      F.L: Focal Length.

In this design we assume that  $(F \cdot L = Y)$ , hence :

$Y = X^2/4$   $X=75$  ,  $y=37.5$  ,  $F.L=37.5$  ,  $A=150$  ,  $1/A=0.006666$

Table 3.2 parabolic chap

X	X <sup>2</sup>	Y		X	X <sup>2</sup>	Y
1	1	0.006666		24	576	3.84
2	4	0.0266		25	625	4.16
3	9	0.06		26	676	4.5
4	16	0.1		27	729	4.86
5	25	0.16		28	784	5.22
6	36	0.24		29	841	5.6
7	49	0.32		30	900	5.99
8	64	0.42		31	961	6.4
9	81	0.54		32	1024	6.82
10	100	0.66		33	1089	7.25
11	121	0.8		34	1156	7.7
12	144	0.96		35	1225	8.16
13	169	1.12		36	1296	8.64
14	196	1.3		37	1369	9.12
15	225	1.49		38	1444	9.62
16	256	1.7		39	1522	10.14



17	289	1.96		40	1600	10.66
18	324	2.16		41	1681	11.2
19	361	2.4		42	1764	11.76
20	400	2.66		43	1849	12.32
21	441	2.94		44	1936	12.9
22	484	3.22		45	2025	13.49
23	529	3.52		46	2116	14.1
X	X <sup>2</sup>	Y		X	X <sup>2</sup>	Y
47	2209	14.72		61	3721	24.8
48	2304	15.36		62	3844	25.62
49	2401	16		63	3969	26.45
50	2500	16.665		64	4096	27.3
51	2601	17.34		65	4225	28.16
52	2704	18.02		66	4356	29.03
53	2809	18.72		67	4489	29.90
54	2916	19.44		68	4624	30.82
55	3025	20.16		69	4761	31.73
56	3136	20.9		70	4900	32.66
57	3249	21.65		71	5041	33.6
58	3364	22.42		72	5184	34.55
59	3481	23.2		73	5329	35.5
60	3600	23.99		74	5476	36.5
				75	5625	37.498

The model had been built using the following parts:

- 1- Blank (board blex).
- 2- Stainless steel (grade 430).
- 3- STM pipe.
- 4- Pressure gauge (20 bar).
- 5- Check valve.
- 6- Control valve.



Figure 3.24 experimental model.

### 3.15.B Parameter of experimental model

Table 3.3 experimental parabolic trough collector parameters

Parameter founded	value
Length of parabolic <b>L</b>	120 cm
Aperture width of parabolic <b>W</b>	150 cm
Focal Length <b>f</b>	37.5 cm
Rim angle <b><math>\Psi</math></b>	90°
Receiver inner diameter <b>Dr. in</b>	1.305 cm
Receiver outer diameter <b>Dr. ext</b>	1.905 cm
Aperture area	0.0358m <sup>2</sup>
Height of Concentrator <b>h</b>	7 cm

### 3.12.C Devices of measurement

- A pyranometer is a type of action meter used to measure broadband solar irradiance on a planar surface and is a sensor that is designed to measure the solar radiation flux density  $\text{W/m}^2$  from a field of view of 180 degrees. The name pyranometer stems from Greek, "pyr- $\pi\rho$ " meaning fire and "ano-v $\omega$ " meaning above sky.



Figure 3.25 pyranometer and avometer.

- Pressure gauge:

It used to read the pressure inside the closed tube which equaled (1.2 bar).



Figure 3.26 pressure gauges.

- Thermometer (hioki):  
It used to read the temperature. And the temperature value of the out fluid (water) was ( $99^{\circ}\text{C}$  ).



Figure 3.27 thermometers (hioki)

# CHAPTER FOUR

## Results and discussion

The formulations of the model discussed in the previous section were programmed using **MATLAB** R2010b and the program outputs were print below.

### 4.1 The number of day in year

Table 4.1 below shown the standard value of the day of the year for all years and the program outputs results for al month and specified day 15 as the average and specified year 2015.

Table 4.1 the number of day in year

<b>Month</b>	<b>standard Day No. in the year</b>	<b>Program output Day No. in the year for 2015</b>
January	17	15
February	47	46
March	75	74
April	105	105
May	135	135
June	162	166
July	198	196
August	228	227
September	258	258
October	288	289
November	318	319
December	344	349

The program to find the number of day in year **N** only need to input specified month, specified day and specified year and it print the value of **N**.

## 4.2 Results for horizontal surface

The program to calculate the solar radiation in horizontal surface only requires the day number of the year, apparent solar irradiation and the atmospheric extinction coefficient. The value of latitude angle is constant which equal to the latitude of the Khartoum  $15.9667^\circ$ , and the ground reflectivity assumed 20%. The program returns to a table of the day number to input new value which presents the average value of the month.

Table 4.2 below shown the results of the written program for 15 January 2015 in this specified Date the value of N equal 15 , result of equation of time is equal to -6.6034 and the declination angle equal to -0.3715 radian .

Hour s  LSt T	Solar time LST	Hour angle h	altitude angle $\beta$	zenith angle $\psi$	azimuth angle $\gamma$	Air mass ratio m	Direct radiation Idn	Diffuse radiation Id	beam radiation Ib	Total radiation It
7	6.6922	1.3896	0.0589	1.5119	-0.3658	16.983	30.5143	4.1194	1.7967	5.9161
8	7.6922	1.1278	0.2815	1.2893	-0.3484	3.6001	507.0960	68.4580	140.8570	209.3149
9	8.6922	0.8660	0.4779	1.0929	-0.3167	2.1745	684.0826	92.3512	314.5981	406.9493
10	9.6922	0.6042	0.6347	0.9361	-0.2590	1.6865	757.8965	102.3160	449.3845	551.7005
11	10.6922	0.3424	0.7413	0.8295	-0.1660	1.4809	791.3323	106.8299	534.3431	641.1730
12	11.6922	0.0806	0.7904	0.7804	-0.0416	1.4072	803.6808	108.4969	571.1163	679.6133
13	12.6922	-0.1812	0.7786	0.7922	0.0920	1.4239	800.8711	108.1176	562.4541	670.5717
14	13.6922	-0.4430	0.7068	0.8640	0.2061	1.5398	781.6050	105.5167	507.5878	613.1044
15	14.6922	-0.7048	0.5799	0.9909	0.2850	1.8251	736.1510	99.3804	403.3377	502.7181
16	15.6922	-0.9666	0.4064	1.1644	0.3313	2.5298	634.8965	85.7110	250.9688	336.6798
17	16.6922	-1.2284	0.1982	1.3726	0.3563	5.0777	371.8147	50.1950	73.2248	123.4198

Table 4.3 below shown the results of the written program for 15 February 2015 in this specified Date the value of N equal 46 , result of equation of time is equal to -14.2119 and the declination angle equal to -0.2321 radian .

Hours <b>LST</b>	Solar time <b>LST</b>	Hour angle <b>h</b>	altitude angle $\beta$	zenith angle $\psi$	azimuth angle $\gamma$	Air mass ratio <b>m</b>	Direct radiation <b>Idn</b>	Diffuse radiation <b>Id</b>	beam radiation <b>Ib</b>	Total radiation <b>It</b>
7	6.5654	1.4228	0.0730	1.4978	-0.2302	13.7094	61.2501	8.2688	4.4678	12.7365
8	7.5654	1.1610	0.3078	1.2630	-0.2233	3.3005	545.0177	73.5774	165.1296	238.7070
9	8.5654	0.8992	0.5172	1.0536	-0.2087	2.0224	712.8244	96.2313	352.4696	448.7009
10	9.5654	0.6374	0.6870	0.8838	-0.1780	1.5768	782.7390	105.6698	496.4014	602.0711
11	10.5654	0.3756	0.8054	0.7654	-0.1221	1.3867	814.6235	109.9742	587.4549	697.4291
12	11.5654	-0.1138	0.8646	0.7062	-0.0403	1.3143	827.0983	111.6583	629.2925	740.9507
13	12.5654	-0.1480	0.8604	0.7104	0.0520	1.3190	826.2801	111.5478	626.4236	737.9715
14	13.5654	-0.4098	0.7932	0.7776	0.1310	1.4033	811.7847	109.5909	578.4733	688.0642
15	14.5654	-0.6716	0.6675	0.9033	0.1833	1.6155	776.4046	104.8146	480.5911	585.4057
16	15.5654	-0.9334	0.4918	1.0790	0.2113	2.1176	698.7115	94.3261	329.9552	424.2812
17	16.5654	-1.1952	0.2782	1.2926	0.2245	3.6408	507.4294	68.5030	139.3717	207.8747

Table 4.4 below shown the results of the written program for 15 March 2015 in this specified Date the value of N equal 74 , result of equation of time is equal to -11.4957 and the declination angle equal to -0.0492 radian .

Hours <b>LST</b>	Solar time <b>LST</b>	Hour angle <b>h</b>	altitude angle $\beta$	zenith angle $\psi$	azimuth angle $\gamma$	Air mass ratio <b>m</b>	Direct radiation <b>Idn</b>	Diffuse radiation <b>Id</b>	beam radiation <b>Ib</b>	Total radiation <b>It</b>
7	6.6106	1.4109	0.1390	1.4318	-0.0491	7.2198	447.64	60.432	62.002	122.43
8	7.6106	1.1491	0.3791	1.1917	-0.0484	2.7020	842.6	113.75	311.84	425.59
9	8.6106	0.8873	0.5925	0.9783	-0.0460	1.7908	957.25	129.23	534.55	663.78
10	9.6106	0.6255	0.7645	0.8063	-0.0399	1.4447	1004.8	135.64	695.5	831.15
11	10.6106	0.3637	0.8835	0.6873	-0.0276	1.2937	1026.2	138.54	793.26	931.81
12	11.6106	0.1019	0.9414	0.6294	-0.0085	1.2371	1034.4	139.64	836.18	975.82
13	12.6106	-0.1599	0.9341	0.6367	0.0132	1.2437	1033.4	139.52	830.97	970.48
14	13.6106	-0.4217	0.8622	0.7085	0.0310	1.3170	1022.9	138.09	776.69	914.78
15	14.6106	-0.6835	0.7307	0.8401	0.0417	1.4984	997.24	134.63	665.53	800.16
16	15.6106	-0.9453	0.5484	1.0224	0.0468	1.9183	940.31	126.94	490.17	617.11
17	16.6106	-1.2071	0.3277	1.2431	0.0486	3.1066	796.19	107.49	256.29	363.78

Table 4.5 below shown the results of the written program for 15 April 2015 in this specified Date the value of N equal 105 , result of equation of time is equal to -2.3111 and the declination angle equal to 0.16446 radian .



<i>Hou rs LStT</i>	<i>Solar time LST</i>	<i>Hour angle h</i>	<i>altitude angle <math>\beta</math></i>	<i>zenith angle <math>\psi</math></i>	<i>azimuth angle <math>\gamma</math></i>	<i>Air mass ratio m</i>	<i>Direct radiation Idn</i>	<i>Diffuse radiation Id</i>	<i>beam radiation Ib</i>	<i>Total radiation It</i>
7	6.7637	1.3709	0.23461	1.3362	0.16574	4.3018	678.99	91.664	157.84	249.5
8	7.7637	1.1091	0.46877	1.102	0.16505	2.2134	909.59	122.79	410.94	533.74
9	8.7637	0.84726	0.67415	0.89665	0.15772	1.602	990.88	133.77	618.54	752.3
10	9.7637	0.58546	0.83673	0.73407	0.13546	1.3469	1026.9	138.63	762.43	901.06
11	10.764	0.32366	0.94544	0.62536	0.089067	1.2334	1043.3	140.85	845.9	986.75
12	11.764	0.061862	0.99287	0.57793	0.018529	1.1939	1049.1	141.63	878.75	1020.4
13	12.764	-0.19994	0.97579	0.595	-0.058044	1.2075	1047.1	141.36	867.18	1008.5
14	13.764	-0.46174	0.89536	0.67543	-0.11692	1.2813	1036.4	139.91	808.82	948.73
15	14.764	-0.72354	0.75707	0.81373	-0.14968	1.456	1011.3	136.53	694.58	831.11
16	15.764	-0.98534	0.57033	1.0005	-0.16283	1.8521	956.77	129.16	516.57	645.74
17	16.764	-1.2471	0.34788	1.2229	-0.16587	2.9334	822.38	111.02	280.35	391.37

Table 4.6 below shown the results of the written program for 15 May 2015 in this specified Date the value of N equal 135 , result of equation of time is equal to 3.7109 and the declination angle equal to 0.32826 radian .

<i>Hou rs LStT</i>	<i>Solar time LST</i>	<i>Hour angle h</i>	<i>altitude angle <math>\beta</math></i>	<i>zenith angle <math>\psi</math></i>	<i>azimuth angle <math>\gamma</math></i>	<i>Air mass ratio m</i>	<i>Direct radiation Idn</i>	<i>Diffuse radiation Id</i>	<i>beam radiation Ib</i>	<i>Total radiation It</i>
7	6.8641	1.3446	0.29517	1.2756	0.33459	3.4376	778.69	105.12	226.52	331.64
8	7.8641	1.0828	0.51776	1.053	0.33389	2.0205	949.56	128.19	469.97	598.16
9	8.8641	0.82098	0.71127	0.85952	0.31672	1.5319	1016.8	137.27	663.76	801.03
10	9.8641	0.55918	0.86252	0.70828	0.26604	1.3167	1047.9	141.46	795.85	937.32
11	10.864	0.29739	0.96119	0.60961	0.16576	1.2197	1062.2	143.4	870.88	1014.3
12	11.864	0.03558	1.0006	0.57024	0.02125	1.188	1066.9	144.04	898.12	1042.2
13	12.864	0.22621	0.97795	0.59285	-0.12978	1.2058	1064.3	143.68	882.67	1026.3
14	13.864	0.48801	0.8949	0.6759	-0.24404	1.2818	1053	142.16	821.5	963.66
15	14.864	0.74981	0.75706	0.81373	-0.30708	1.456	1027.6	138.73	705.77	844.51
16	15.864	1.0116	0.57384	0.99695	-0.33145	1.8421	973.58	131.43	528.52	659.95
17	16.864	1.2734	0.35772	1.2131	-0.33533	2.856	844.74	114.04	295.78	409.82

Table 4.7 below shown the results of the written program for 15 June 2015 in this specified Date the value of N equal 166 , result of equation of time is equal to 1.8665 and the declination angle equal to 0.40726 radian .

Hour s <i>LStT</i>	<i>Solar time LST</i>	<i>Hour angle h</i>	<i>altitude angle <math>\beta</math></i>	<i>zenith angle <math>\psi</math></i>	<i>azimuth angle <math>\gamma</math></i>	<i>Air mass ratio m</i>	<i>Direct radiation <math>I_{dn}</math></i>	<i>Diffuse radiation <math>I_d</math></i>	<i>beam radiation <math>I_b</math></i>	<i>Total radiation <math>I_t</math></i>
7	6.8333	1.3526	0.30293	1.2679	0.41715	3.3521	775.55	104.7	231.36	336.06
8	7.8333	1.0908	0.51949	1.0513	0.41669	2.0144	935.29	126.26	464.31	590.57
9	8.8333	0.82903	0.70826	0.86253	0.39468	1.5372	999.9	134.99	650.45	785.43
10	9.8333	0.56723	0.8564	0.7144	0.33084	1.3237	1030.2	139.08	778.34	917.42
11	10.833	0.30543	0.95379	0.61701	0.20734	1.2261	1044.4	141.0	851.84	992.84
12	11.833	0.043634	0.99381	0.57699	0.031678	1.1932	1049.2	141.65	879.38	1021
13	12.833	-0.21817	0.97372	0.59707	-0.15308	1.2092	1046.9	141.33	865.76	1007.1
14	13.833	-0.47996	0.8949	0.67589	-0.29669	1.2818	1036.3	139.9	808.47	948.37
15	14.833	-0.74176	0.76272	0.80808	-0.37916	1.4474	1012.6	136.69	699.56	836.26
16	15.833	-1.0036	0.58618	0.98461	-0.41262	1.8077	962.74	129.97	532.58	662.55
17	16.833	-1.2654	0.37732	1.1935	-0.41845	2.7142	848.76	114.48	312.43	426.9

Table 4.8 below shown the results of the written program for 15 July 2015 in this specified Date the value of N equal 196 , result of equation of time is equal to -3.8526 and the declination angle equal to 0.37301 radian .

Hour s <i>LSt T</i>	<i>Solar time LST</i>	<i>Hour angle h</i>	<i>altitude angle <math>\beta</math></i>	<i>zenith angle <math>\psi</math></i>	<i>azimuth angle <math>\gamma</math></i>	<i>Air mass ratio m</i>	<i>Direct radiation <math>I_{dn}</math></i>	<i>Diffuse radiation <math>I_d</math></i>	<i>beam radiatio n <math>I_b</math></i>	<i>Total radiation <math>I_t</math></i>
7	6.738	1.3776	0.27483	1.296	0.38071	3.6849	731.29	98.724	198.46	297.18
8	7.738	1.1158	0.49638	1.0744	0.38145	2.0998	912.99	123.25	434.81	558.06
9	8.738	0.85399	0.69112	0.87968	0.36458	1.5689	983.44	132.76	626.84	759.61
10	9.738	0.59219	0.84577	0.72502	0.31176	1.336	1016	137.16	760.48	897.64
11	10.738	0.33039	0.9498	0.62099	0.20461	1.2296	1031.3	139.22	838.74	977.97
12	11.738	0.068588	0.99612	0.57468	0.04596	1.1914	1036.8	139.97	870.27	1010.2
13	12.738	-0.19321	0.98157	0.58923	-0.12625	1.2028	1035.1	139.74	860.59	1000.3
14	13.738	-0.45501	0.90713	0.66366	-0.26301	1.2695	1025.5	138.45	807.86	946.31
15	14.738	-0.71681	0.77789	0.7929	-0.34275	1.4249	1003.5	135.47	704.21	839.67
16	15.738	-0.97861	0.60266	0.96814	-0.37581	1.7642	956.91	129.18	542.41	671.59
17	16.738	-1.2404	0.39336	1.1774	-0.38247	2.6089	850.18	114.77	325.87	440.64

Table 4.9 below shown the results of the written program for 15 August 2015 in this specified Date the value of N equal 227 , result of equation of time is equal to -4.7156 and the declination angle equal to 0.37301 radian .

Hours LSiT	Solar time LST	Hour angle h	altitude angle $\beta$	zenith angle $\psi$	azimuth angle $\gamma$	Air mass ratio m	Direct radiation Idn	Diffuse radiation Id	beam radiation Ib	Total radiation It
7	6.7236	1.3814	0.24317	1.3276	0.24369	4.1532	620.59	83.78	149.43	233.2
8	7.7236	1.1196	0.47451	1.0963	0.24364	2.1886	817.05	110.3	373.31	483.62
9	8.7236	0.85775	0.6781	0.89269	0.23372	1.5941	887.97	119.88	557.04	676.92
10	9.7236	0.59595	0.84008	0.73072	0.20191	1.3428	919.77	124.17	684.94	809.11
11	10.724	0.33415	0.94939	0.62141	0.13474	1.2299	934.42	126.15	759.74	885.88
12	11.724	0.072354	0.99859	0.57221	0.03184	1.1895	939.73	126.86	790.03	916.9
13	12.724	-0.18945	0.98433	0.58647	-0.081228	1.2006	938.26	126.67	781.48	908.14
14	13.724	-0.45125	0.90757	0.66322	-0.16972	1.269	929.32	125.46	732.31	857.77
15	14.724	-0.71304	0.77356	0.79724	-0.21979	1.4313	908.45	122.64	634.72	757.36
16	15.724	-0.97484	0.59142	0.97938	-0.24002	1.7936	863.52	116.57	481.44	598.02
17	16.724	-1.2366	0.37356	1.1972	-0.24438	2.7402	756.34	102.11	276.01	378.12

Table 4.10 below shown the results of the written program for 15 September 2015 in this specified Date the value of N equal 258 , result of equation of time is equal to 2.7207 and the declination angle equal to 0.038725 radian .

Hours LSiT	Solar time LST	Hour angle h	altitude angle $\beta$	zenith angle $\psi$	azimuth angle $\gamma$	Air mass ratio m	Direct radiation Idn	Diffuse radiation Id	beam radiation Ib	Total radiation It
7	6.8476	1.3489	0.22236	1.3484	0.038729	4.5345	424.08	57.251	93.523	150.77
8	7.8476	1.0871	0.45771	1.1131	0.038216	2.263	683.3	92.245	301.94	394.19
9	8.8476	0.82531	0.66261	0.90819	0.036089	1.6256	781.17	105.46	480.56	586.01
10	9.8476	0.56351	0.8231	0.7477	0.030418	1.3638	825.31	111.42	605.17	716.58
11	10.848	0.30171	0.92824	0.64256	0.019199	1.2491	845.43	114.13	676.82	790.95
12	11.848	0.039907	0.97087	0.59993	0.0027358	1.2116	852.12	115.04	703.32	818.36
13	12.848	-0.22189	0.94808	0.62272	-0.014609	1.2311	848.64	114.57	689.34	803.91
14	13.848	-0.48369	0.86143	0.70937	-0.027645	1.3179	833.3	112.5	632.29	744.78
15	14.848	-0.74549	0.71681	0.85398	-0.034842	1.5221	798.32	107.77	524.49	632.26
16	15.848	-1.0073	0.5241	1.0467	-0.037813	1.9983	722.35	97.518	361.49	459.01
17	16.848	-1.2691	0.29641	1.2744	-0.038662	3.4237	535.49	72.291	156.41	228.7

Table 4.11 below shown the results of the written program for 15 October 2015 in this specified Date the value of N equal 289 , result of equation of time is equal to 12.602 and the declination angle equal to -0.17409 radian .

Hour s LSiT	Solar time LST	Hour angle h	altitude angle $\beta$	zenith angle $\psi$	azimuth angle $\gamma$	Air mass ratio m	Direct radiation Idn	Diffuse radiation Id	beam radiation Ib	Total radiation It
7	7.0123	1.3058	0.19909	1.3717	-0.17137	5.0562	370.04	49.955	73.184	123.14
8	8.0123	1.044	0.42716	1.1436	-0.16526	2.4138	644.53	87.011	267.02	354.03
9	9.0123	0.78219	0.62278	0.94802	-0.15088	1.7144	746.5	100.78	435.43	536.2
10	10.012	0.52039	0.77263	0.79817	-0.12057	1.4326	792	106.92	552.83	659.75
11	11.012	0.25859	0.86649	0.70431	-0.068461	1.3122	812.28	109.66	619.01	728.66
12	12.012	-0.003207	0.89797	0.67283	0.0008916	1.2787	818.02	110.43	639.75	750.18
13	13.012	-0.26501	0.86492	0.70588	0.069993	1.314	811.98	109.62	617.95	727.57
14	14.012	-0.52681	0.76959	0.80121	0.12156	1.4371	791.26	106.82	550.59	657.41
15	15.012	-0.78861	0.61848	0.95231	0.15139	1.7247	744.88	100.56	431.88	532.44
16	16.012	-1.0504	0.42189	1.1489	0.16548	2.4421	640.71	86.496	262.36	348.86
17	17.012	-1.3122	0.19322	1.3776	0.17147	5.2078	358.45	48.39	68.829	117.22

Table 4.12 below shown the results of the written program for 15 November 2015 in this specified Date the value of N equal 319 , result of equation of time is equal to 15.044 and the declination angle equal to -0.33448 radian .

Hours <i>LStT</i>	Solar time <i>LST</i>	Hour angle <i>h</i>	altitude angle $\beta$	zenith angle $\psi$	azimuth angle $\gamma$	Air mass ratio <i>m</i>	Direct radiation <i>Idn</i>	Diffuse radiation <i>Id</i>	beam radiation <i>Ib</i>	Total radiation <i>It</i>
7	7.053	1.2951	0.15448	1.4163	-0.3254	6.4993	275.85	37.24	42.443	79.683
8	8.053	1.0333	0.37222	1.1986	-0.30755	2.7496	606.25	81.844	220.49	302.33
9	9.053	0.77153	0.55829	1.0125	-0.27325	1.8877	726.54	98.083	384.87	482.95
10	10.053	0.50973	0.69999	0.87081	-0.21099	1.5523	779.56	105.24	502.2	607.44
11	11.053	0.24793	0.78766	0.78313	-0.11444	1.411	803.04	108.41	569.12	677.53
12	12.053	-0.013866	0.81535	0.75545	0.006638	1.3737	809.36	109.26	589.18	698.45
13	13.053	-0.27567	0.78115	0.78965	0.12616	1.4203	801.48	108.2	564.32	672.52
14	14.053	-0.53746	0.68739	0.8834	0.2192	1.576	775.7	104.72	492.2	596.92
15	15.053	-0.79926	0.54048	1.0303	0.27801	1.9435	718.09	96.942	369.49	466.43
16	16.053	-1.0611	0.35041	1.2204	0.31003	2.913	585.8	79.083	201.1	280.18
17	17.053	-1.3229	0.13015	1.4406	0.32673	7.7051	214.14	28.909	27.792	56.701

Table 4.13 below shown the results of the written program for 15 December 2015 in this specified Date the value of N equal 349 , result of equation of time is equal to 6.8438 and the declination angle equal to -0.40762 radian .

Hours <i>LStT</i>	Solar time <i>LST</i>	Hour angle <i>h</i>	altitude angle $\beta$	zenith angle $\psi$	azimuth angle $\gamma$	Air mass ratio <i>m</i>	Direct radiation <i>Idn</i>	Diffuse radiation <i>Id</i>	beam radiation <i>Ib</i>	Total radiation <i>It</i>
7	6.9163	1.3309	0.097752	1.473	-0.39729	10.246	123.26	16.64	12.03	28.67
8	7.9163	1.0691	0.31251	1.2583	-0.37392	3.2526	535.38	72.277	164.6	236.88
9	8.9163	0.80731	0.49834	1.0725	-0.33212	2.0922	683.12	92.221	326.51	418.73
10	9.9163	0.54552	0.64259	0.92821	-0.25985	1.6687	746.65	100.8	447.44	548.24
11	10.916	0.28372	0.73541	0.83539	-0.15021	1.4906	775.11	104.64	520.01	624.65
12	11.916	0.021917	0.77048	0.80032	-0.012107	1.4358	784.08	105.85	546.09	651.95
13	12.916	-0.23988	0.74542	0.82538	0.12853	1.4743	777.76	105	527.54	632.54
14	13.916	-0.50168	0.66193	0.90887	0.2441	1.627	753.22	101.68	462.96	564.64
15	14.916	-0.76348	0.5257	1.0451	0.32246	1.9928	697.53	94.167	350.03	444.2
16	15.916	-1.0253	0.34601	1.2248	0.36853	2.9485	570.68	77.042	193.55	270.59
17	16.916	-1.2871	0.13512	1.4357	0.39421	7.4234	222.99	30.103	30.038	60.141

The results show in figures (4.1) to (4.12) respectively, shown the relation between hours of the day and solar flux for one year 2015, It is seen that, as expected, the solar radiation component starts to increase from morning hours reaching a peak value at noon and gradually decreases towards sunset time. The direct component is much greater than the diffuse component except during early and late times of the day. This is due to the fact that during these hours the solar altitude is very low( longer path of the solar ray) , and much of the solar radiation is depleted by atmospheric components through scattering and absorption processes. The results also indicated that the maximum value of solar radiation reaching the earth surface occurs during mid day very close to noon Time, The highest values of total solar radiation occur during summer solstice while lower values occur winter solstice. The figure 4.1 showed the relation between hours of the day and solar flux for 15 January 2015.

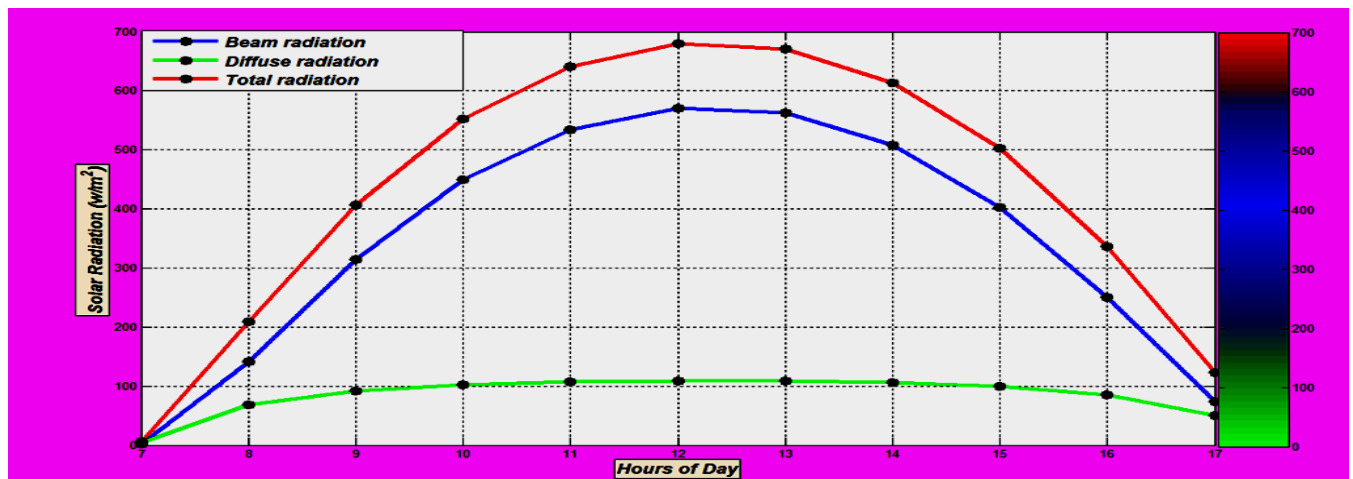


figure 4.1 Direct, diffuse, and total solar radiation components during 15 January 2015.

The figure 4.2 shown the relation between hours of the day and solar flux for 15 February 2015.

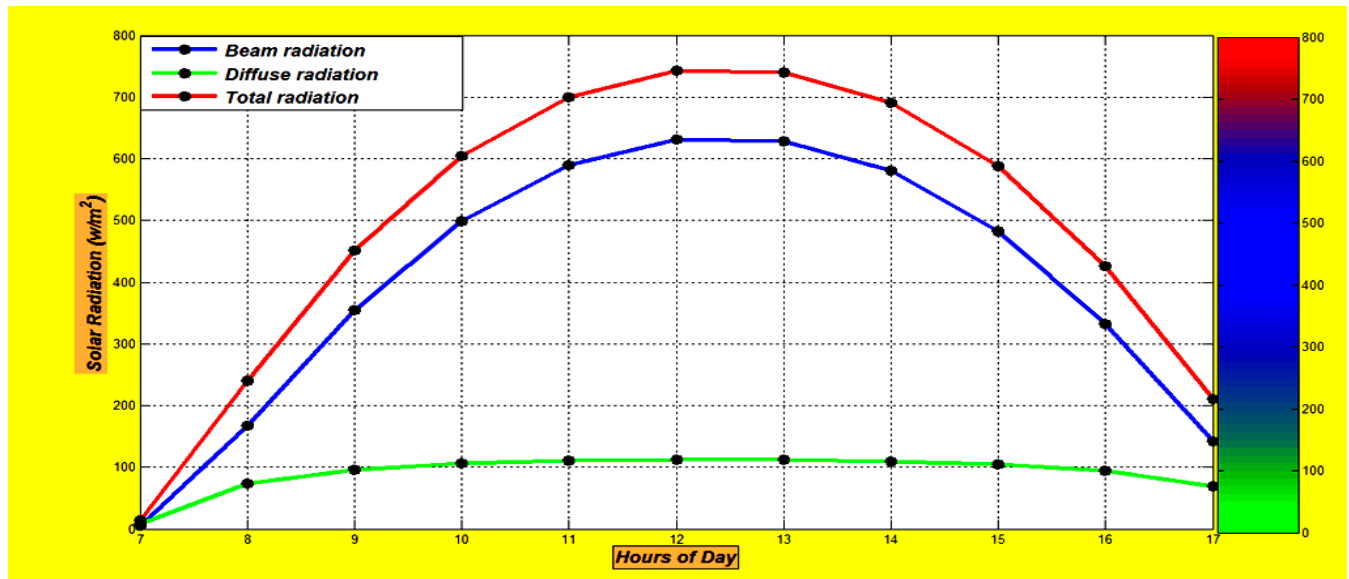


figure 4.2 Direct, diffuse, and total solar radiation components during 15 February 2015.

The figure 4.3 shown the relation between hours of the day and solar flux for 15 March 2015.

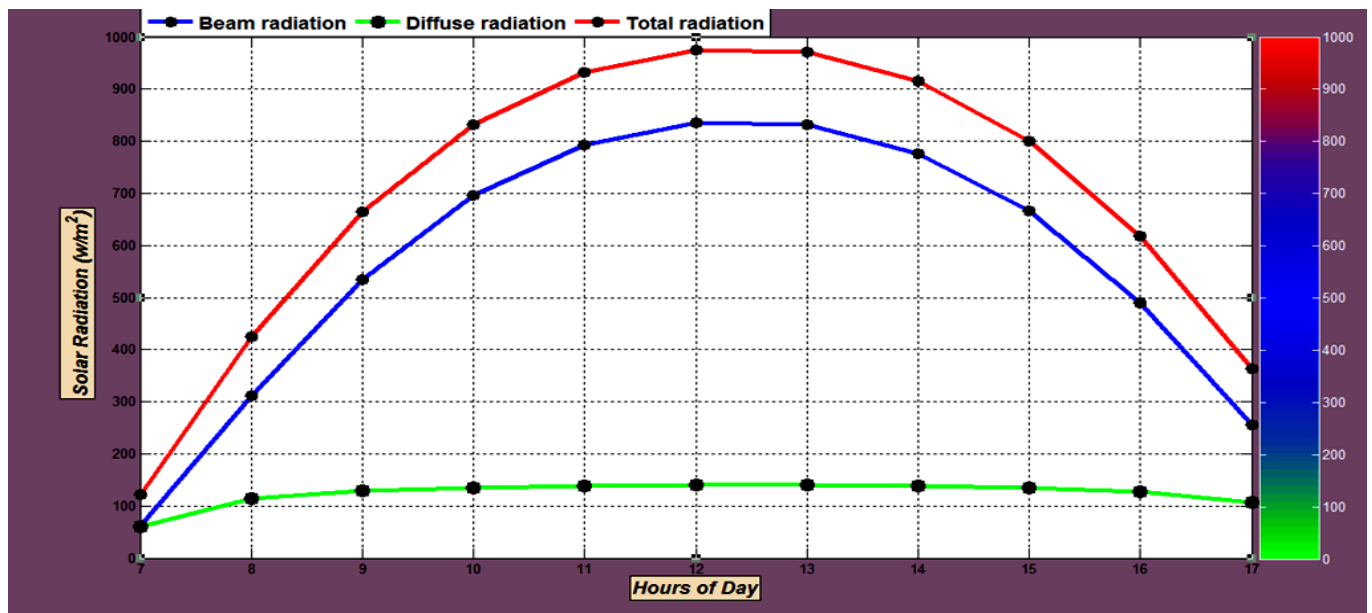


figure 4.3 Direct, diffuse, and total solar radiation components during 15 March 2015

The figure 4.4 shown the relation between hours of the day and solar flux for 15 April 2015.

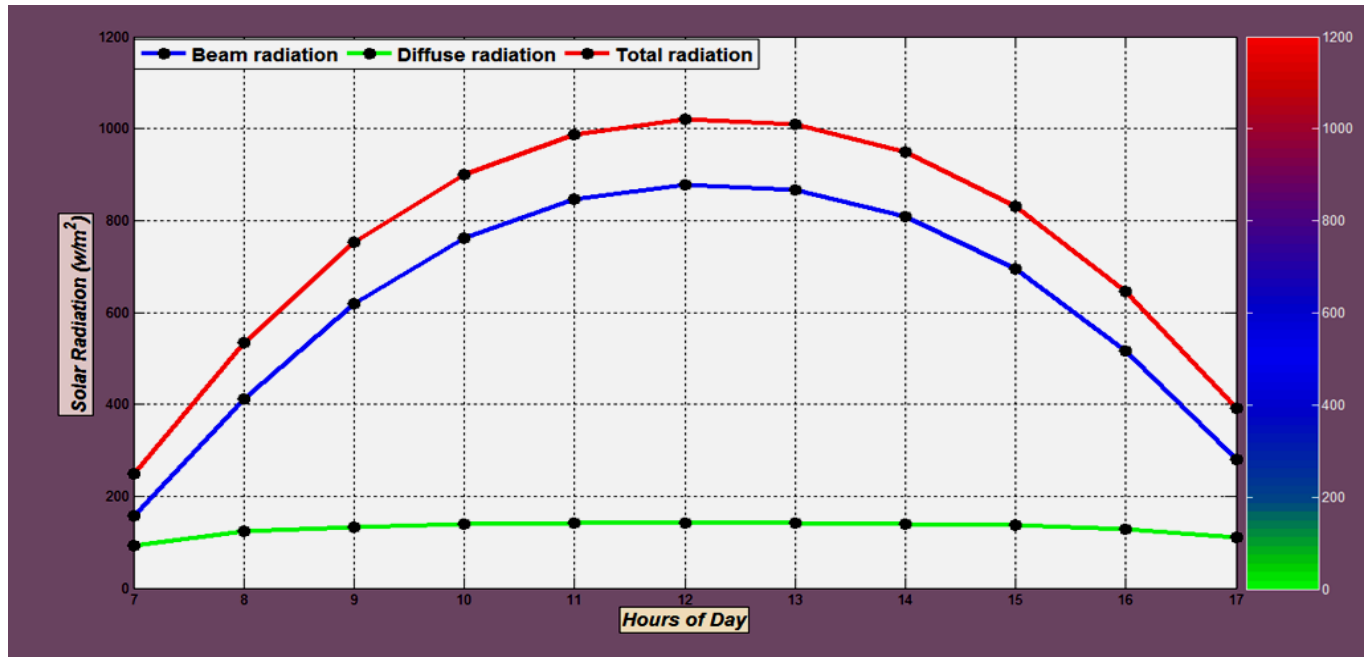


figure 4.4Direct, diffuse, and total solar radiation components during 15 April 2015.

The figure 4.5 shown the relation between hours of the day and solar flux for 15 May 2015.

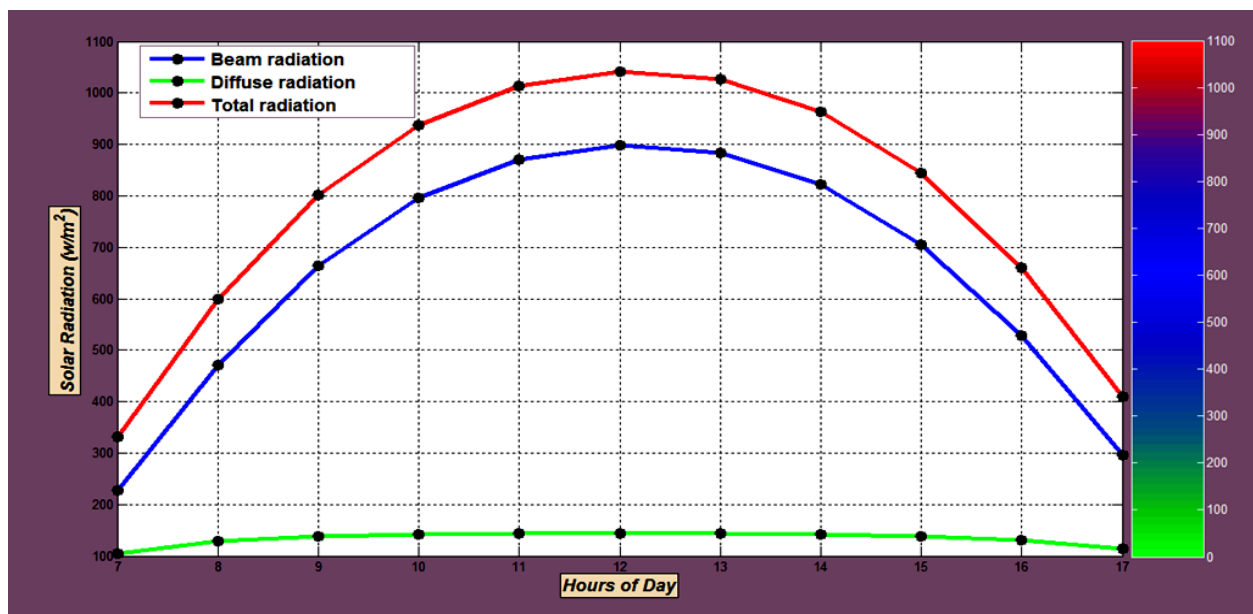


figure 4.5Direct, diffuse, and total solar radiation components during 15 May 2015.

The figure 4.6 shown the relation between hours of the day and solar flux for 15 June 2015.

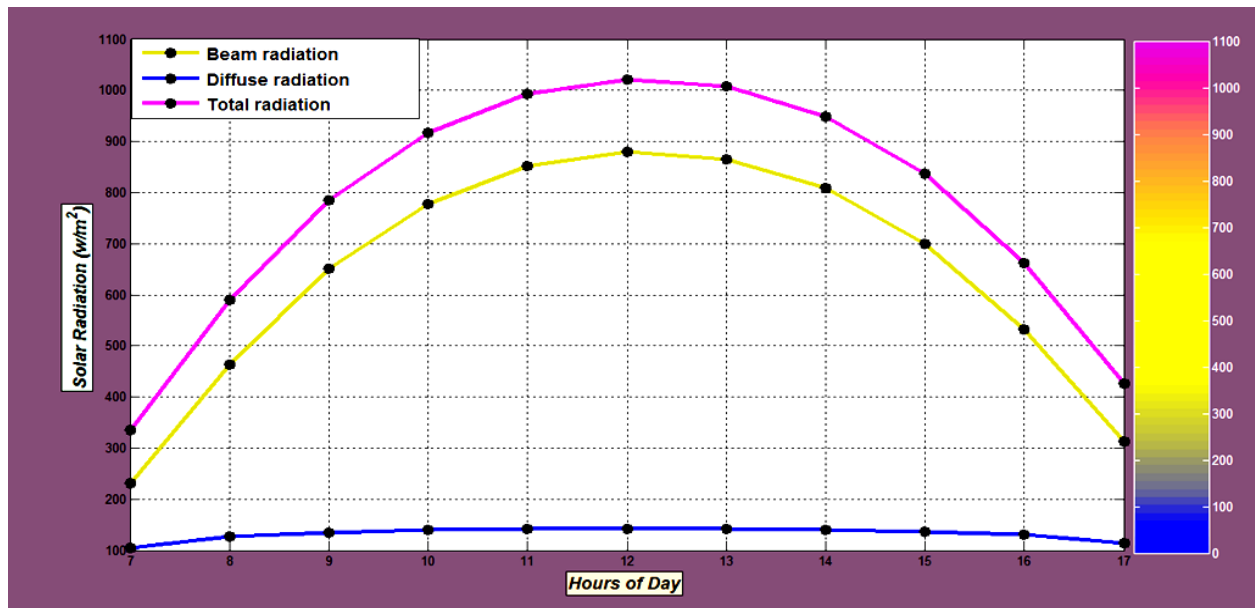


figure 4.6 Direct, diffuse, and total solar radiation components during 15 June 2015.

The figure 4.7 shown the relation between hours of the day and solar flux for 15 July 2015.

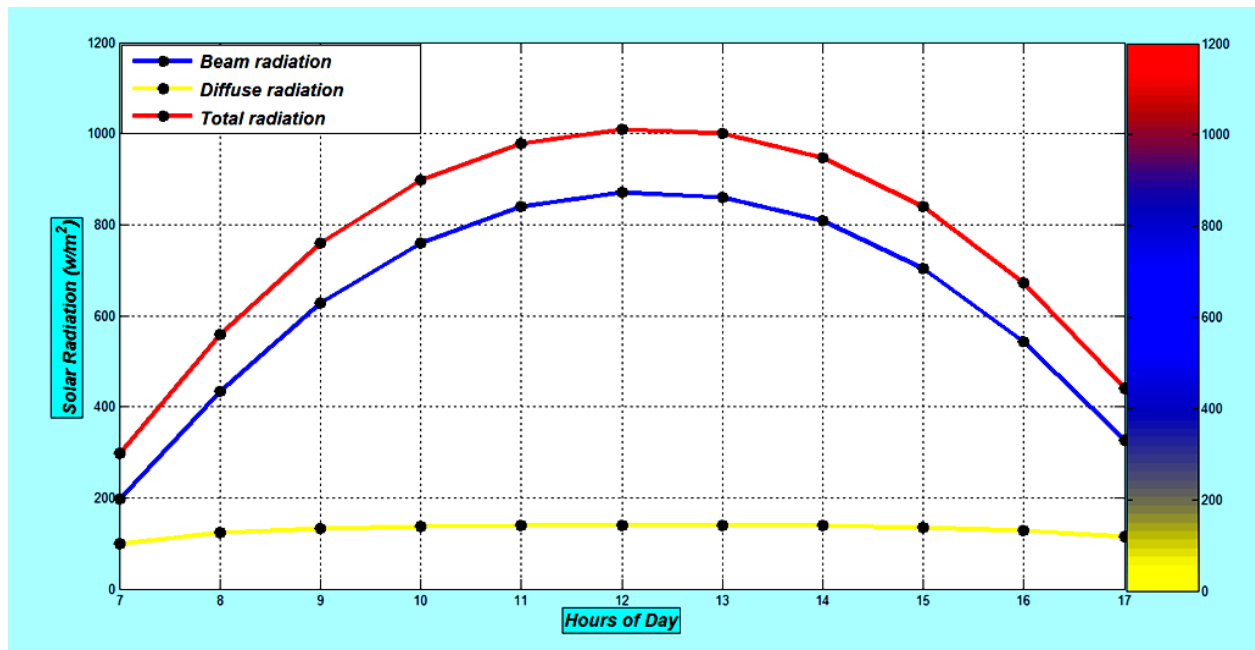


figure 4.7 Direct, diffuse, and total solar radiation components during 15 July 2015



The figure 4.8 shown the relation between hours of the day and solar flux for 15 August 2015.

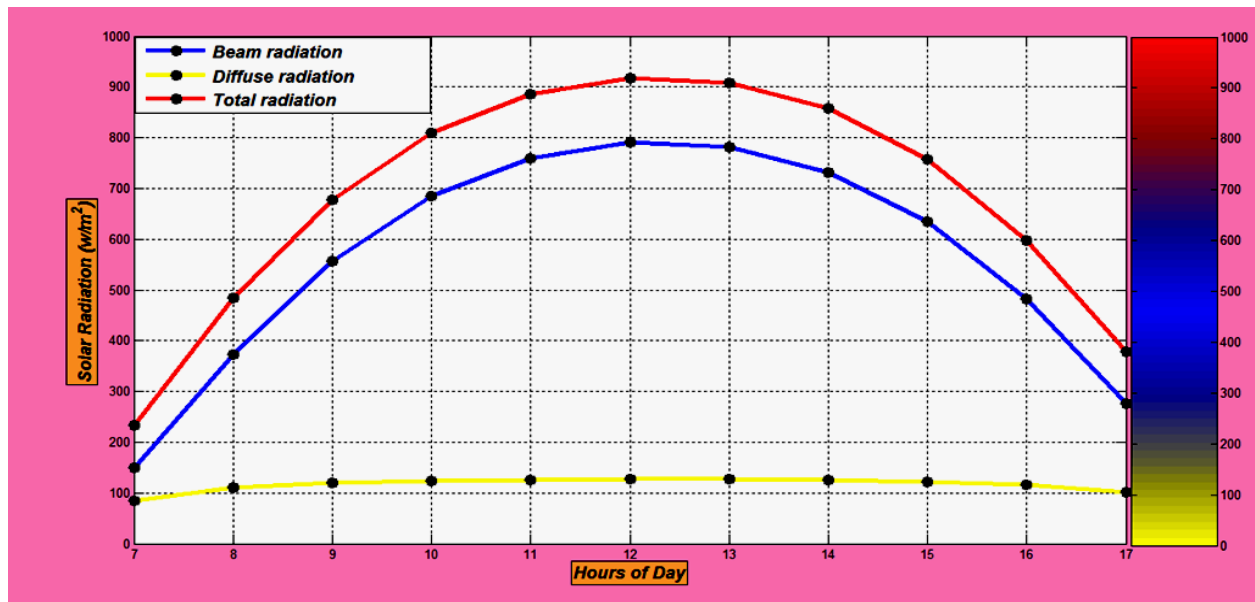


figure 4.8 Direct, diffuse, and total solar radiation components during 15 August 2015.

The figure 4.9 shown the relation between hours of the day and solar flux for 15 September 2015.

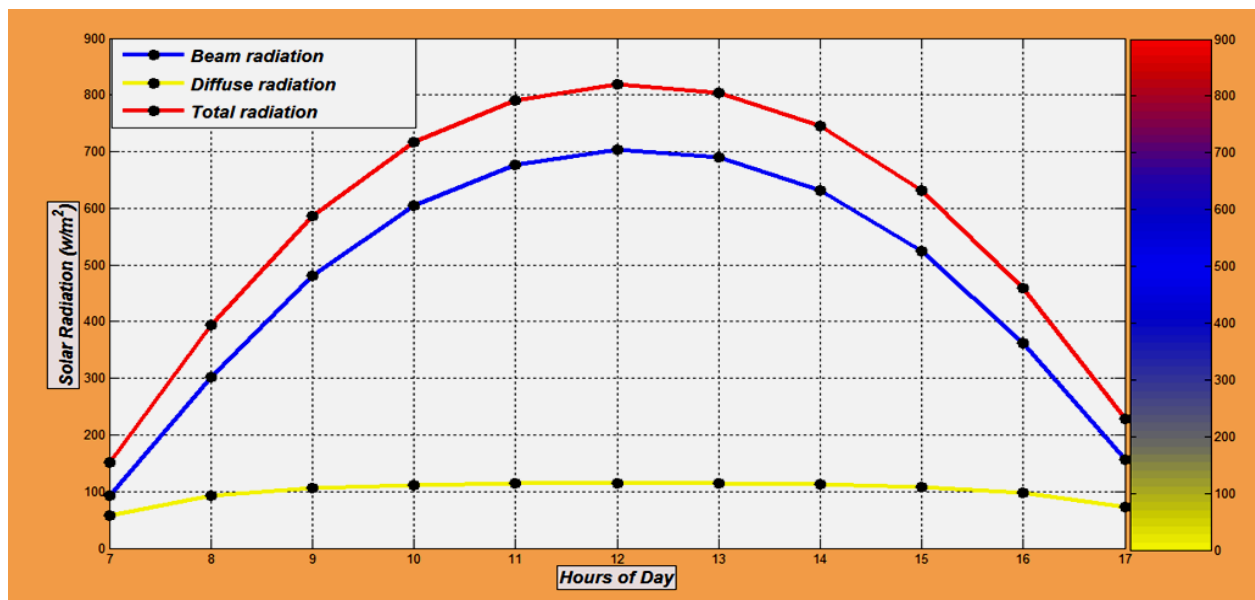


figure 4.9 Direct, diffuse, and total solar radiation components during 15 September 2015.

The figure 4.10 shown the relation between hours of the day and solar flux for 15 October 2015.

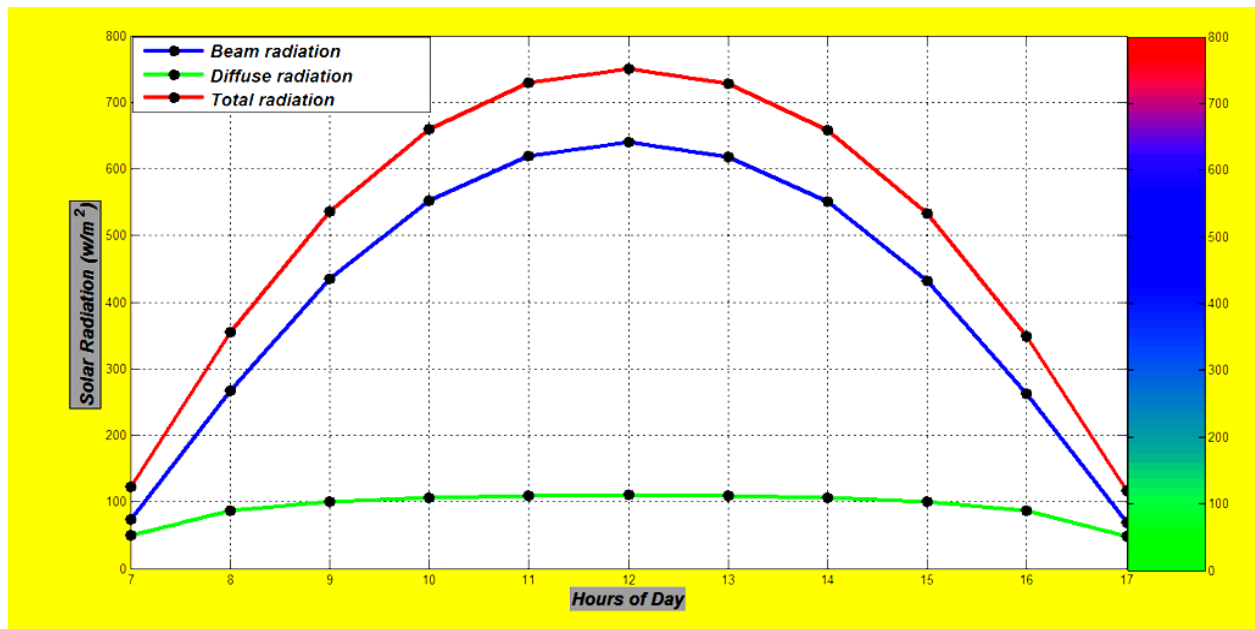


figure 4.10 Direct, diffuse, and total solar radiation components during 15 October 2015.

The figure 4.11 shown the relation between hours of the day and solar flux for 15 November 2015.

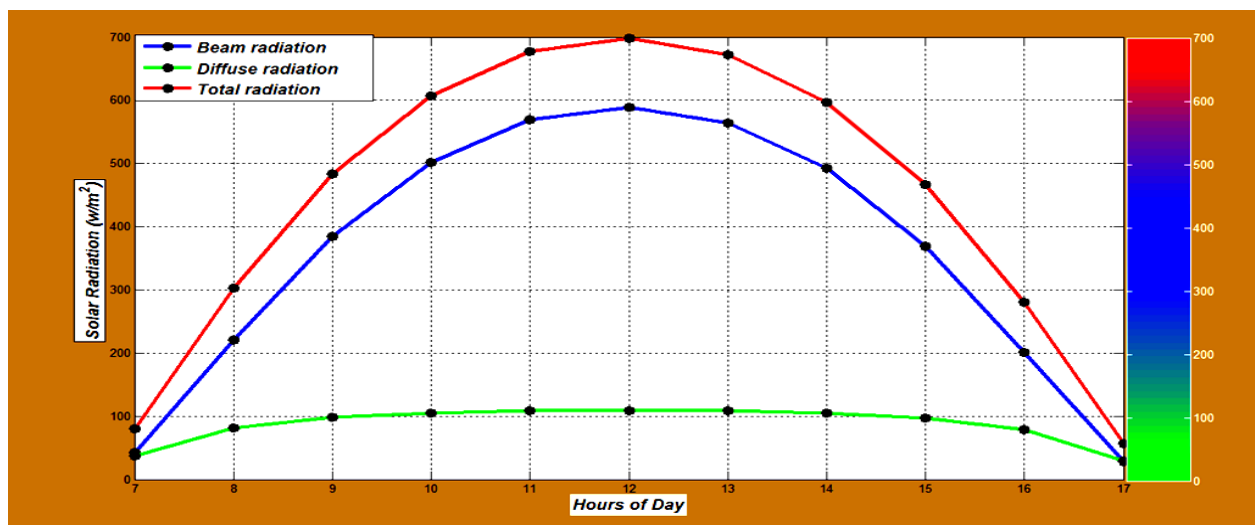


figure 4.11 Direct, diffuse, and total solar radiation components during 15 November 2015.

The figure 4.12 shown the relation between hours of the day and solar flux for 15 December 2015 .

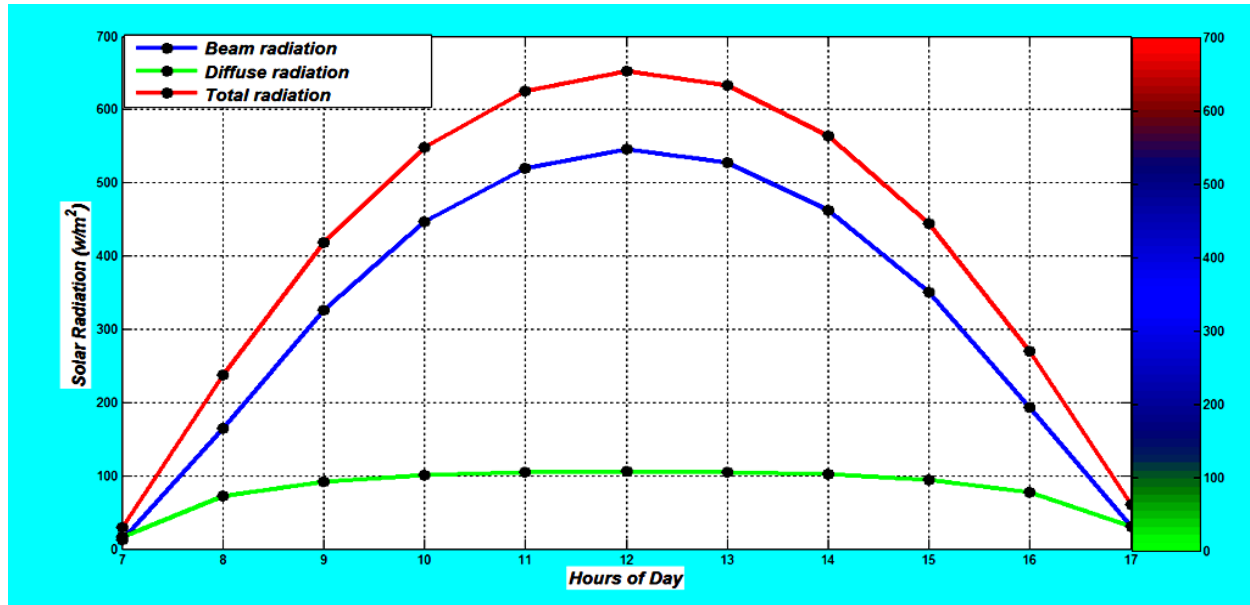


figure 4.12 Direct, diffuse, and total solar radiation components during 15 December 2015.

Table 4.14 below shown the daily average solar radiation components for 2015.

Months	average Daily diffuse radiation $\text{W/m}^2$	average Daily direct radiation $\text{W/m}^2$	average Daily total radiation $\text{W/m}^2$
January	931.49	3809.7	4741.2
February	996.31	4410.6	5406.9
March	1363.9	6253	7616.9
April	1427.3	6841.9	8269.2
May	1457.9	7102.5	8560.4
June	1450.1	7074.5	8524.5
July	1284.9	6220.5	7505.4
August	1081.2	5135	6216.2
September	1016.6	4518.8	5535.5
October	949.06	3926.5	4875.6
November	944.63	3908.2	4852.8
December	900.42	3580.8	4481.2

figure 4.13 below shown the relation between daily average solar radiation components and month of year .

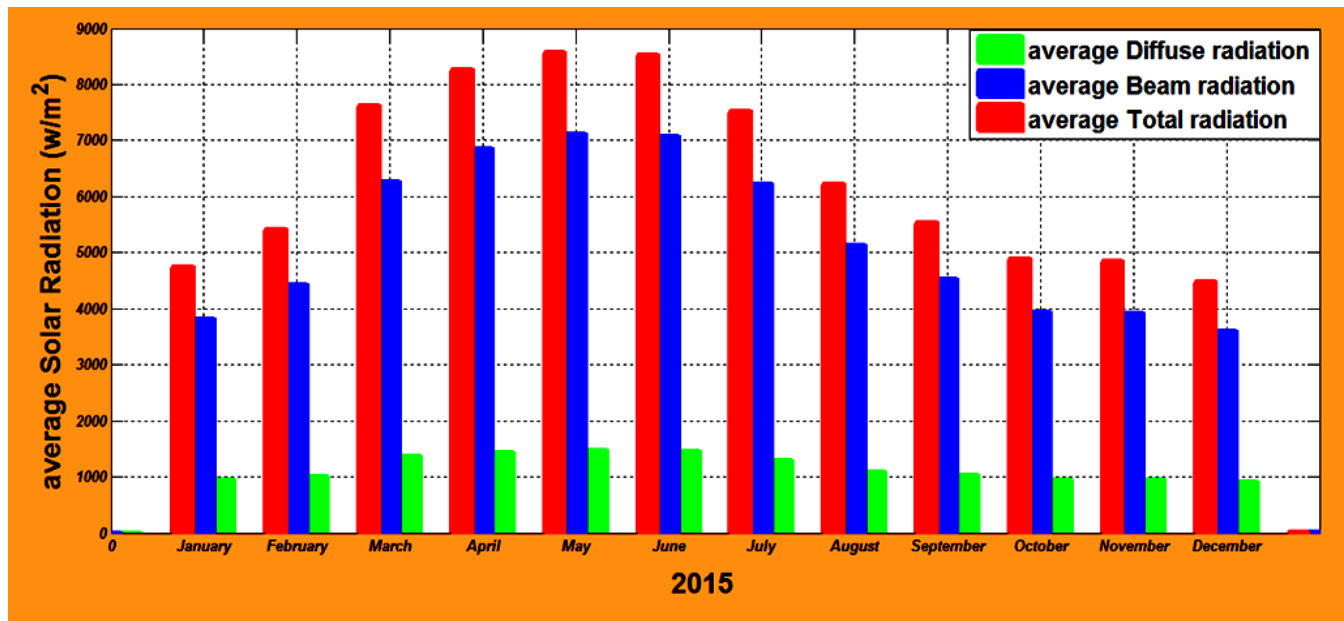


figure 4.13 average Direct, diffuse, and total solar radiation components during 2015.

### 4.3 Results for Inclined surface

The next tables below shows the results of written program for calculation the solar radiation in an Inclined surface. The program to calculate the solar radiation in Inclined surface only requires the day number of the year, apparent solar irradiation, the atmospheric extinction coefficient, surface azimuth angle (tilted) and surface tilt angle from the horizontal. The outputs of the program were shown the results for February, May, August and November which present the seasons of year Winter, summer, Autumn, and Winter respectively. The Table(4.15) below shown the outputs of the program for 15 February 2015 in this specified Date the value of N day number of the year equal to 47. for surface azimuth angle equal to (0, 90, 180, 270) degree and collector facing South, West, North, and East directions respectively. For 15 February 2015, and surface tilt angle from the horizontal equal to (20, 40, 60, 80) degrees. The table showed the results of total solar

radiation  $Q_t$  by  $\text{w/m}^2$  with different tilt angles and different orientation for 15 February as average of the month. The Table(4.16) below shown the outputs of the program for 15 May 2015 in this specified Date the value of N day number of the year equal to 135 .for surface azimuth angle equal to( 0,90,180,270) degree and collector facing South , West , North, and East directions respectively. For 15 May 2015, and surface tilt angle from the horizontal equal to(20,40,60,80) degrees. The table shown the results of total solar radiation  $Q_t$  by  $\text{w/m}^2$  with different tilt angles and different orientation for 15 May as average of the month. The Table(4.17) below shown the outputs of the program for 15 August 2015 in this specified Date the value of N day number of the year equal to 227 .for surface azimuth angle equal to( 0,90,180,270) degree and collector facing South , West , North, and East directions respectively. For 15 August 2015, and surface tilt angle from the horizontal equal to(20,40,60,80) degrees. The table shown the results of total solar radiation  $Q_t$  by  $\text{w/m}^2$  with different tilt angles and different orientation for 15 August as average of the month. The Table(4.17) below shown the outputs of the program for 15 November 2015 in this specified Date the value of N day number of the year equal to 319 .for surface azimuth angle equal to( 0,90,180,270) degree and collector facing South , West , North, and East directions respectively. For 15 November 2015, and surface tilt angle from the horizontal equal to (20,40,60,80) degrees.

The table shown the results of total solar radiation  $Q_t$  by  $\text{w/m}^2$  with different tilt angles and different orientation for 15 November as average of the month.

**The Table (4.15)** Total radiation with different tilted angles during 15 February 2015

Orient ation	Hour Tilted At	7	8	9	10	11	12	13	14	15	16	17
South Facing	20°	28.101	290.89	537.51	731.77	862.68	924.4	914.59	833.6	684.62	474.67	216.95
	40°	37.692	326.61	569.72	755.47	879.16	937.17	927.96	851.77	710.67	508.81	250.52
	60°	45.03	335.98	551.52	709.37	812.6	860.62	853.01	789.84	671.66	498.73	264.78
	80°	49.231	317.86	485.08	599.03	671.03	703.97	698.78	655.3	572.27	445.63	257.99
West Facing	20°	55.805	399.6	626.7	765.65	825.76	812.26	731.45	591.92	406.22	195.59	40.12
	40°	89.759	530.92	737.36	819.15	809.78	726.42	583.78	397.55	187.46	83.637	49.402
	60°	115.18	611.25	777.37	795.17	719.12	576.67	389.29	177.88	128.07	103.96	63.622
	80°	129	630.88	741.92	696.59	564.73	381.08	179.54	172.98	156.21	128.88	81.06
North Facing	20°	7.4247	160.27	342.96	494.47	598.35	647.64	639.8	575.19	457.34	295.02	109.89
	40°	9.5666	81.129	204.1	309.49	382.37	417.04	411.52	366.1	283.53	171.18	49.402
	60°	12.848	77.059	111.75	132.8	144.83	159.84	157.21	142.3	128.07	103.96	63.622
	80°	16.874	97.318	137.81	161.49	174.79	180.41	179.54	172	156.21	128.88	81.066
East Facing	20°	7.4247	51.558	253.76	460.58	635.27	759.78	822.93	816.87	735.74	469.23	187.99
	40°	9.5666	60.543	90.513	245.81	451.76	627.79	755.7	820.32	806.75	512.22	198.23
	60°	12.848	77.059	111.75	132.8	236.76	443.79	620.93	747.47	801.09	520.43	156.34
	80°	16.874	97.318	137.81	161.49	174.79	229.98	434.86	607.12	719.47	642.23	218.45

**The Table (4.16)** Total radiation with different tilted angles during 15 May 2015

orientation	Hours Tilted At	6	8	10	12	14	16	18
South Facing	20°	0.10557	544.96	1076.6	1299.8	1178.7	729.96	89.351
	40°	0.13249	432.41	920.4	1126.5	1014.6	601.3	72.236
	60°	0.17374	303.24	704.29	873.43	781.71	441.67	88.069
	80°	0.22433	275.44	454.35	571.14	508.04	323.76	107.49
West Facing	20°	0.59886	876.71	1298.4	1344.3	1060.3	524.36	61.902
	40°	1.0341	1055.9	1337.3	1210.1	792.21	252.82	72.236
	60°	1.375	1143.3	1266	986.13	482.07	284.68	88.069
	80°	1.5803	1128.3	1093.1	699.3	420.32	323.76	107.49
North Facing	20°	0.29362	669.55	1143.4	1335.8	1231.7	837.92	195.6
	40°	0.46047	666.56	1046	1194	1114.3	804.19	237.76
	60°	0.6021	618.72	873.5	964.43	916.09	715.02	265.46
	80°	0.7014	531.79	646.77	674.63	660.83	581.17	275.35
East Facing	20°	0.10557	337.8	921.58	1291.2	1350.1	1043.5	231.87
	40°	0.13249	209.91	629.07	1110.4	1336.7	1190.6	287.35
	60°	0.17374	239.34	357.76	851.72	1215.7	1235.6	234.56
	80°	0.22433	275.44	400.83	546.46	1001.6	1173.2	276.87

**The Table (4.17)** Total radiation with different tilted angles during 15 August 2015

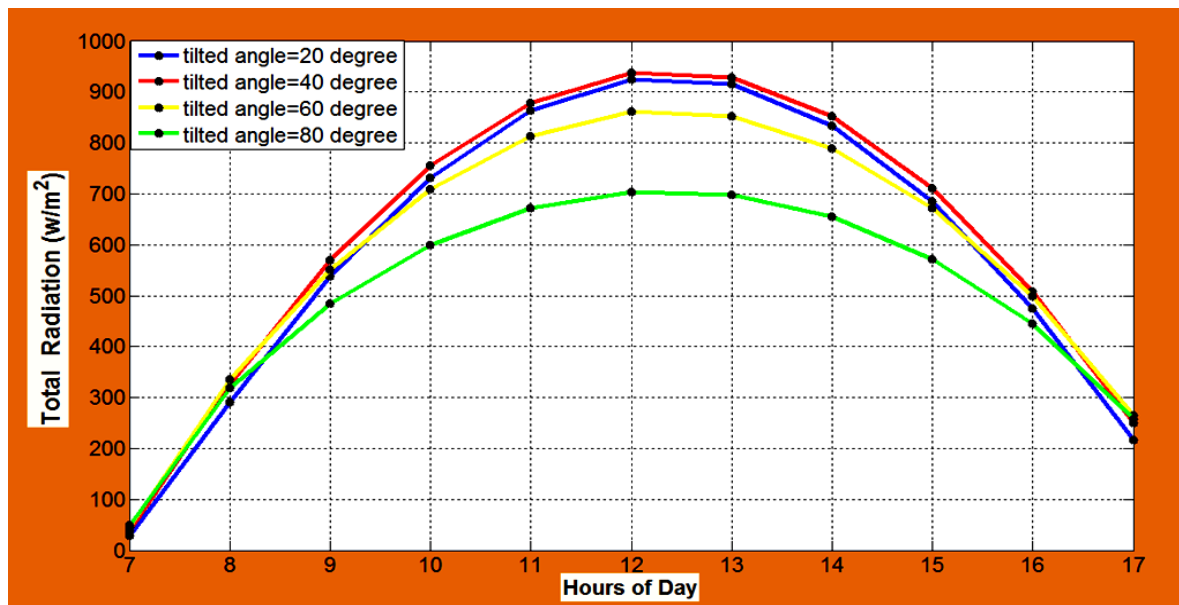
orientation	Hours Tilted At	6	8	10	12	14	16	18
South Facing	20°	0.10352	455.32	875.91	1046.4	930.56	551.98	40.686
	40°	0.12858	373.59	756.52	912.6	806.53	461.09	36.019
	60°	0.16698	269.61	574.65	699.17	614.56	339.07	45.871
	80°	0.21408	173.02	352.23	431.85	377.81	200.63	57.957
West Facing	20°	0.57392	732.13	1044.3	1050.1	786.87	335.87	29.588
	40°	0.98811	893.83	1073	919.56	536.48	128.65	36.019
	60°	1.312	970.54	1001.1	708.55	250.72	154.45	45.871
	80°	1.5064	953	837.16	442.51	224.73	186.1	57.957
North Facing	20°	0.23847	516.48	878.92	1022.1	924.97	601.57	91.249
	40°	0.35767	488.54	762.19	866.86	796.02	554.3	113.19
	60°	0.46257	424.49	582.28	637.55	600.4	464.64	129.24
	80°	0.54052	332.05	360.92	361.77	361.71	343.42	137.48
East Facing	20°	0.10352	239.66	710.51	1018.4	1068.7	817.68	179.75
	40°	0.12858	117.99	445.67	859.9	1066.1	960.45	279.51
	60°	0.16698	142.71	185.63	628.17	964.24	1011.8	353.33
	80°	0.21408	173.02	220.15	351.1	775.45	965.68	392.3



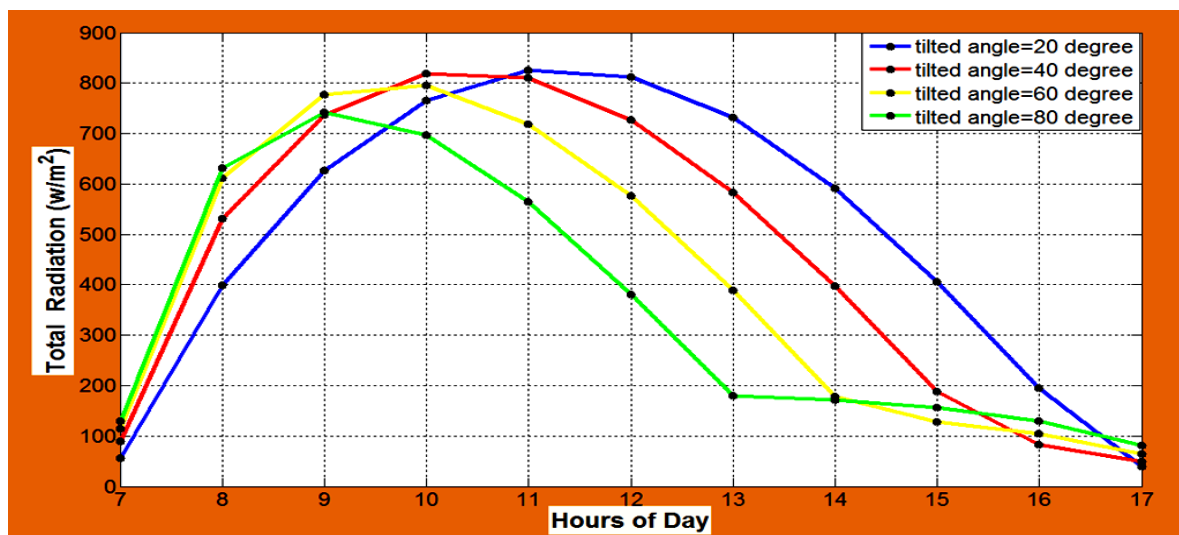
**The Table (4.18)** Total radiation with different tilted angles during 15 November 2015

orientation	Hours Tilted At	7	8	9	10	11	12	13	14	15	16	17
South Facing	20°	82.45	346.51	572.82	742.54	847.42	883.1	848.26	744.19	575.2	349.5	85.54
	40°	110.49	401.14	626.6	790.44	890.38	924.22	891.18	792.02	628.92	404.2	114.28
	60°	129.92	420.23	621.91	762.59	846.86	875.18	847.53	763.92	623.93	423.06	134.1
	80°	138.4	401.49	559.31	662.34	722.11	741.91	722.57	663.3	560.83	403.81	142.6
West Facing	20°	60.45	424.67	615.6	724.58	758.37	722.23	623.15	471.09	281.64	84.521	14.1
	40°	88.89	548.03	707.02	756.68	723.02	621.88	468.12	278.75	80.966	56.92	18.938
	60°	97.76	618.13	730.25	717.1	621.37	467.85	277.54	119.31	102.2	74.346	26.35
	80°	99.45	626.54	682.51	610.62	465.68	278.7	157.86	147.55	128.25	95.722	35.442
North Facing	20°	14.714	160.51	322.04	451.04	532.57	560.54	533.23	452.31	323.82	162.51	15.804
	40°	18.361	56.567	155.3	242.6	298.66	317.99	299.12	243.47	156.48	56.92	18.938
	60°	25.574	73.925	101.94	119.15	128.52	131.5	128.59	119.31	102.2	74.346	26.35
	80°	34.421	95.217	127.95	147.38	157.78	161.06	157.86	147.55	128.25	95.722	35.442
East Facing	20°	13.654	82.349	279.25	469	621.63	721.41	758.34	725.42	617.37	427.49	116.9
	40°	18.361	56.567	80.736	276.36	466.03	620.33	722.18	756.74	708.18	550.77	145
	60°	25.574	73.925	101.94	119.15	275.13	465.75	619.83	716.39	730.71	620.54	135.8
	80°	34.421	95.217	127.95	147.38	157.78	276.32	463.65	609.25	682.25	628.38	281.2

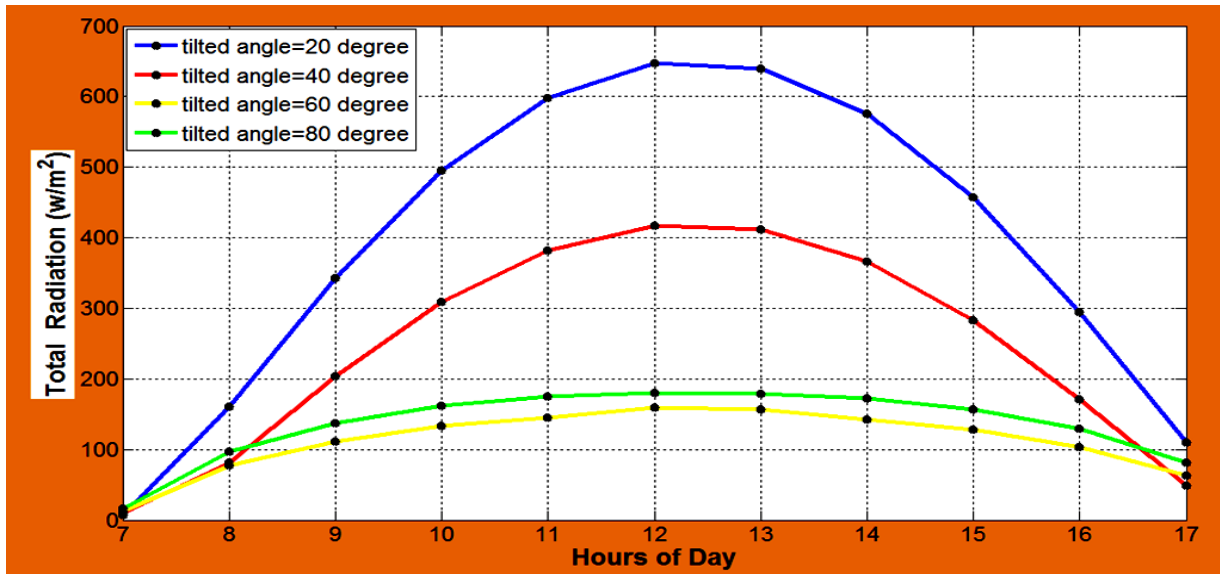
Figure (4.14 to 4.17) below shown total Solar radiation in Khartoum with different tilted angles and directions towards South facing (4.14) , West facing (4.15) , North facing (4.16) and East facing (4.17) respectively for 15 February 2015.



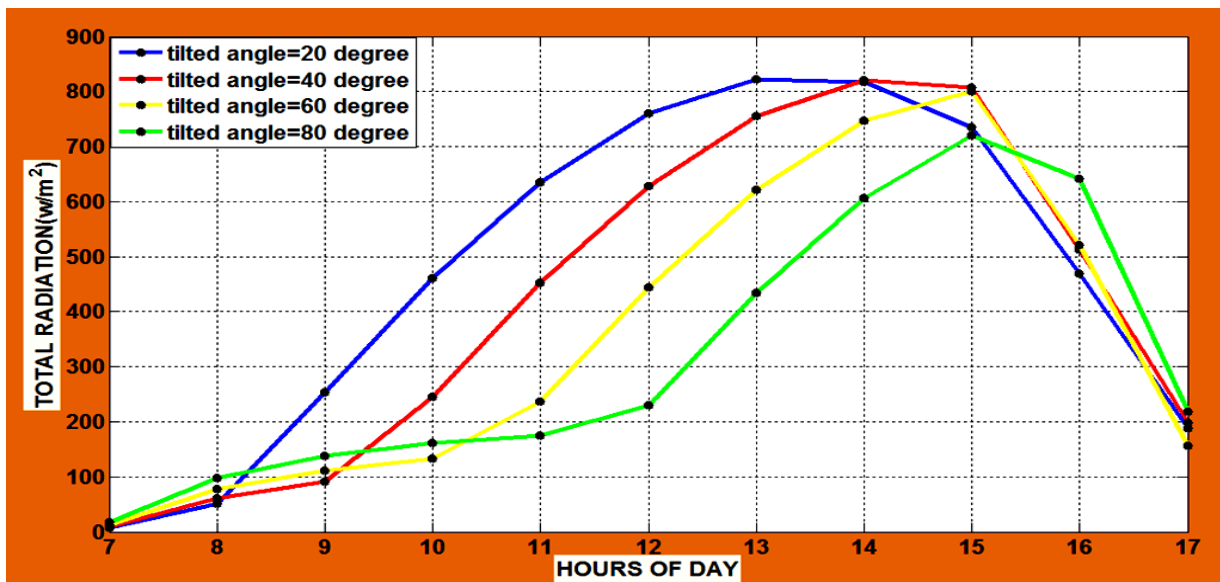
The figure 4.14 shown the relation between hours of the day and solar flux for 15 February 2015 with different tilting angles, collector facing South direction .



The figure 4.15 shown the relation between hours of the day and solar flux for 15 February 2015 with different tilting angles, collector facing West direction .

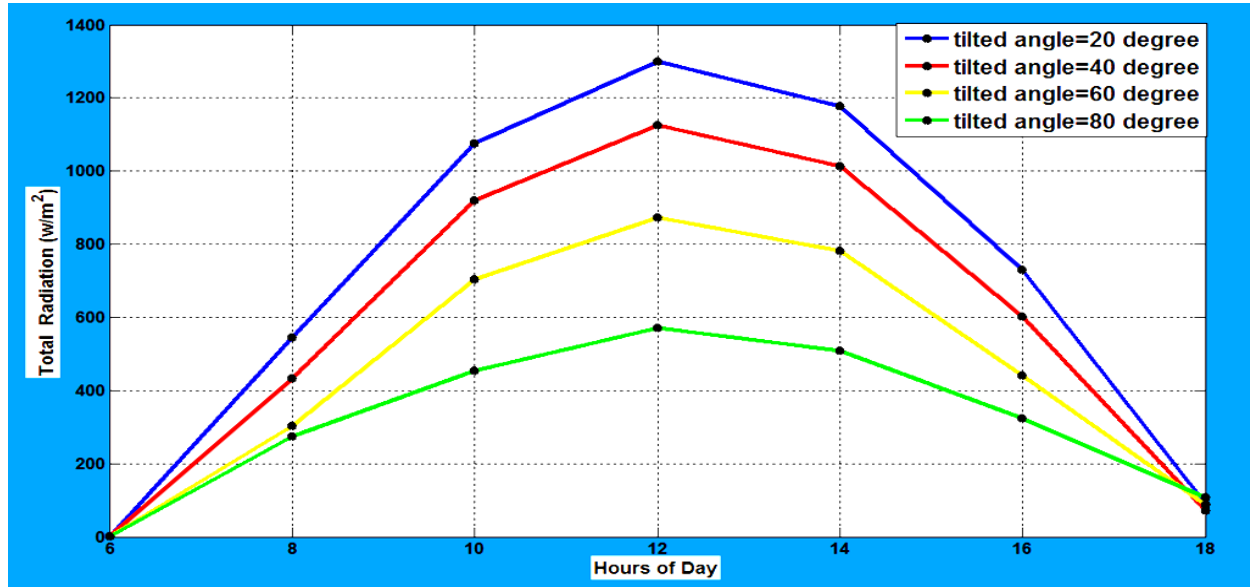


The figure 4.16 shown the relation between hours of the day and solar flux for 15 February 2015 with different tilting angles, collector facing North direction

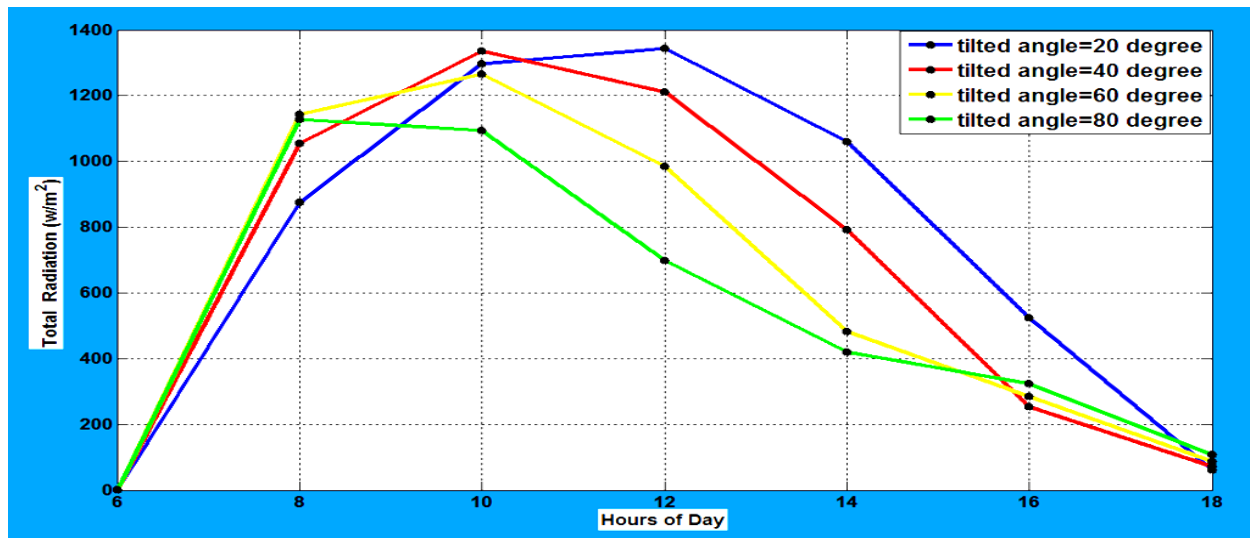


The figure 4.17 shown the relation between hours of the day and solar flux for 15 February 2015 with different tilting angles, collector facing East direction.

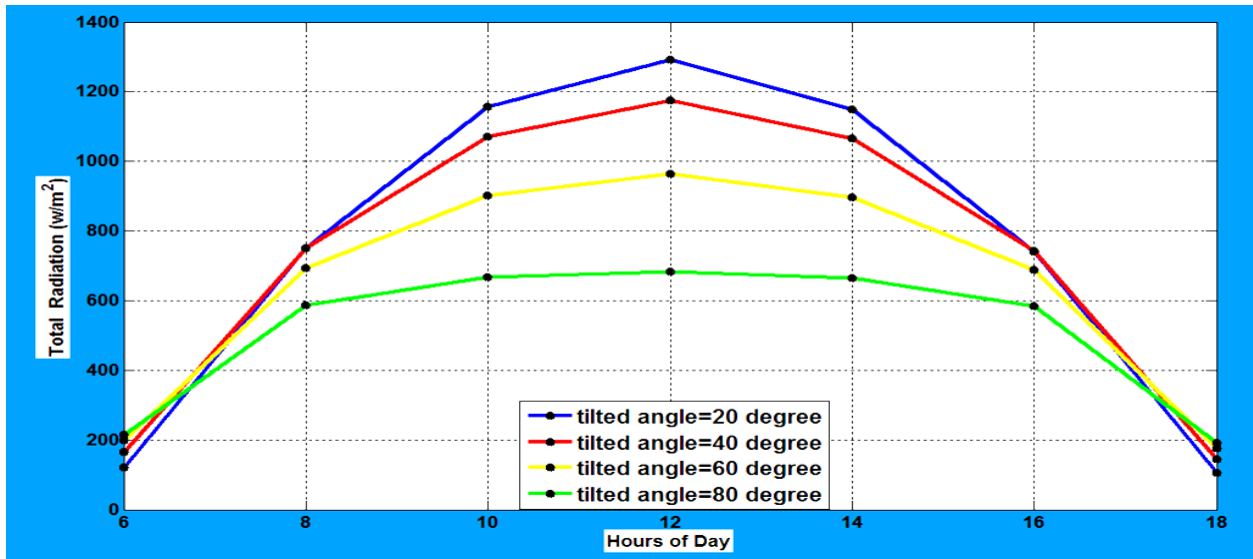
Figure (4.18 to 4.21) below shown total Solar radiation in Khartoum with different tilted angles and directions towards South facing (4.18) , West facing (4.19) , North facing (4.20) and East facing (4.21) respectively for 15 May 2015.



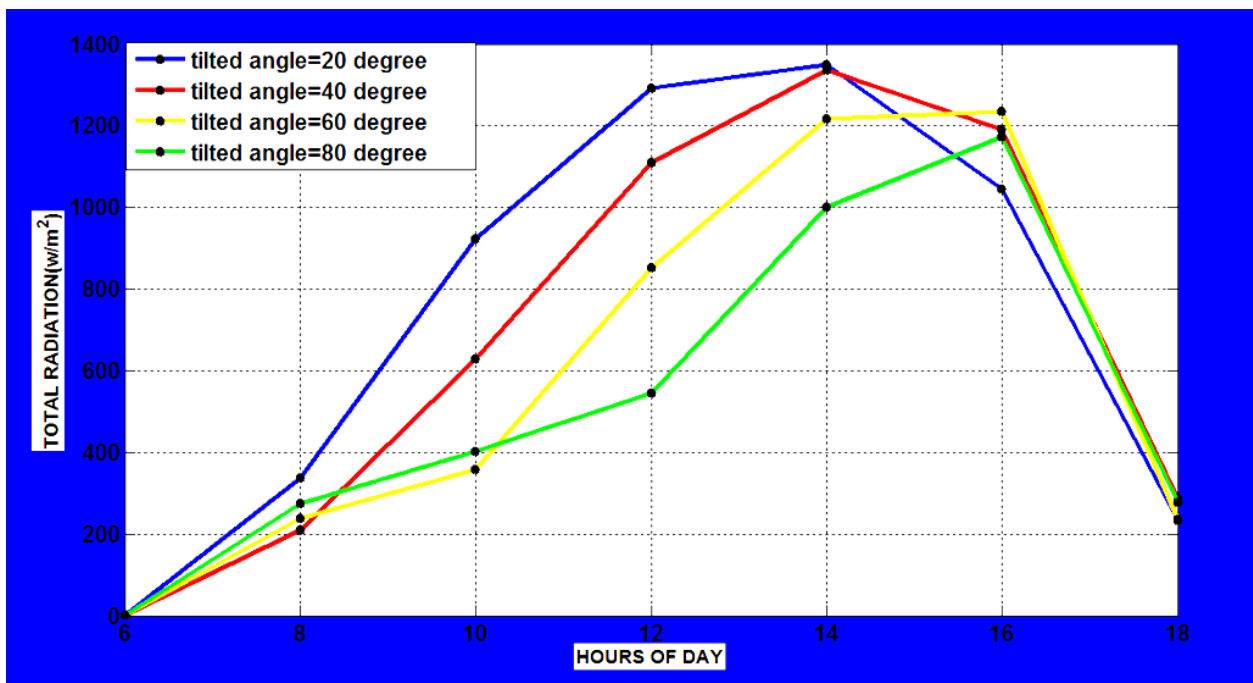
The figure 4.18 shown the relation between hours of the day and solar flux for 15 May 2015 with different tilting angles, collector facing South direction.



The figure 4.19 shown the relation between hours of the day and solar flux for 15 May 2015 with different tilting angles, collector facing West direction.

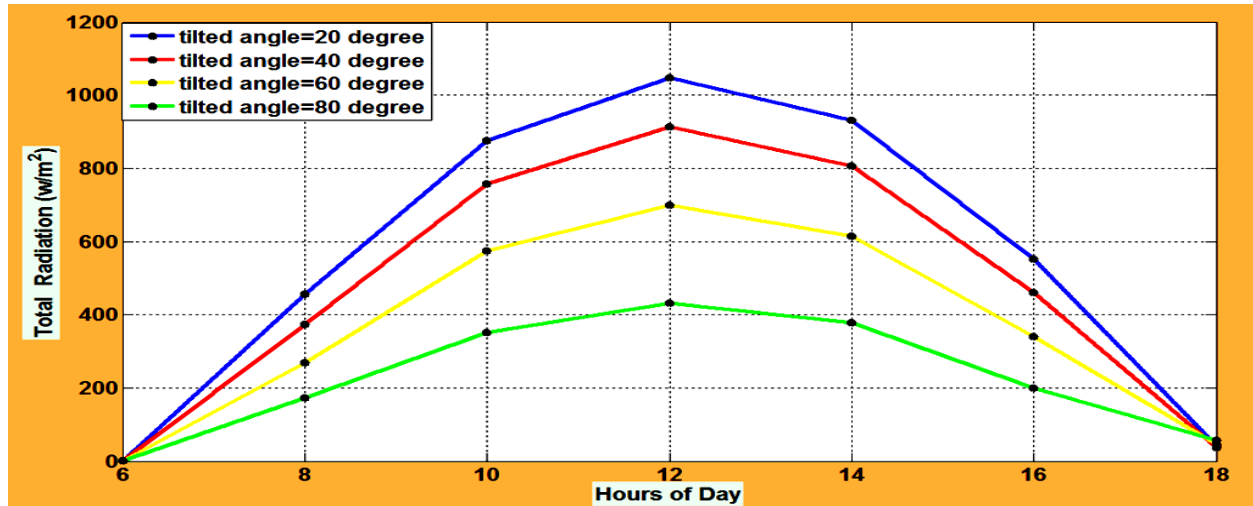


The figure 4.20 shown the relation between hours of the day and solar flux for 15 May 2015 with different tilting angles, collector facing North direction.

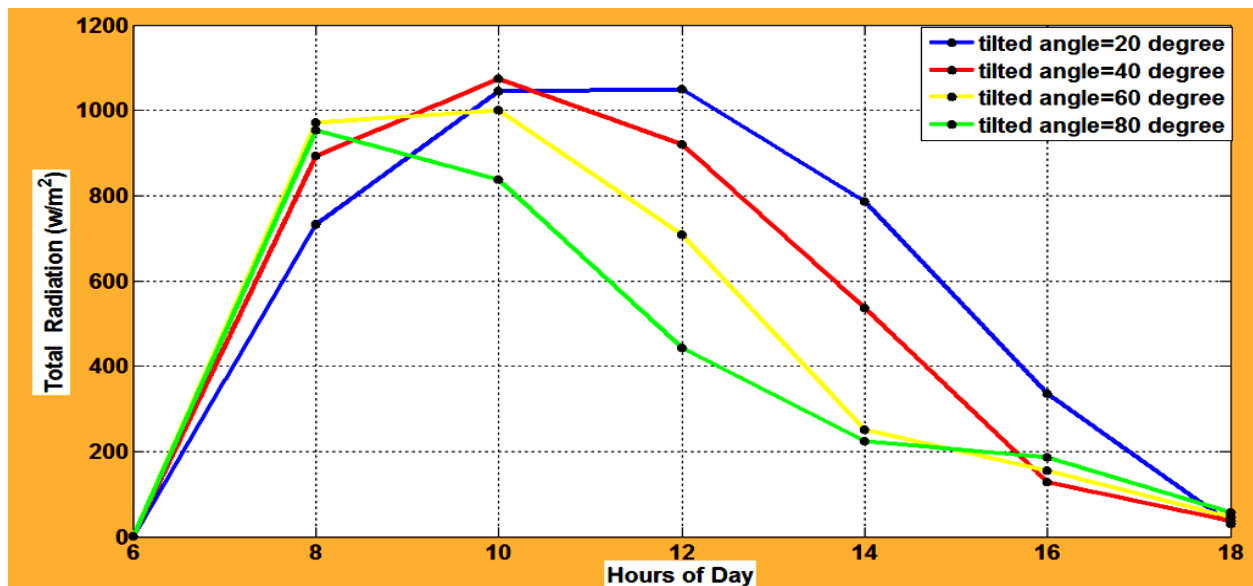


The figure 4.21 shown the relation between hours of the day and solar flux for 15 May 2015 with different tilting angles, collector facing East direction.

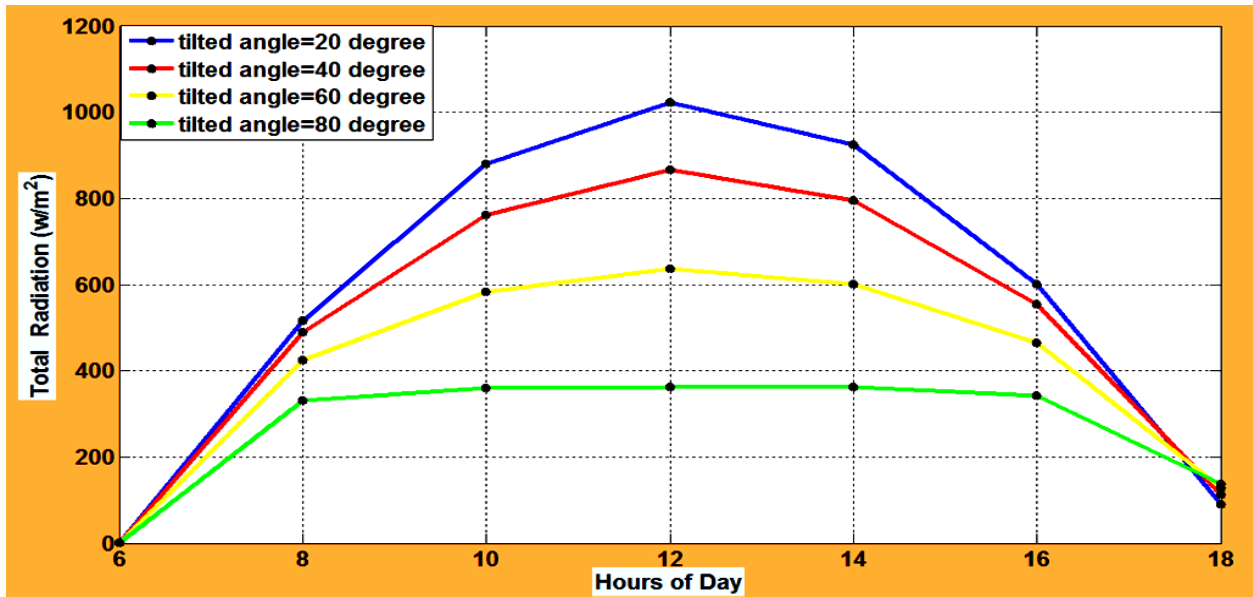
Figure (4.22 to 4.25) below shown total Solar radiation in Khartoum with different tilted angles and directions towards South facing (4.22) , West facing (4.23) , North facing (4.24) and East facing (4.25) respectively for 15 August 2015.



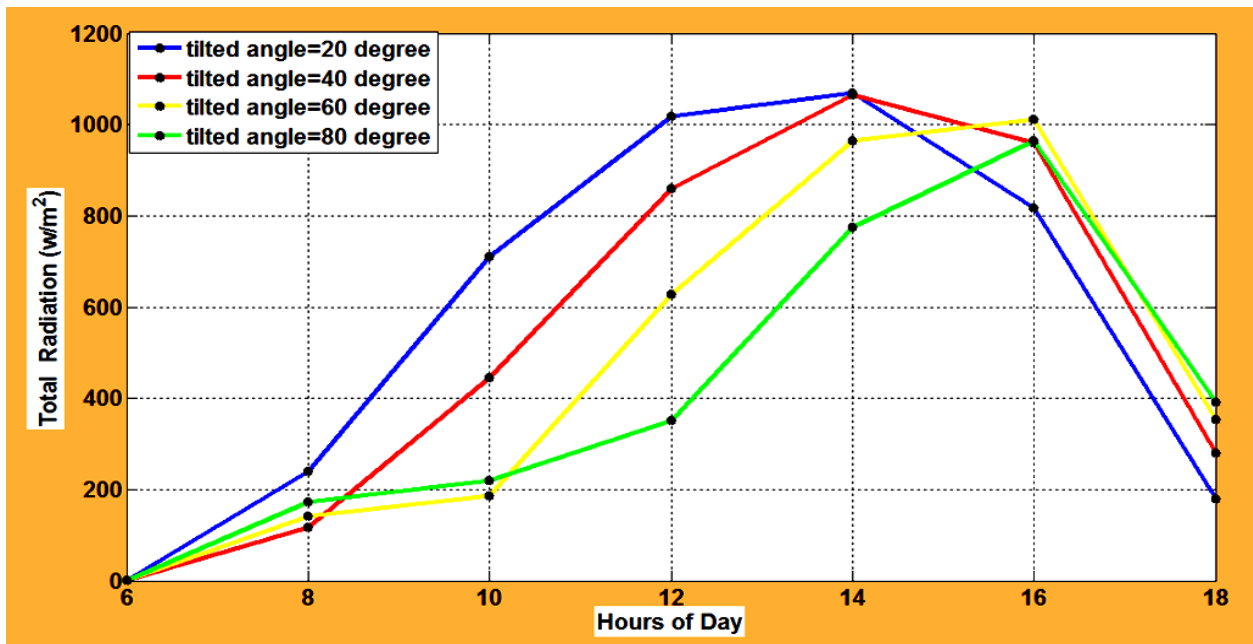
The figure 4.22 shown the relation between hours of the day and solar flux for 15 August 2015 with different tilting angles, collector facing South direction



The figure 4.23 shown the relation between hours of the day and solar flux for 15 August 2015 with different tilting angles, collector facing West direction.

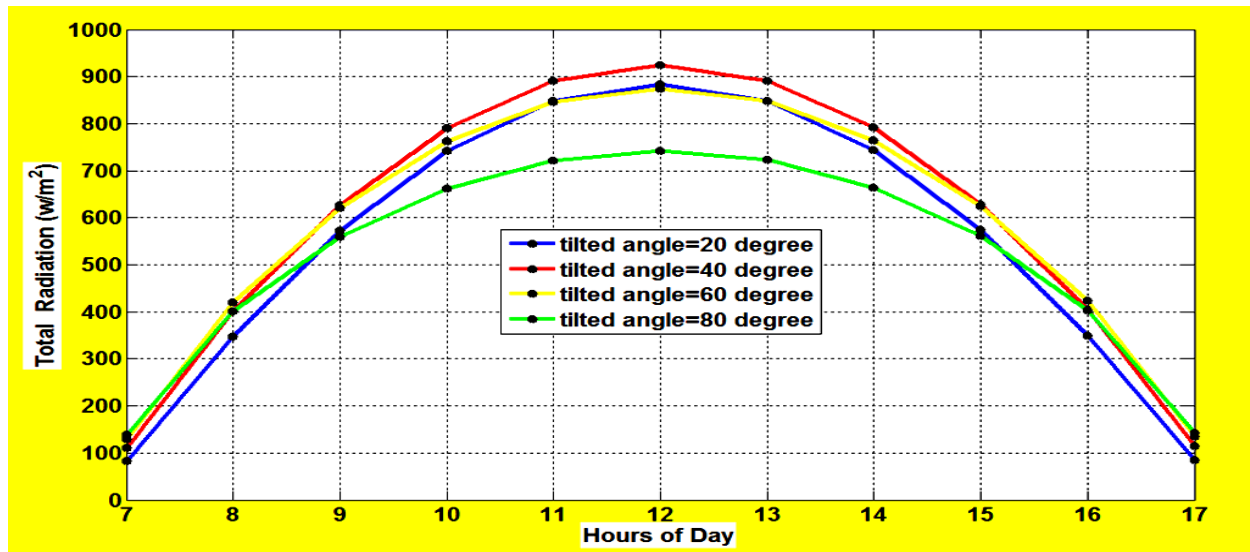


The figure 4.24 showed the relation between hours of the day and solar flux for 15 August 2015 with different tilting angles, collector facing North direction.

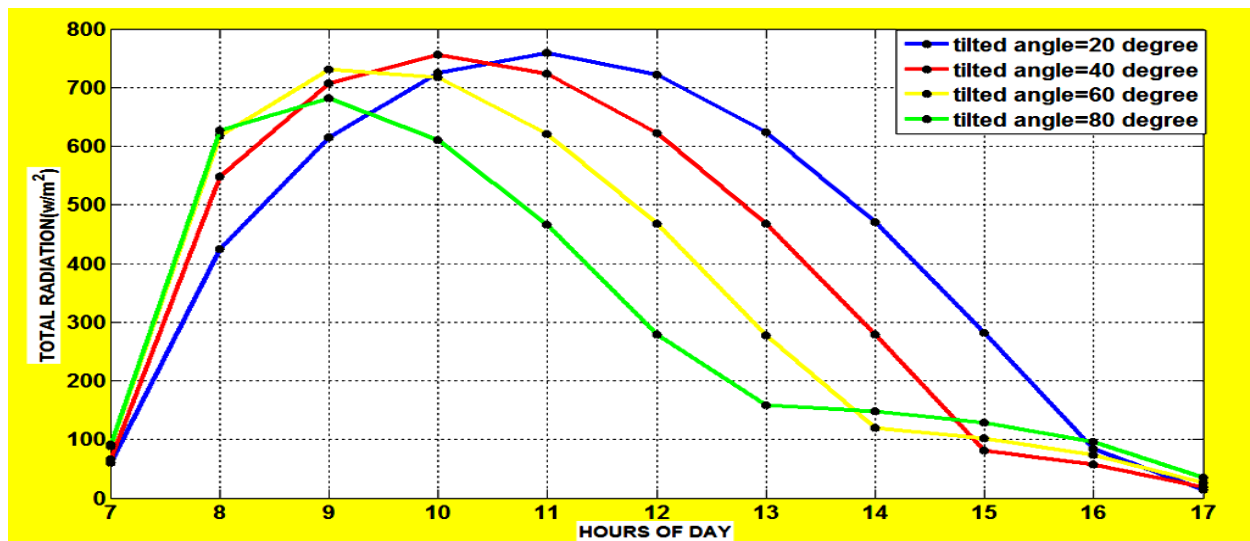


The figure 4.25 showed the relation between hours of the day and solar flux for 15 August 2015 with different tilting angles, collector facing East direction.

Figure (4.26 to 4.29) below shown total Solar radiation in Khartoum with different tilted angles and directions towards South facing (4.26) , West facing (4.27) , North facing (4.28) and East facing (4.29) respectively for 15 November 2015.

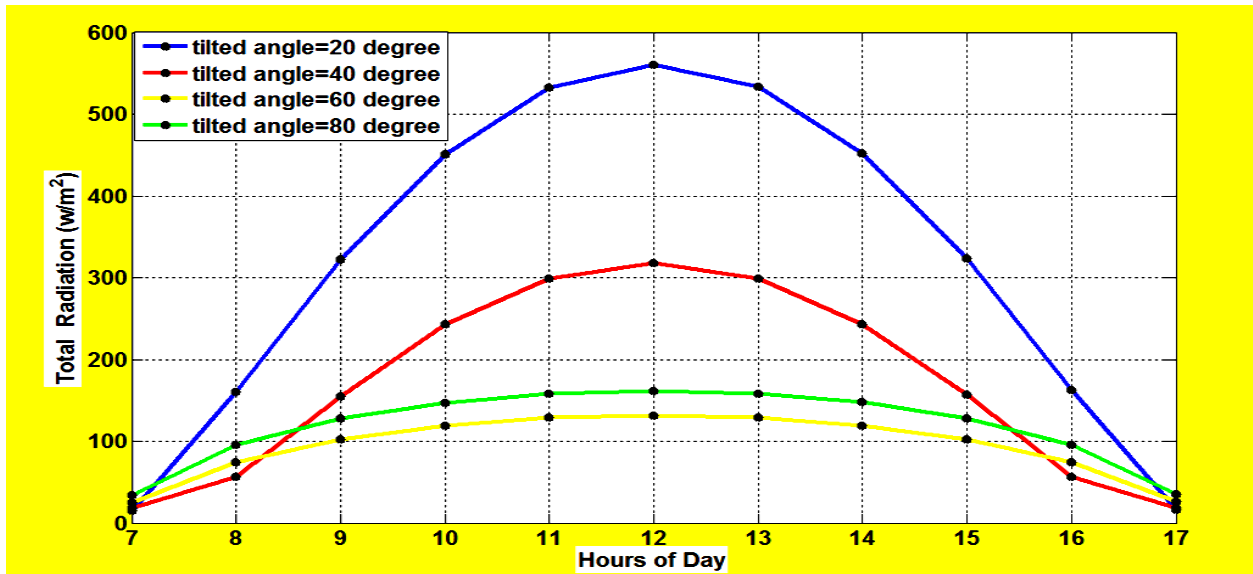


The figure 4.26 showed the relation between hours of the day and solar flux for 15 November 2015 with different tilting angles, collector facing South direction.

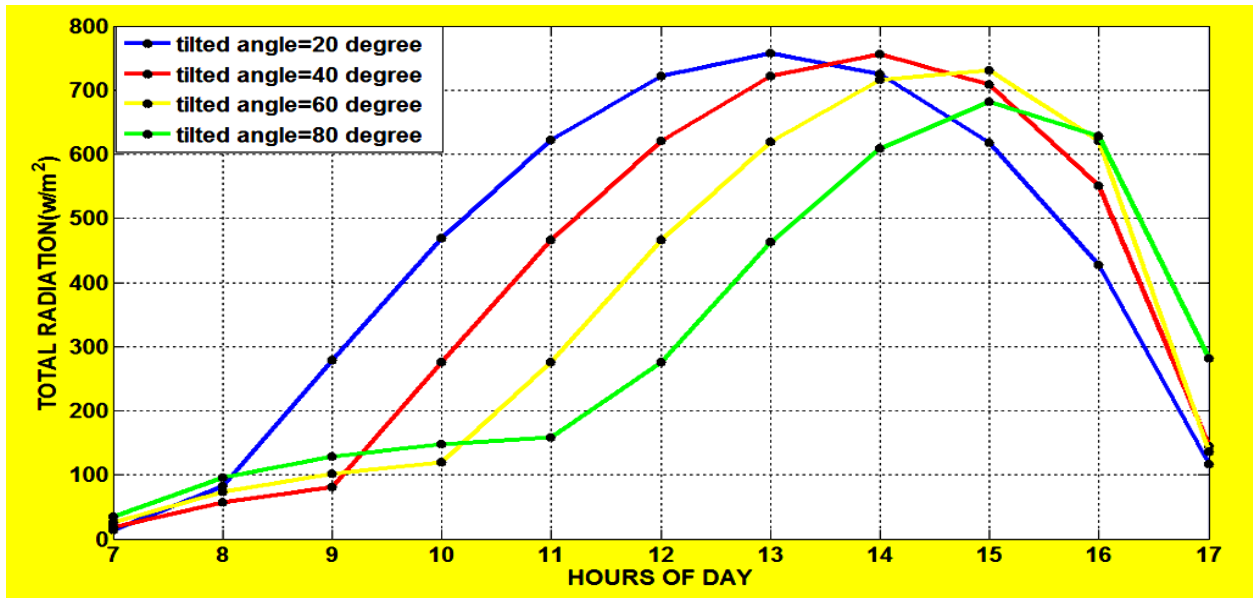


The figure 4.27 showed the relation between hours of the day and solar flux for 15 November 2015 with different tilting angles, collector facing West direction.





The figure 4.28 showed the relation between hours of the day and solar flux for 15 November 2015 with different tilting angles, collector facing North direction.



The figure 4.29 shown the relation between hours of the day and solar flux for 15 November 2015 with different tilting angles, collector facing East direction.

## 4.4 Results for theoretical Study of a Parabolic Trough Solar Collector

The program to calculate theoretical efficiency of Parabolic Trough Solar Collector is written using MATLAB . Results were obtained in the process of refining the model by repeating the steps shown in Figure 3.8. The acceptable parameters to achieved high efficiency of Parabolic Trough Solar Collector have been founded. The next Table (4.19) shows model parameters and constant value used in simulation to calculate theoretical efficiency of Parabolic Trough Solar Collector.

**Table (4.19)** theoretical model parameters.

Parameter founded	value	Considered and constant Parameters	value
Length of parabolic <b>L</b>	3.5 m	Inlet fluid temperature <b><math>T_{f.i}</math></b>	27°C
Aperture width of parabolic <b>W</b>	1.414m	Ambient temperature <b><math>T_{amb}</math></b>	29°C
Focal Length <b>f</b>	0.25 m	Cylindrical tube receiver temperature <b><math>T_r</math></b>	80°C
Height of Concentrator <b>h</b>	0.50 m	reflectivity <b><math>\rho</math></b>	0.94
Rim angle <b><math>\Psi</math></b>	90°	Absorptivity <b><math>\alpha</math></b>	0.95
Receiver inner diameter <b>Dr.int</b>	0.03 m		
Receiver outer diameter <b>Dr.ext</b>	0.0315 m		
Wind velocity <b>V</b>	5 m/s		

The simulation was repeated for three mass flow rate in the receiver 100kg/hr ,50kg/hr and 20kg/hr it shows that the model's efficiency increased with increasing in mass flow rate . The average daily efficiency of Parabolic Trough Solar Collector with mass flow rate equal to 20kg/hr is 43.23% , for mass flow rate equal to 50kg/hr is 62.393% and for mass flow rate equal to 100kg/hr is 71.492%.

The figure 4.30 shown the efficiency of Parabolic Trough Solar Collector with different mass flow rate.

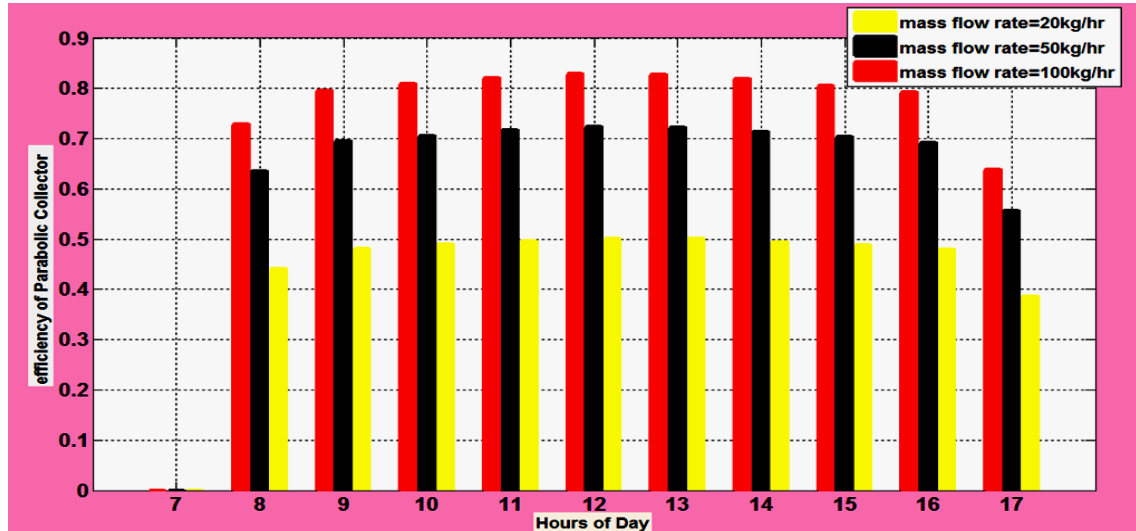


figure 4.30 variation in efficiency of Parabolic Trough Solar Collector with different mass flow rate.

The next Table (4.20) below shown the output of the program to calculate efficiency of Parabolic Trough Solar Collector with different mass flow rate and the value of useful energy from parabolic trough solar collector  $q_o$  and the power input to collector  $q_i$  by  $w/m^2$ .

**Table (4.20)** efficiency, useful energy and input power with different mass flow rate.

Mass flow		M=20kg/hr		M=50kg/hr		M=100kg/hr	
hours	$q_i$	$q_o$	$\eta. th$	$q_o$	$\eta. th$	$q_o$	$\eta. th$
8	399.71	176.01	0.44033	254.02	0.63552	291.07	0.72819
9	1087.5	523.49	0.48138	755.54	0.69477	865.71	0.79609
10	1632.9	798.3	0.48887	1152.2	0.70558	1320.2	0.80847
11	1963.9	974.87	0.49639	1407	0.71642	1612.2	0.8209
12	2106.3	1055.5	0.5011	1523.4	0.72323	1745.5	0.82869
13	2089.8	1045.9	0.50049	1509.5	0.72234	1729.7	0.82768
14	1910.2	945.31	0.49488	1364.3	0.71425	1563.3	0.81841
15	1533.9	747.4	0.48725	1078.7	0.70324	1236	0.80579
16	945.59	453.11	0.47918	653.96	0.69159	749.32	0.79244
17	261.83	100.92	0.38545	145.66	0.55632	166.9	0.63744

The figure 4.31 shown the useful energy from parabolic trough solar collector During the day hours with different mass flow rate.

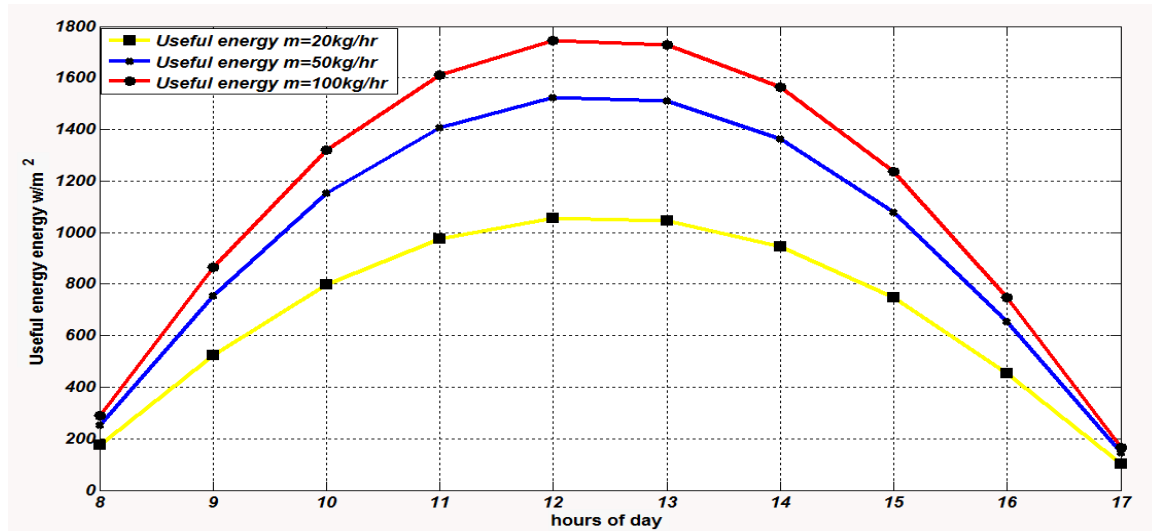


figure 4.31 variation in useful energy with different mass flow rate.

The next Table (4.21) shown the relation between concentration ratio and useful energy from parabolic trough solar collector  $q_o$  and power input to collector  $q_i$ .

**Table (4.21)** useful energy and input power with different concentration ratio.

$Cr$	$q_o$	$q_i$
0	0	0
50	338.11	541.25
100	2506.5	2922
150	5771	6564.2
200	9395.4	10512

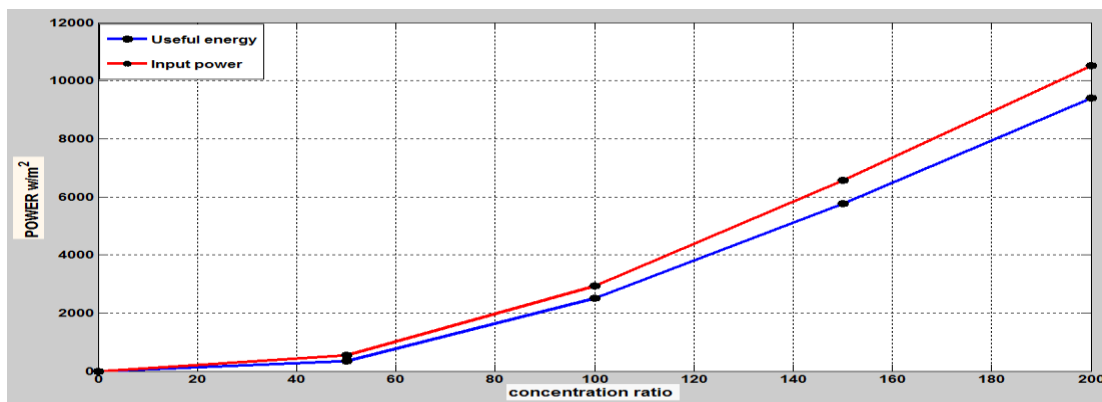


Figure 4.32 rate of energy gained as the concentration ratio increases.

The model has been tested in summer and winter and shown that in summer as expected efficiency of Parabolic Trough Solar Collector increases.

**Table (4.22)** shows the efficiency during summer and winter.

Season	Winter			summer		
Hours of day	$qi$	$qo$	$\eta.th$	$qi$	$qo$	$\eta.th$
8	2529.6	1178.5	0.46432	1087.5	772.66	0.69052
9	3281.3	1841.6	0.49589	1632.9	1236.4	0.71716
10	3710.1	2305.1	0.56125	1963.9	1534.4	0.78126
11	3902.8	2578	0.62129	2106.3	1670.4	0.79303
12	3963.6	2690.4	0.66054	2089.8	1654.2	0.79158
13	3949.8	2662.7	0.67878	1910.2	1484.5	0.77714
14	3846.4	2489.2	0.67412	1533.9	1150.5	0.75005
15	3572.2	2142.8	0.64714	945.59	653.9	0.69153
16	3019.7	1597.7	0.59987	399.71	186.3	0.68769

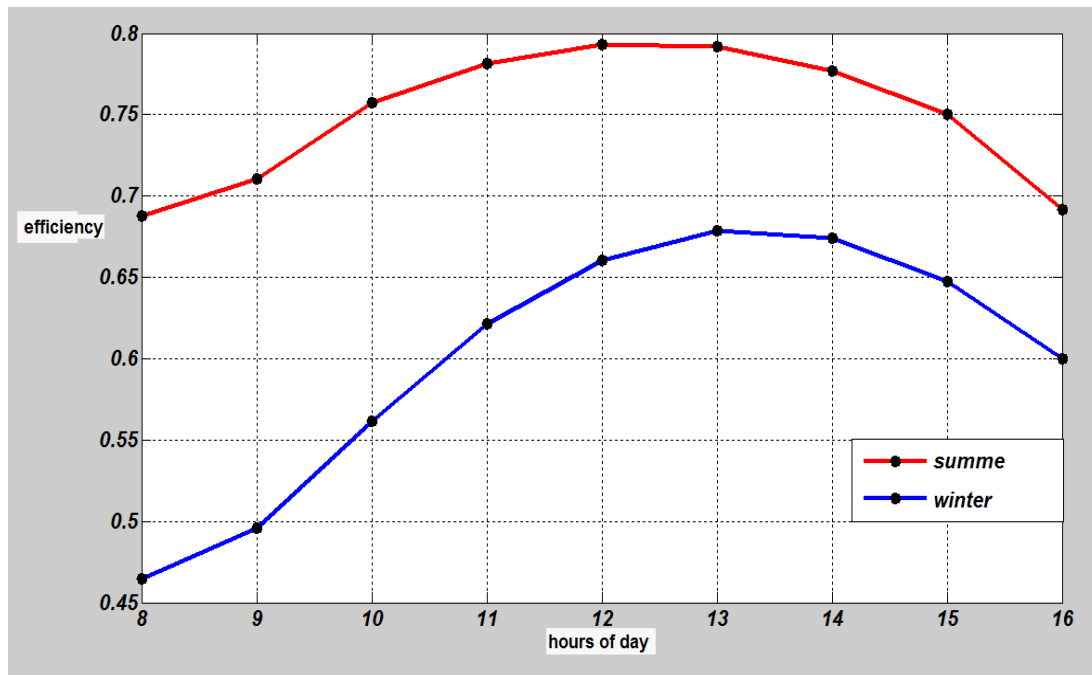


figure 4.33 variation in efficiency of Parabolic Trough Solar Collector during summer and winter.

The next figure 4.34 shown variation of efficiency of Parabolic Trough Solar and heat removal factor with mass flow rate.

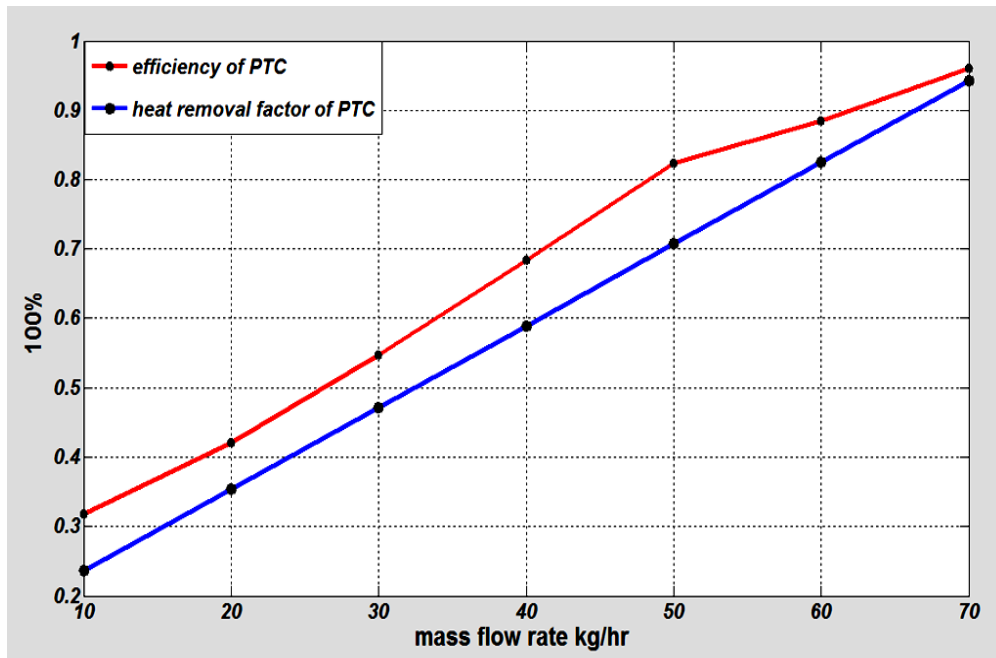


Figure 4.34 variation of efficiency and heat removal factor of PTC with different mass flow rate.

**Table (4.23)** variation of efficiency and heat removal factor of PTC with different mass flow rate

Mass flow rate Kg/hr	heat removal factor	Useful energy $\text{w/m}^2$	Power input $\text{w/m}^2$	Efficiency
10	0.11789	638.94	638.94	0.44927
20	0.23579	1800.7	1800.7	0.31883
30	0.35368	2043.5	2043.5	0.42142
40	0.47157	2100.4	2100.4	0.54668
50	0.58946	2100.3	2100.3	0.68337
60	0.70736	2091.6	2091.6	0.82345
70	0.82525	2092.9	2092.9	0.96008

## 4.5 Numerical result of FLUENT

The result of analyzing by using FLUENT 6.3.26 for the flow inside the tube shows that:

- The lower arch which faces the mirror transfer high heat to the fluid inside the tube, while the upper arch transfers heat from the tube to surrounding. So there is a hugely heat losses in the process.
- There is a back mass flow rate from the nozzle caused by throttling process, also a highly pressure inside the tube.
- The velocity of the steam increase rapidly because of the change in the density of water as the phase exchange from liquid phase to a vapour phase.

1- Total temperature in the tube:

The minimum temperature = 299.990 k

The maximum temperature = 375.477 k

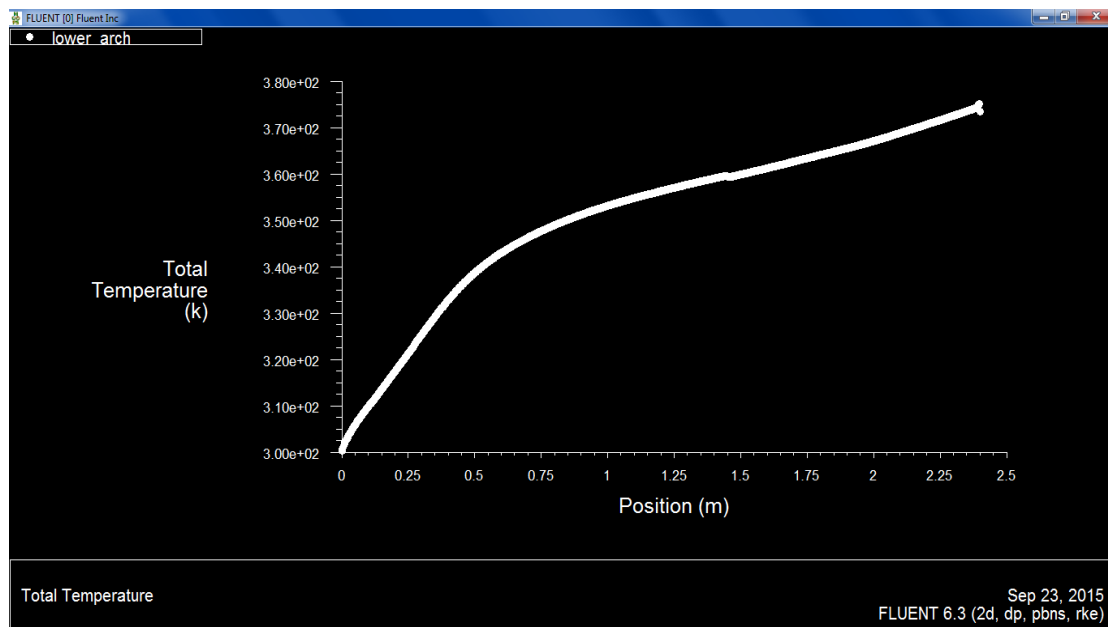


Figure 4.35 Total Temperature

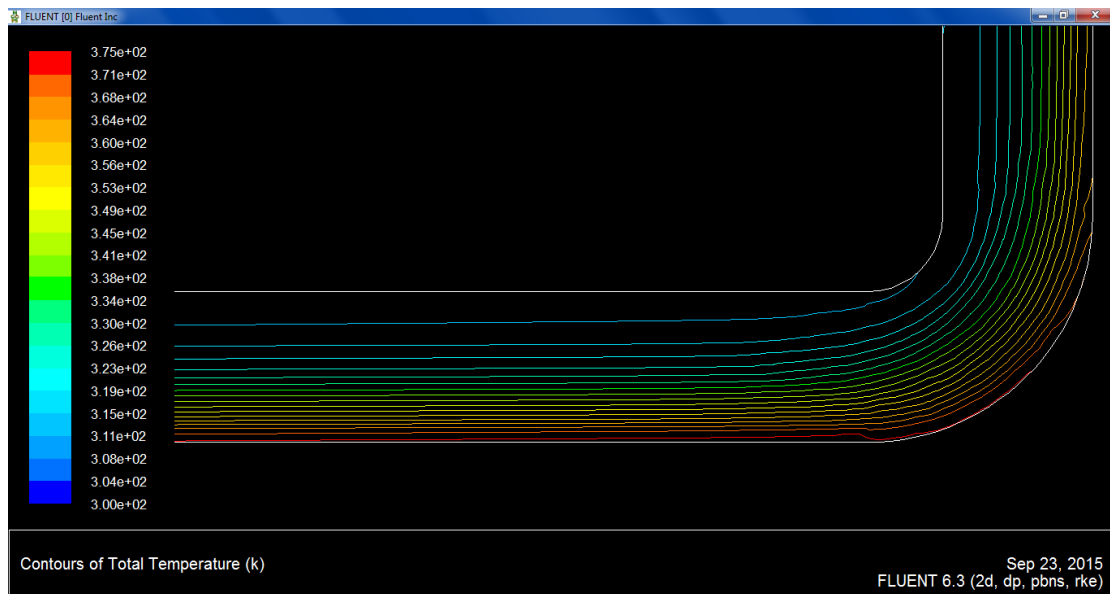


Figure 4.36 Contours of Total Temperature

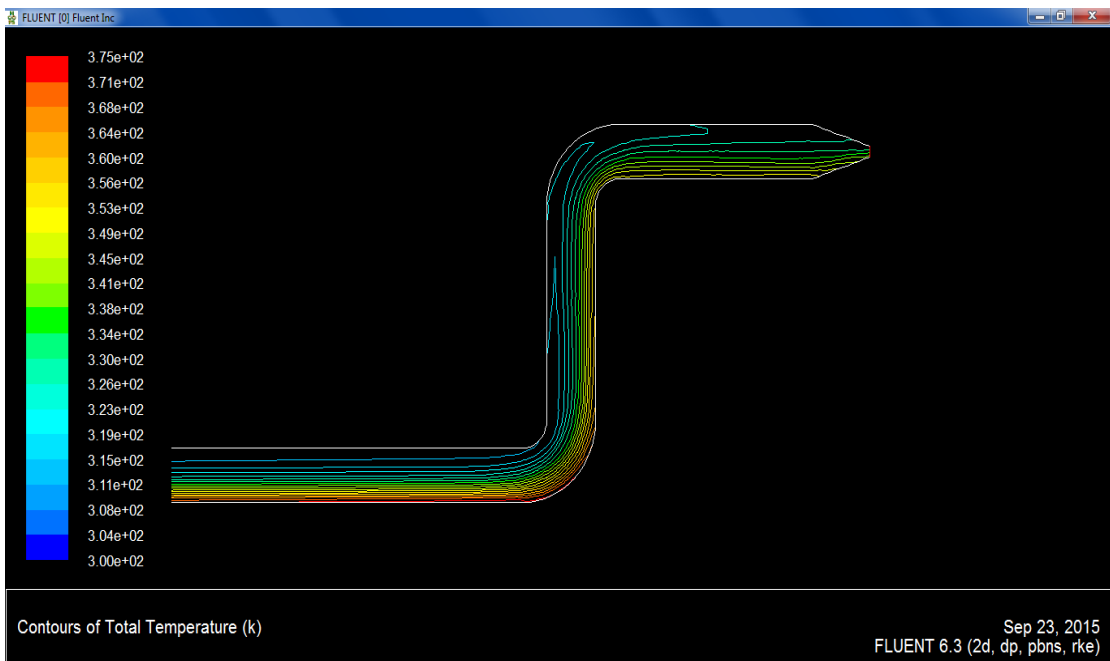


Figure 4.37 Contour of Total Temperature

2- Total pressure:

The minimum pressure = 7.00147 bar

The maximum pressure = 7.00705 bar



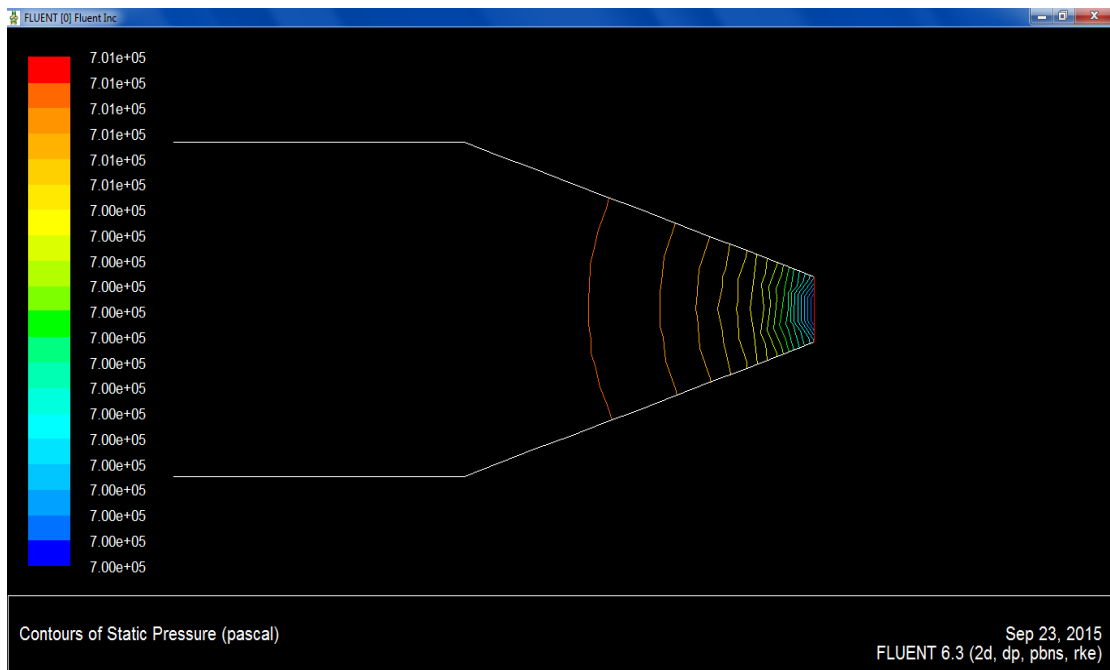


Figure 4.38 Contours of Static Pressure

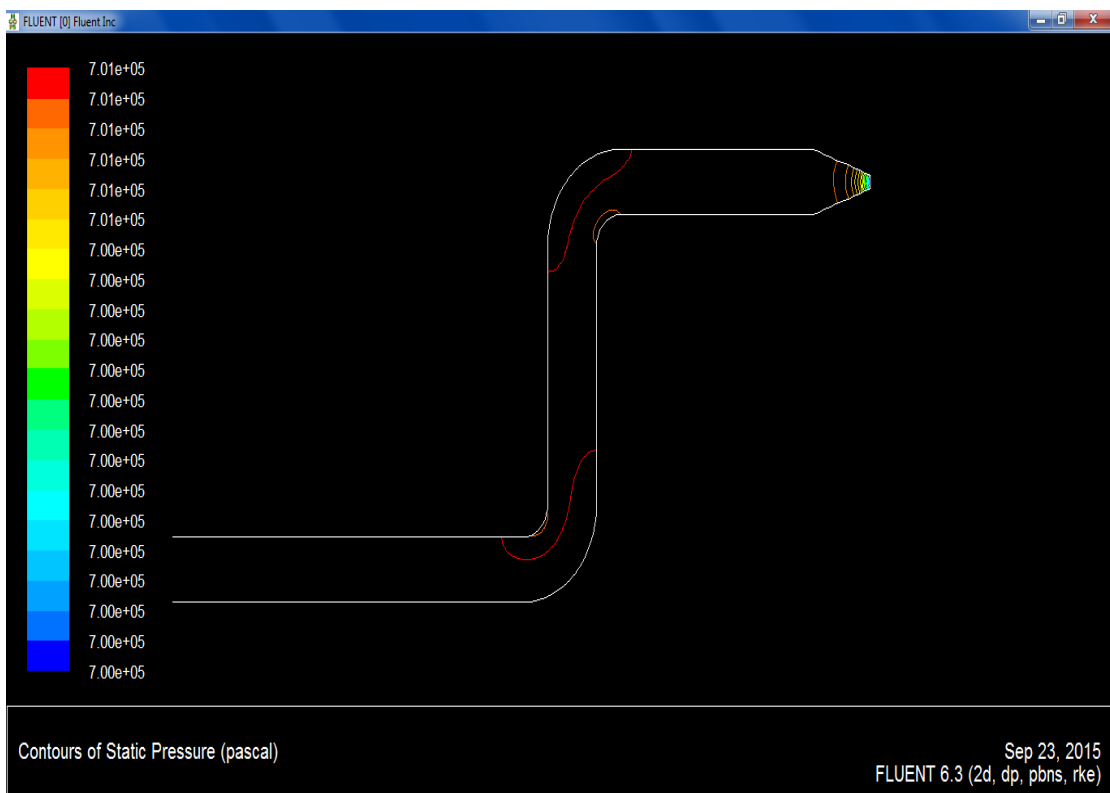


Figure 4.39 Contours of Static Pressure

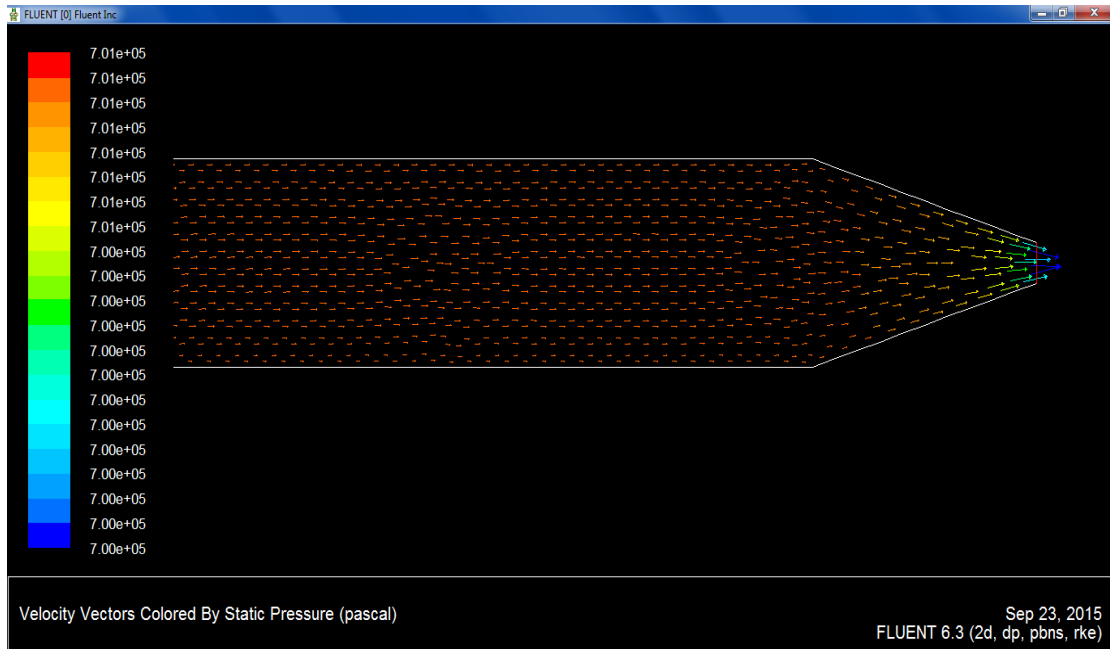


Figure 4.40 Velocity Vector Colored by Static Pressure

3- Velocity at the nozzle:

The minimum velocity = 1.453587 m/s

The maximum velocity = 32.521 m/s

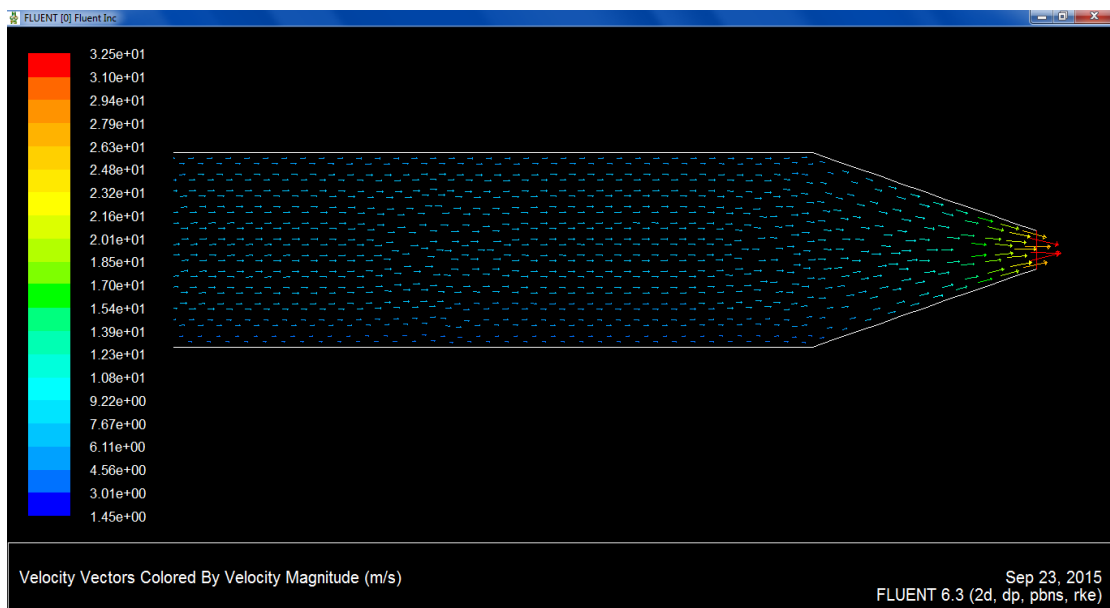


Figure 4.41 Velocity Vector Colored by Velocity Magnitude.

4- The kinetic Energy in the tube:

The minimum kinetic energy =  $0.01606 \text{ m}^2/\text{s}^2$

The maximum kinetic energy =  $2.332145 \text{ m}^2/\text{s}^2$

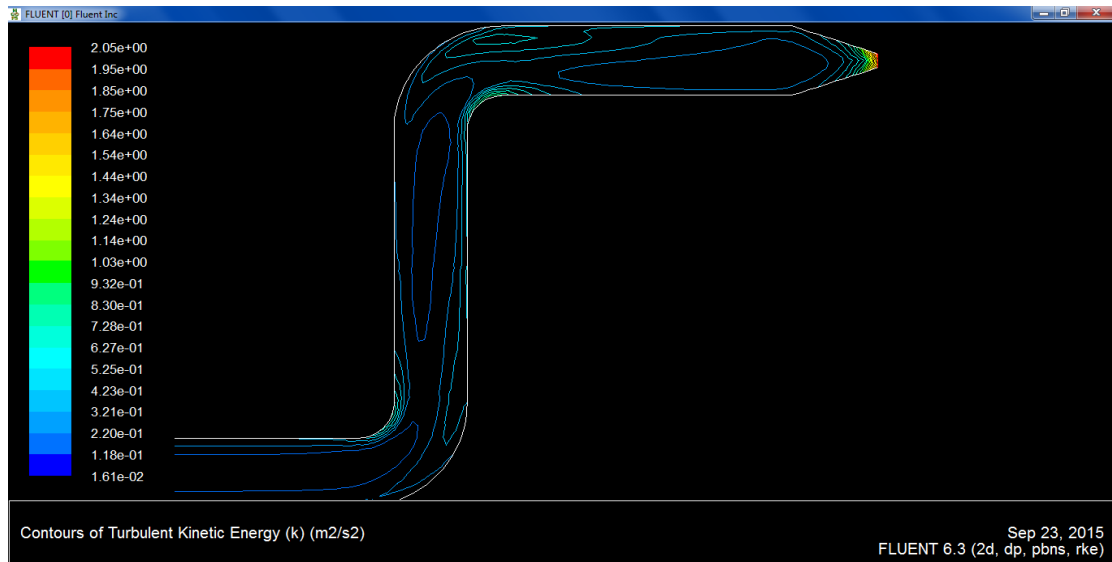


Figure 4.42 Contours of Turbulent kinetic Energy.

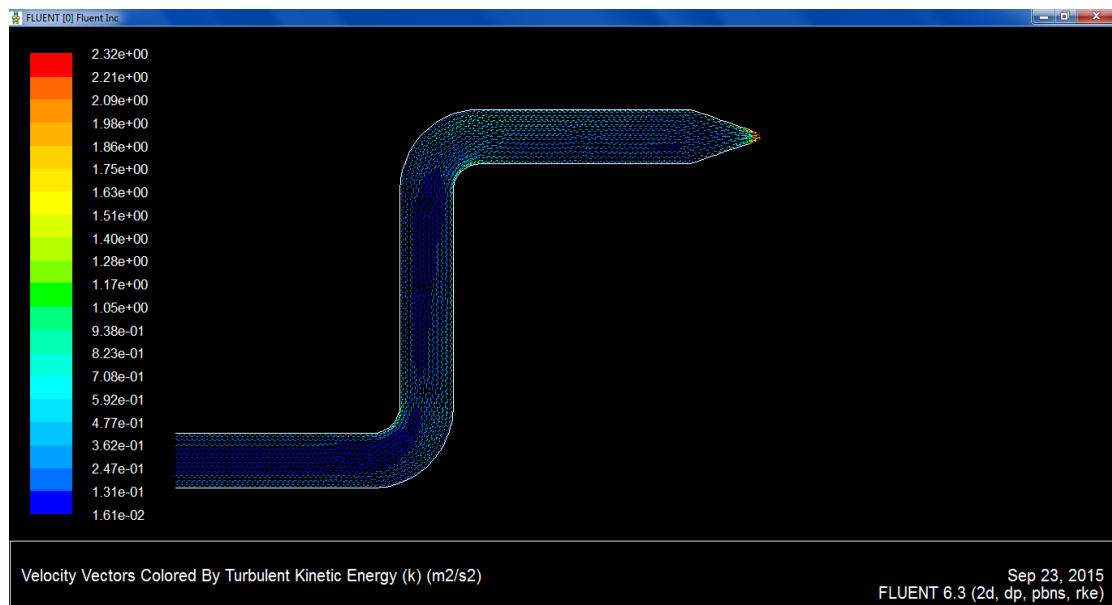


Figure 4.43 Velocity Vector Colored by Turbulent kinetic Energy.

## Mass flow rate

**Table 4.24** Mass flow rate.

<b>Mass flow rate:</b>	<b>Kg/s</b>
Inlet	0.2
Outlet	0.2000001
<b>Net</b>	<b>-1.0006e-06</b>

## Total heat transfer

**Table 4.25** Total heat transfer.

<b>Total heat transfer:</b>	<b>W</b>
Lower arch	5933.5818
Upper arch	-11.281953
<b>Net</b>	<b>5922.2999</b>

## Force report

**Table 4.26** Force report.

<b>Zone name</b>	<b>Pressure force (N)</b>	<b>Viscous force (N)</b>	<b>Total force (N)</b>	<b>Pressure coefficient</b>	<b>Viscous coefficient</b>	<b>Total coefficient</b>
<b>Wall</b>	14292.02	0.08187	14292.109	23333.922	0.13367619	23334.055
<b>Lower arch</b>	0	0.38187	0.381873	0	0.62346611	0.62346611
<b>Upper arch</b>	0	0.38337	0.38337376	0	0.62591634	0.62591634
<b>Net</b>	<b>14292.027</b>	<b>0.84711</b>	<b>14292.874</b>	<b>23333.922</b>	<b>1.3830586</b>	<b>23335.305</b>

## Moment report

**Table 4.27** Moment report.

Zone name	Pressure moment (N-m)	Viscous moment (N-m)	Total moment (N-m)	Pressure coefficient	Viscous coefficient	Total coefficient
Wall	529.03574	0.058218382	529.09395	863.73181	0.095050419	863.82686
Lower arch	-336316.29	0.0048497869	-336316.29	-549087.83	0.0079180195	-549087.82
Upper arch	336315.99	-0.0048688467	336315.99	549087.34	-0.0079491374	549087.33
Net	<b>528.7358</b>	<b>0.058199322</b>	<b>528.794</b>	<b>863.24212</b>	<b>0.095019301</b>	<b>863.33714</b>

## 4.6 Results of measured Data

To validate the model presented in above work theoretical estimation of hourly solar radiation using MATLAB, a comparison between hourly theoretical estimation and hourly measured data has been conducted.

**Table 4.28** shows the measured Data for 15 October 2015.

Hours	Total radiation		Diffuse radiation		Beam radiation	
	Voltage mV	Solar radiation $W/M^2$	Voltage mV	Solar radiation $W/M^2$	Voltage mV	Solar radiation $W/M^2$
10	3.1	685.84	0.3	66.37	2.8	619.47
11	3.6	796.46	0.6	132.74	3	663.72
12	4.3	951.33	0.5	110.62	3.8	840.70
13	3.75	829.84	0.35	77.43	3.4	752.21
14	3.2	707.96	0.2	44.25	3	663.72

## 4.7 Comparison with Measured Data

Based on the above formulations to estimate the solar radiation theoretically a experimental test has been developed to calculate the hourly solar Radiation parameters. As a test, the diffuse, direct, and total components of solar radiation were calculated for Khartoum for 15 October 2015.

The next table 4.29 below showed the comparison between MATLAB R2010b outputs and measured data.

hours	measured data			Theoretical result		
	diffuse	beam	total	diffuse	beam	total
10	66.37	619.47	685.84	106.92	552.83	659.75
11	132.74	663.72	796.46	109.66	619.01	728.66
12	110.62	840.70	951.33	110.43	639.75	750.18
13	77.43	752.21	829.84	109.62	617.95	727.57
14	44.25	663.72	707.96	106.82	550.59	657.41

The figure below show the variation between measured data and theoretical results .The average difference between theoretical and measured data does not exceed 9.5%.

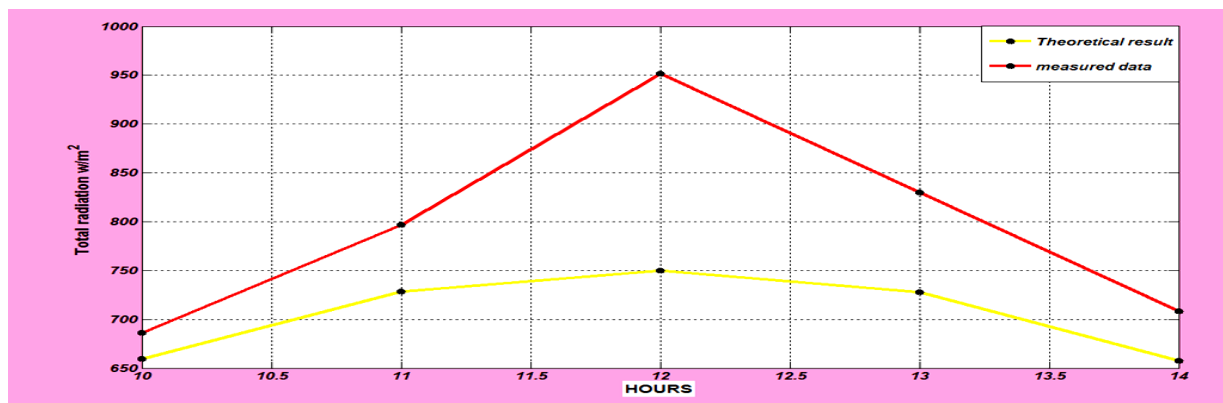


Figure 4.44 variation between measured data and theoretical results.

## 4.8 Result of experimental model

### Efficiency of experimental model

The test had been done at 14:00 o'clock parabolic trough solar collector efficiency estimated by the following equation:

$$\eta. ex = \frac{Mw \cdot Cw(T. out - T. in)}{Ib \cdot A}$$

Where:

$Mw \equiv$  water mass flow rate = 30mL/15min =  $0.0333 \times 10^{-3}$  Kg/s

$Cw \equiv$  the specific heat of water = 4.18 KJ/Kg.°C

$Ib \equiv$  direct radiation = 663.72 w/m<sup>2</sup>

$A \equiv$  aperture area =  $(\pi dL)/2 = (\pi \times 0.019m \times 1.2m)/2 = 0.0358$  m<sup>2</sup>

$T.out \equiv$  outlet water temperature = 99 °C

$T.in \equiv$  inlet water temperature = 29 °C

$$\eta. ex = 40.99\%$$

## 4.9 Discussion

From Table 4.14 we found that the total radiation has risen from January to February by 12.3%, from February to March by 29%, March to April by 7.8%, April to May by 3.4% and has digressed from May to June by 0.42%, June to July By 11.9%, July to August by 17.1%, August to September by 10.9%, September to October by 12.3%, October to November by 0.47%, November to December by 7.6%. The maximum daily average solar radiation is 8560.4 w/m<sup>2</sup> on May and minimum daily average solar radiation is 4481.2 w/m<sup>2</sup> on December. Also we discovered the average variation between theoretical result and measured data not exceed than 9.5%, this variation comes with different in location.

From FLUENT results we found that there is a reversed flow inside the tube; because of through nozzle. And there is a waste in heat from the upper arch which is equals -11.281953. Also there is high pressure in the wall of the tube especially on the elbow position. In addition there a huge losses (about 147°C) heat transfer due to thickness and conductivity of the tube. From experimental model results we found that:

There was a huge heat losses in input power; because there was no tracking system. The generated heat power by the model is instantaneously and depend on the reflected rays into the focal point, which is need to track the sun to be a system with continuously generating power. Also there was no evacuated tube to a void heat losses around the tube. And there was a high wind velocity cause a high heat losses in the name of convection losses, also it effects on the stability of the model. In addition there was a leakage in the check valve due to relaxant of the spring inside the valve which cause by generated heat.



# CHAPTER FIVE

## 5.1 Conclusion

In this Research the component of solar radiation diffuse, direct and total were calculated theoretically using MATLAB and practically using pyranometer and avometer and the value of direct radiation is high in Sudan which is good for solar thermal applications . And used GUMBIT and FLUENT to simulation the flow inside the tube.

Also the model had been designed and built practically, and experimental test had been developed to estimate the experimental efficiency of the parabolic trough collector. It compared with theoretical efficiency, which is less than theoretical value; because reasons mentioned in the previous discussion.

## 5.2 Recommendation

1. The location of Sudan is good for thermal solar application; because the average daily beam radiation about 5231.8 w/m<sup>2</sup>.
2. The technology of Parabolic Trough Collector (PTC) must be built completely with all parts (reflected surface, receiver tube with evacuated glass, sun tracking devise, the heat transfer fluid (working fluid) which must be circulated and construction supports) to get high performance with high efficiency. Any consoled part caused input power losses according to experimental test.

## REFERENCES

- [1] Solar energy engineering processes and systems. Soteris Kalogirou Cyprus University of Technology
- [2] Energy in the 21<sup>st</sup> century. JOHN R. FANCHI. (Texas Christian University, USA) copyright © 2013 by world scientific publishing . ISBN978-981-4434-66-9
- [3] Design of Solar Distillation System Prof. Alpesh Mehta, Arjun Vyas, Nitin Bodar, Dharmesh Lathiya Asst.Professor, G.H.Patel College of Engg, & Technology. V.V.Nagar, INDIA
- [4] Solar thermal collectors and applications, Soteris A. Kalogirou\*, Progress in Energy and Combustion Science 30 (2004) 231-295.
- [5] Solar Energy. Asian and Pacific Centre for Transfer of Technology of the United Nations – Economic and Social Commission for Asia and the Pacific (ESCAP)  
By Dr. P. Jayakumar September 2009
- [6] Adapted from D. Green and R. Perry (editors), Perry's chemical engineers' handbook, 8th ed. McGraw-Hill, New York, 2008.
- [7] L. Theodore, Heat transfer for the practicing engineer, John Wiley & Sons, Hoboken, NJ, 2011.
- [8] R. Dorf (adapted from), Energy resources and policy, Addison Wesley, Reading.
- [9] Matthias Günther, Michael Joemann, Simon Csambor. Parabolic trough technology. Institute for Electrical Engineering, Rational Energy Conversion, University of Kassel, Wilhelmshöher Allee 73, 34121 Kassel
- [10] Duffie, J.A., and Beckman, W.A. "Solar Engineering of Thermal Processes", John Wiley and Sons, New York, (1980).
- [11] ASHRAE Handbooks (4 volumes). Air conditioning and ventilation of buildings by D.J. Croome and B.M. Roberts, Pergamon Press
- [12] M.Tech Research Scholar, Mechanical Engineering, N.I.T Patna, India)

IOSR Journal of Mechanical and Civil Engineering (IOSR-JMCE) e-ISSN: 2278-1684, p-ISSN: 2320-334X, Volume 7, Issue 6 (Jul. – Aug. 2013)

[13] Faik A. Hamad, "The Performance Of Cylindrical Parabolic Solar Concentrator", Solar Energy Res. Vol. 5, No. 2, P.P. (1-19), Basrah, Iraq, 1987.

## Appendix

### Mat lab codes

- The day of year program:-

```
%Purpose;
%This program calculates the day of year
corresponding to a specified date;
disp('This program calculate the day of year given
the');
disp('specified date');
month = input('enter specified month{1-12}:' );
day = input ('enter specified day{1-31}');
year = input('enter specified year{yyyy}');
%check for leap year and add extra day if necessary
if rem(year,400)==0
    leap_ day = 1
elseif rem (year,100)==0
    leap_ day = 0
elseif rem (year,4)==0
    leap_ day = 1
else
    leap_ day = 0
end
% calculate the day of year
day_ of _year = day;
for ii= 1:month-1
    switch(ii)
        case{1,3,5,7,8,10,12}
            day_ of _year = day_of_year+31;
        case{4,6,9,11}
            day_ of _year = day_of_year+30;
        case 2,
            day_ of _ year = day_of_year+28+leap_ day
    end
end
fprintf ('the date %2d/%2d/%4d is day of year
%d.\n', month ,day ,year ,day _of _year);
```

- **Solar radiation in horizontal surface program :-**

```
% purpose : Estimation of Hourly Solar Radiation on Horizontal Surfaces
clear
clc
H=input ('altitude of Khartoum in (km): H') %altitude of Khartoum in (km)
LSM=input ('standard Longitude of Khartoum: LSM')%standard Longitude of
Khartoum
LON=input ('local Longitude of Khartoum: LON')% local Longitude of Khartoum
L=input ('latitude of the Khartoum (N) in (degrees): L') % latitude of the
Khartoum
Dr=360/365; % Conversion factor
N=input ('THE DAY NUMBER IN THE YEAR: N')%THE DAY NUMBER IN THE YEAR
W=input ('APPARENT SOLAR IRRADIATION: W')%APPARENT SOLAR IRRADIATION
t=input ('Reflectivity coefficient: t')%Reflectivity coefficient
S=1367; %Solar constant (w/m^2)
hours=[7,8,9,10,11,12,13,14,15,16,17];% local time
format short g
B=2*pi.*(N-1)./365; % Angle to find solar time
EOT=0.2292*(0.075+1.868*cos(B)-32.077*sin(B)-4.615*cos(2*B)-40.89*sin(2*B))%
Equation of Time
T=hours+EOT./60+4.*(Lon- Lsm)./60 % Solar time
hangle=(12.0-T)*15.0*pi/180.0 % Hour angle . pi/180.0 is the factor to
convert angles in degrees to radians.
Declangle =23.47*sin(2.0*pi*(284.0+N)/365.0)*pi/180.0 % Declination angle

alpha=asin(lati*pi/180.0)*sin(declangle)+cos(lati*pi/180.0)*cos(declangle)*co
s(hangle)% Solar altitude angle
beta=alpha.*180/pi;
cosz=90-beta;
zen=cosz.*pi/180 %solar zenith angle
azm=asin(sin(declangle).*sin(hangle)./cos(alpha))%solar azimuth angle
B=input ('atmospheric extinction coefficient :')
Idn=W*exp(-B./sin(alpha))% Direct solar radiation from sun
m=1./sin(alpha)% Air mass ratio
Sd=Idn.*0.135 %Diffuse radiation from sky on a horizontal surface
Sb=Idn .*cos( zen)% Sb is the beam radiation on a horizontal surface
St=Sb+Sd % total radiation on a horizontal surface
plot(hours ,Sb,'--
b*','linewidth',3,'MarkerEdgeColor','k','MarkerFaceColor','k','MarkerSize',7)
; % Plot the beam radiation
hold on
plot(hours ,Sd,'--
g*','linewidth',3,'MarkerEdgeColor','k','MarkerFaceColor','k','MarkerSize',7)
; % % Plot the diffuse radiation
plot(hours ,St,'--
r*','linewidth',3,'MarkerEdgeColor','k','MarkerFaceColor','k','MarkerSize',7)
; % Plot the total radiation
hold off
grid
xlabel('Hours of Day');
ylabel('Solar Radiation (w/m^2)');
legend('Beam radiation' ,'Diffuse radiation' ,'Total radiation' ,'Location'
,'Best')
```

- **Solar radiation in an incident surface program**

```

clear
clc
H=input ('altitude of Khartoum in (km): H') %altitude of Khartoum in (km)
LSM=input ('standard Longitude of Khartoum: LSM')%standard Longitude of
Khartoum
LON=input ('local Longitude of Khartoum: LON')% local Longitude of Khartoum
L=input ('latitude of the Khartoum (N) in (degrees): L') % latitude of the
Khartoum
Dr=360/365; % Conversion factor
N=input ('THE DAY NUMBER IN THE YEAR: N')%THE DAY NUMBER IN THE YEAR
W=input ('APPARENT SOLAR IRRADIATION: W')%APPARENT SOLAR IRRADIATION
t=input ('Reflectivity coefficient: t')%Reflectivity coefficient
S=1367; %Solar constant (w/m^2)
hours=[7,8,9,10,11,12,13,14,15,16,17];% local time
format short g
B=Dr*(N-1);% Angle to find solar time
EOT=0.2292*(0.075+1.868*cos(B)-32.077*sin(B)-4.615*cos(2*B)-40.89*sin(2*B));%
Equation of Time
T=hours+EOT./60+4.*(Lsm-Lon)./60;% Solar time
hangle=(12.0-T)*15.0*pi/180.0;% Note pi/180.0 is the factor to convert
angles in degrees in radians.
declangle=23.45*sin(2.0*pi*(284.0+N)/365.0)*pi/180.0;% Declination angle

altitude=sin(lati*pi/180.0)*sin(declangle)+cos(lati*pi/180.0)*cos(declangle)*
cos(hangle);%altitude angle
M=altitude.*180/pi;
U=90-M;
zen=U.*pi/180;%zenith angle
C=input ('atmospheric extinction coefficient ')
p= exp(-0.0001184.*w);
Idn=0.*exp(-C.*p./(sin( altitude)));% Direct solar radiation from sun
c=0.0965.*(1-.42.*cos(.986.*N))-0.0075.*(1-cos(1.95.*N));%_diffuse
radiation factor
for beta=20% tilted angle
    A=input ('ORIENTATION')
    W=sin(declangle).*sin(lati*pi/180.0).*cos(beta*pi/180.0);

Z=sin(declangle).*cos(lati*pi/180.0).*sin(beta*pi/180.0).*cos(A*pi/180.0);
Q=cos(declangle).*cos(lati*pi/180.0).*cos(beta*pi/180.0).*cos(hangle);

V=cos(declangle).*sin(lati*pi/180.0).*sin(beta*pi/180.0).*cos(A*pi/180.0).*co
s(hangle);
K=cos(declangle).*sin(beta*pi/180.0).*sin(A*pi/180.0).*sin(hangle);
theta =acos(W-Z+Q+V+K);% incident angle
SB=cos(theta).*Idn;% beam radiation in tilted surface
SB(SB<0)=0;
SD=Idn.*(c.*.45+.5.*t.*(c+sin(alpha)));% diffuse radiation in tilted surface
SD(SD<0)=0;
uu=t.*(1-cos(beta.*pi/180))./2;
SG=(SD+Idn).*uu;% reflected radiation
It=SB+SD+SG% total radiation
plot(hours,It,'-
b*','linewidth',3,'MarkerEdgeColor','k','MarkerFaceColor','k','MarkerSize',7)
; % % Plot the total radiation

```

```

hold on
end

for beta=40% tilted angle
    A=input ('ORINTATION')
    W=sin(declangle).*sin(lati*pi/180.0).*cos(beta*pi/180.0);

    Z=sin(declangle).*cos(lati*pi/180.0).*sin(beta*pi/180.0).*cos(A*pi/180.0);
    Q=cos(declangle).*cos(lati*pi/180.0).*cos(beta*pi/180.0).*cos(hangle);

    V=cos(declangle).*sin(lati*pi/180.0).*sin(beta*pi/180.0).*cos(A*pi/180.0).*cos(hangle);
    K=cos(declangle).*sin(beta*pi/180.0).*sin(A*pi/180.0).*sin(hangle);
    theta =acos(W-Z+Q+V+K);% incident angle
    SB=cos(theta).*Idn;% beam radiation in tilted surface
    SB(SB<0)=0;
    SD=Idn.*(c.*.45+.5.*t.*(c+sin(alpha)));% diffuse radiation in tilted surface
    SD(SD<0)=0;
    uu=.2.*(1-cos(beta.*pi/180))./2;
    SG=(SD+Idn).*uu; % reflected radiation
    It=SB+SD+SG% total radiation
    plot(hours,It,'-r*','linewidth',3,'MarkerEdgeColor','k','MarkerFaceColor','k','MarkerSize',7)
; % % Plot the total radiation
end

for beta=60% tilted angle
    A=input ('ORINTATION')
    W=sin(declangle).*sin(lati*pi/180.0).*cos(beta*pi/180.0);

    Z=sin(declangle).*cos(lati*pi/180.0).*sin(beta*pi/180.0).*cos(A*pi/180.0);
    Q=cos(declangle).*cos(lati*pi/180.0).*cos(beta*pi/180.0).*cos(hangle);

    V=cos(declangle).*sin(lati*pi/180.0).*sin(beta*pi/180.0).*cos(A*pi/180.0).*cos(hangle);
    K=cos(declangle).*sin(beta*pi/180.0).*sin(A*pi/180.0).*sin(hangle);
    theta =acos(W-Z+Q+V+K);% incident angle
    SB=cos(theta).*Idn;% beam radiation in tilted surface
    SB(SB<0)=0;
    SD=Idn.*(c.*.45+.5.*t.*(c+sin(alpha)));% diffuse radiation in tilted surface
    SD(SD<0)=0;
    uu=.2.*(1-cos(beta.*pi/180))./2;
    SG=(SD+Idn).*uu; % reflected radiation
    It=SB+SD+SG% total radiation
    plot(hours,It,'-y*','linewidth',3,'MarkerEdgeColor','k','MarkerFaceColor','k','MarkerSize',7)
; % % Plot the total radiation
end

for beta=80% tilted angle
    A=input ('ORINTATION')
    W=sin(declangle).*sin(lati*pi/180.0).*cos(beta*pi/180.0);

    Z=sin(declangle).*cos(lati*pi/180.0).*sin(beta*pi/180.0).*cos(A*pi/180.0);
    Q=cos(declangle).*cos(lati*pi/180.0).*cos(beta*pi/180.0).*cos(hangle);

```



```

V=cos(declangle).*sin(lati*pi/180.0).*sin(beta*pi/180.0).*cos(A*pi/180.0).*cos(hangle);
K=cos(declangle).*sin(beta*pi/180.0).*sin(A*pi/180.0).*sin(hangle);
theta =acos(W-Z+Q+V+K);% incident angle
SB=cos(theta).*Idn;% beam radiation in tilted surface
SB(SB<0)=0;
SD=Idn.*(c.*.45+.5.*t.*(c+sin(alpha)));% diffuse radiation in tilted surface
SD(SD<0)=0;
uu=.2.*(1-cos(beta*pi/180))./2;
SG=(SD+Idn).*uu;% reflected radiation
It=SB+SD+SG% total radiation
plot(hours,It,'-g*','linewidth',3,'MarkerEdgeColor','k','MarkerFaceColor','k','MarkerSize',7)
; % % Plot the total radiation
hold off
grid
xlabel('Hours of Day');
ylabel('Total Radiation (w/m^2)');
legend('tilted angle=20 degree','tilted angle=40 degree','tilted angle=60 degree','tilted angle=80 degree','Location','Best')
end

```

- **Parabolic trough solar collector program**

```

clear
clc
H=input('altitude of Khartoum in (km): H') %altitude of Khartoum in (km)
LSM=input('standard Longitude of Khartoum: LSM')%standard Longitude of Khartoum
LON=input('local Longitude of Khartoum: LON')% local Longitude of Khartoum
L=input('latitude of the Khartoum in (degrees): L') % latitude of the Khartoum
Dr=360/365; % Conversion factor
N=input('THE DAY NUMBER IN THE YEAR: N')%THE DAY NUMBER IN THE YEAR
W=input('APPARENT SOLAR IRRADIATION: W')%APPARENT SOLAR IRRADIATION
t=input('Reflectivity coefficient: t')%Reflectivity coefficient
S=1367; %Solar constant (w/m^2)
hours=[7,8,9,10,11,12,13,14,15,16,17];% local time
format short g
B=Dr*(N-1);% Angle to find solar time
EOT=0.2292*(0.075+1.868*cos(B)-32.077*sin(B)-4.615*cos(2*B)-40.89*sin(2*B));% Equation of Time
T=hours+EOT./60+4.*(LSM-LON)./60;% Solar time
hangle=(12.0-T)*15.0*pi/180.0;% Note pi/180.0 is the factor to convert angles in degrees in radians.
declangle=23.45*sin(2.0*pi*(284.0+N)/365.0)*pi/180.0;% Declination angle

altitude=sin(lati*pi/180.0)*sin(declangle)+cos(lati*pi/180.0)*cos(declangle)*cos(hangle);%altitude angle
M=altitude.*180/pi;
U=90-M;
zen=U.*pi/180;%zenith angle
C=input('atmospheric extinction coefficient ')

```

```

p=exp(-0.0001184.*w);
Idn=0.*exp(-C.*p./(sin(altitude)));% Direct solar radition from sun
c=0.0965.*((1-.42.*cos(.986.*N))-0.0075.*(1-cos(1.95.*N)));%_diffuse
radiation factor
azm=asin(sin(declangle).*sin(hangle)./cos(alpha));% solar azimuth angle
MM=1./sin(alpha);% Air mass ratio
beta =input('tilted angle ')% tilted angle
A=input ('ORINTATION')
W=sin(declangle).*sin(lati*pi/180.0).*cos(beta*pi/180.0);

Z=sin(declangle).*cos(lati*pi/180.0).*sin(beta*pi/180.0).*cos(A*pi/180.0);
Q=cos(declangle).*cos(lati*pi/180.0).*cos(beta*pi/180.0).*cos(hangle);

V=cos(declangle).*sin(lati*pi/180.0).*sin(beta*pi/180.0).*cos(A*pi/180.0).*cos(hangle);
K=cos(declangle).*sin(beta*pi/180.0).*sin(A*pi/180.0).*sin(hangle);
theta =acos(W-Z+Q+V+K);% incident angle
r=cos(zen)./cos(theta);% beam radiation in tilted surface
SB=cos(theta).*Idn;% diffuse radiation in tilted surface
SB(SB<0)=0;
SD=Idn.*(c.*.45+.5.*t.*(c+sin(alpha)));
SD(SD<0)=0;
uu=.2.*(1-cos(beta.*pi/180))./2;
SG=(SD+Idn).*uu;% reflected radiation
It=SB+SD+SG;% total radiation
rb=Ib./SB;%hourly geometric factor for beam radiation
rd=SD./Id;% hourly geometric factor for diffuse radiation
L=input ('Length of parabola: L')
F=input ('Focal Length: F')
h=input('Height of Concentrator')
Dri=input ('Receiver inner diameter')
Dro=input ('Receiver outer diameter')
W=input ('Aperture of parabola')
MM=input ('mass flow rate')
Tfi=input ('Inlet fluid temperature')
Ta=input ('Ambient temperature')
Tsky=input ('Sky temperature')
Tr=input ('Cylindrical tube receiver temperature')
V=input ('Kinetic viscosity of air')
vv=input ('Kinetic viscosity of water')
Cpw=input ('specific heat constant of water')
Cpa=input ('specific heat constant of air')

P=input ('reflectivity')
Emr=input ('Emissivity of receiver tube surface')
abs=input ('Absorptivity')
tra=input ('Transmittivity of tube')
kair=input ('Thermal conductivity of air')
kw=input ('Thermal conductivity of water')
Wv=input ('Wind velocity')
d=input ('Density')
c=(W-Dro)./(pi.*Dro.*L);%concentration ratio
Vavg=(4.*M1)./(pi.*Dri).^(2.*P);% average speed
Re=(Vavg.*Dro)./V %Reynolds number of air
Nu=0.3.*Re.^(0.6)%Nussle number of air
hw=(Nu.*kair)./Dro;%convective heat transfer coefficient between receiver
and ambient

```

```

xx=1./ul;
Ac=(pi.*Dri.^2)./4;%cross sectional area of receiver
uw=M1./(1000.*Ac);
Rew=(uw.*Dri)./vv %Reynolds number of water
prw=vv.*cpw
xxx=0.0668.*(Dri./L).*Rew.*prw
xxxx=1+0.04.*((Dri./L).*Rew.*prw).^(2./3)
zxxx=3.6+xxx./xxxx
hc=(kw./Dri).*(zxxx)%convective heat transfer coefficient between receiver
and fluid
ul=hc+hw%overall heat loss coefficient
zxxz=Dro.*(log(Dro./Dri))./(2.*kr)
ZZ=ul.*(xx+(Dro./Dri)+zxxz).^(-1)
Ao=pi.*Dro.*L;%external surface area of receiver
Ai=pi.*Dri.*L;%internal surface area of receiver
yy=(M1.*Cp)./(Ai.*ul);
yx=(Ai.*ul.*ZZ)./(M1.*Cp);
Fr=yy.*(1-exp(-yx))%heat removal factor of collector
Ap=(W-Dro).*L;%aperture area
hp=Ib.*abs.*Emr;%absorbed radiation
qo=Fr.*Ap.*(hp-((Ao./Ap).*ul.*(Tfi-Ta)))%theoretical useful energy
qi=(Ib.*rb).*(W.*L)% power input
effl=qo./qi

```

## Summary of analyzing by Fluent 6.3.26:

FLUENT

Version: 2d, dp, pbns, rke (2d, double precision, pressure-based, realizable k-epsilon)

Release: 6.3.26

Title:

### Models:

-----	
Model	Setting
-----	
Space	2D
Time	Steady
Viscous	Realizable k-epsilon turbulence model
Wall Treatment	Standard Wall Functions
Heat Transfer	Enabled
Solidification and Melting	Disabled
Radiation	None
Species Transport	Disabled
Coupled Dispersed Phase	Disabled
Pollutants	Disabled
Pollutants	Disabled
Soot	Disabled

### Boundary Conditions:

#### Zones:

-----		
name	id	type
-----		

fluid	2	fluid
wall	3	wall
interior	4	interior
lower_arch	5	wall
upper_arch	6	wall
outlet	7	outlet-vent
inlet	8	mass-flow-inlet
default-interior	10	interior

### Boundary Conditions:

#### Fluid:

Condition	Value
Material Name	air
Specify source terms?	no
Source Terms	()
Specify fixed values?	no
Fixed Values	()
Motion Type	0
X-Velocity of Zone (m/s)	0
Y-Velocity Of Zone (m/s)	0
Rotation speed (rad/s)	0
X-Origin of Rotation-Axis (m)	0
Y-Origin of Rotation-Axis (m)	0
Deactivated Thread	no
Laminar zone?	no

Set Turbulent Viscosity to zero within laminar zone?	yes
Porous zone?	no
X-Component of Direction-1 Vector	1
Y-Component of Direction-1 Vector	0
Relative Velocity Resistance Formulation?	yes
Direction-1 Viscous Resistance (1/m <sup>2</sup> )	0
Direction-2 Viscous Resistance (1/m <sup>2</sup> )	0
Choose alternative formulation for inertial resistance?	no
Direction-1 Inertial Resistance (1/m)	0
Direction-2 Inertial Resistance (1/m)	0
C0 Coefficient for Power-Law	0
C1 Coefficient for Power-Law	0
Porosity	1
Solid Material Name	aluminum

## Wall

Condition	Value
Wall Thickness (m)	0.0020000001
Heat Generation Rate (w/m <sup>3</sup> )	100
Material Name	aluminum
Thermal BC Type	1
Temperature (k)	523
Heat Flux (w/m <sup>2</sup> )	1000
Convective Heat Transfer Coefficient (w/m <sup>2</sup> -k)	1.5
Free Stream Temperature (k)	300
Wall Motion	0

Shear Boundary Condition	0
Define wall motion relative to adjacent cell zone?	yes
Apply a rotational velocity to this wall?	no
Velocity Magnitude (m/s)	0
X-Component of Wall Translation	1
Y-Component of Wall Translation	0
Define wall velocity components?	no
X-Component of Wall Translation (m/s)	0
Y-Component of Wall Translation (m/s)	0
External Emissivity	1
External Radiation Temperature (k)	350
Wall Roughness Height (m)	0
Wall Roughness Constant	0.5
Rotation Speed (rad/s)	0
X-Position of Rotation-Axis Origin (m)	0
Y-Position of Rotation-Axis Origin (m)	0
X-component of shear stress (pascal)	0
Y-component of shear stress (pascal)	0
Surface tension gradient (n/m-k)	0
Specularity Coefficient	0

**Interior:**

**Condition Value:**

**Lower arch:**

---

Condition	Value
-----------	-------

---

Wall Thickness (m)	0.0020000001
Heat Generation Rate (w/m3)	100
Material Name	aluminum
Thermal BC Type	5
Temperature (k)	300
Heat Flux (w/m2)	1000
Convective Heat Transfer Coefficient (w/m2-k)	1.5
Free Stream Temperature (k)	300
Wall Motion	0
Shear Boundary Condition	0
Define wall motion relative to adjacent cell zone?	yes
Apply a rotational velocity to this wall?	no
Velocity Magnitude (m/s)	0
X-Component of Wall Translation	1
Y-Component of Wall Translation	0
Define wall velocity components?	no
X-Component of Wall Translation (m/s)	0
Y-Component of Wall Translation (m/s)	0
External Emissivity	1
External Radiation Temperature (k)	523
Wall Roughness Height (m)	0
Wall Roughness Constant	0.5
Rotation Speed (rad/s)	0
X-Position of Rotation-Axis Origin (m)	0
Y-Position of Rotation-Axis Origin (m)	0
X-component of shear stress (pascal)	0
Y-component of shear stress (pascal)	0



Surface tension gradient (n/m-k)	0
Specularity Coefficient	0

#### Upper arch:

Condition	Value
Wall Thickness (m)	0.0020000001
Heat Generation Rate (w/m3)	100
Material Name	aluminum
Thermal BC Type	2
Temperature (k)	523
Heat Flux (w/m2)	1000
Convective Heat Transfer Coefficient (w/m2-k)	1.5
Free Stream Temperature (k)	300
Wall Motion	0
Shear Boundary Condition	0
Define wall motion relative to adjacent cell zone?	yes
Apply a rotational velocity to this wall?	no
Velocity Magnitude (m/s)	0
X-Component of Wall Translation	1
Y-Component of Wall Translation	0
Define wall velocity components?	no
X-Component of Wall Translation (m/s)	0
Y-Component of Wall Translation (m/s)	0
External Emissivity	1
External Radiation Temperature (k)	350

Wall Roughness Height (m)	0
Wall Roughness Constant	0.5
Rotation Speed (rad/s)	0
X-Position of Rotation-Axis Origin (m)	0
Y-Position of Rotation-Axis Origin (m)	0
X-component of shear stress (pascal)	0
Y-component of shear stress (pascal)	0
Surface tension gradient (n/m-k)	0
Specularity Coefficient	0

**Outlet:**

Condition	Value
Gauge Pressure (pascal)	700000
Backflow Total Temperature (k)	523
Backflow Direction Specification Method	1
X-Component of Flow Direction	1
Y-Component of Flow Direction	0
X-Component of Axis Direction	1
Y-Component of Axis Direction	0
Z-Component of Axis Direction	0
X-Coordinate of Axis Origin (m)	0
Y-Coordinate of Axis Origin (m)	0
Z-Coordinate of Axis Origin (m)	0
Turbulent Specification Method	0
Backflow Turbulent Kinetic Energy (m2/s2)	1

Backflow Turbulent Dissipation Rate (m2/s3)	1
Backflow Turbulent Intensity (%)	0.1
Backflow Turbulent Length Scale (m)	1
Backflow Hydraulic Diameter (m)	1
Backflow Turbulent Viscosity Ratio	10
is zone used in mixing-plane model?	no
Specify targeted mass flow rate	no
Targeted mass flow (kg/s)	1
Loss Coefficient	(polynomial normal-velocity 0 )

#### **Inlet:**

Condition	Value
Mass Flow Specification Method	0
Mass Flow-Rate (kg/s)	0.2
Mass Flux (kg/m2-s)	1
Average Mass Flux (kg/m2-s)	1
Upstream Torque Integral (n-m)	1
Upstream Total Enthalpy Integral (w/m2)	1
Total Temperature (k)	300
Supersonic/Initial Gauge Pressure (pascal)	1000
Direction Specification Method	0
Reference Frame	0
X-Component of Flow Direction	1
Y-Component of Flow Direction	0
X-Component of Axis Direction	1

Y-Component of Axis Direction	0
Z-Component of Axis Direction	0
X-Coordinate of Axis Origin (m)	0
Y-Coordinate of Axis Origin (m)	0
Z-Coordinate of Axis Origin (m)	0
Turbulent Specification Method	0
Turbulent Kinetic Energy (m2/s2)	1
Turbulent Dissipation Rate (m2/s3)	1
Turbulent Intensity (%)	0.1
Turbulent Length Scale (m)	1
Hydraulic Diameter (m)	1
Turbulent Viscosity Ratio	10
is zone used in mixing-plane model?	no

#### **Default-interior:**

#### **Equations:**

-----	
Equation	Solved
-----	
Flow	yes
Turbulence	yes
Energy	yes

#### **Numeric:**

-----	
Numeric	Enabled
-----	
Absolute Velocity Formulation	yes

**Relaxation:**

---

Variable	Relaxation Factor
Pressure	0.3
Density	1
Body Forces	1
Momentum	0.7
Turbulent Kinetic Energy	0.8
Turbulent Dissipation Rate	0.8
Turbulent Viscosity	1
Energy	1

**Linear Solver:**

---

	Solver	Termination	Residual
Variable	Type	Criterion	Reduction Tolerance
Pressure	V-Cycle	0.1	
X-Momentum	Flexible	0.1	0.7
Y-Momentum	Flexible	0.1	0.7
Turbulent Kinetic Energy	Flexible	0.1	0.7
Turbulent Dissipation Rate	Flexible	0.1	0.7
Energy	Flexible	0.1	0.7

**Discretization Scheme:**

Variable	Scheme
Pressure	Standard
Momentum	First Order Upwind
Turbulent Kinetic Energy	First Order Upwind
Turbulent Dissipation Rate	First Order Upwind
Energy	First Order Upwind

**Solution Limits:**

Quantity	Limit
Minimum Absolute Pressure	1
Maximum Absolute Pressure	5e+10
Minimum Temperature	1
Maximum Temperature	5000
Minimum Turb. Kinetic Energy	1e-14
Minimum Turb. Dissipation Rate	1e-20
Maximum Turb. Viscosity Ratio	100000

**Material Properties:**

**Material: water-vapor (fluid):**

Property	Units	Method	Value(s )
Density	kg/m <sup>3</sup>	constant	0.55419999
Cp (Specific Heat)	J/kg-K	constant	2014
Thermal Conductivity	W/m-K	constant	0.0261
Viscosity	kg/m-s	constant	1.34e-05
Molecular Weight	kg/kgmol	constant	18.01534
L-J Characteristic Length	angstrom	constant	2.605
L-J Energy Parameter	K	constant	572.4
Thermal Expansion Coefficient	1/K	constant	0
Degrees of Freedom		constant	0
Speed of Sound	m/s	none	#f

**Material: air (fluid):**

Property	Units	Method	Value(s )
Density	kg/m <sup>3</sup>	constant	1.225
Cp (Specific Heat)	J/kg-K	constant	1006.43
Thermal Conductivity	W/m-K	constant	0.0242
Viscosity	kg/m-s	constant	1.7894e-05
Molecular Weight	kg/kg.mol	constant	28.966
L-J Characteristic Length	angstrom	constant	3.711
L-J Energy Parameter	K	constant	78.6
Thermal Expansion Coefficient	1/K	constant	0

Degrees of Freedom		constant	0
Speed of Sound	m/s	none	#f

**Material: aluminum (solid):**

Property	Units	Method	Value(s)
Density	kg/m3	constant	2719
Cp (Specific Heat)	j/kg-k	constant	871
Thermal Conductivity	w/m-k	constant	202.4